



NUREG/CR-7124

# Validation of LAPUR 6.0 Code

Office of Nuclear Reactor Regulation

**AVAILABILITY OF REFERENCE MATERIALS  
IN NRC PUBLICATIONS**

**NRC Reference Material**

As of November 1999, you may electronically access NUREG-series publications and other NRC records at NRC's Public Electronic Reading Room at <http://www.nrc.gov/reading-rm.html>. Publicly released records include, to name a few, NUREG-series publications; *Federal Register* notices; applicant, licensee, and vendor documents and correspondence; NRC correspondence and internal memoranda; bulletins and information notices; inspection and investigative reports; licensee event reports; and Commission papers and their attachments.

NRC publications in the NUREG series, NRC regulations, and *Title 10, Energy*, in the Code of *Federal Regulations* may also be purchased from one of these two sources.

1. The Superintendent of Documents  
U.S. Government Printing Office  
Mail Stop SSOP  
Washington, DC 20402-0001  
Internet: [bookstore.gpo.gov](http://bookstore.gpo.gov)  
Telephone: 202-512-1800  
Fax: 202-512-2250
2. The National Technical Information Service  
Springfield, VA 22161-0002  
[www.ntis.gov](http://www.ntis.gov)  
1-800-553-6847 or, locally, 703-605-6000

A single copy of each NRC draft report for comment is available free, to the extent of supply, upon written request as follows:

Address: U.S. Nuclear Regulatory Commission  
Office of Administration  
Publications Branch  
Washington, DC 20555-0001  
E-mail: [DISTRIBUTION.RESOURCE@NRC.GOV](mailto:DISTRIBUTION.RESOURCE@NRC.GOV)  
Facsimile: 301-415-2289

Some publications in the NUREG series that are posted at NRC's Web site address <http://www.nrc.gov/reading-rm/doc-collections/nuregs> are updated periodically and may differ from the last printed version. Although references to material found on a Web site bear the date the material was accessed, the material available on the date cited may subsequently be removed from the site.

**Non-NRC Reference Material**

Documents available from public and special technical libraries include all open literature items, such as books, journal articles, and transactions, *Federal Register* notices, Federal and State legislation, and congressional reports. Such documents as theses, dissertations, foreign reports and translations, and non-NRC conference proceedings may be purchased from their sponsoring organization.

Copies of industry codes and standards used in a substantive manner in the NRC regulatory process are maintained at—

The NRC Technical Library  
Two White Flint North  
11545 Rockville Pike  
Rockville, MD 20852-2738

These standards are available in the library for reference use by the public. Codes and standards are usually copyrighted and may be purchased from the originating organization or, if they are American National Standards, from—

American National Standards Institute  
11 West 42<sup>nd</sup> Street  
New York, NY 10036-8002  
[www.ansi.org](http://www.ansi.org)  
212-642-4900

Legally binding regulatory requirements are stated only in laws; NRC regulations; licenses, including technical specifications; or orders, not in NUREG-series publications. The views expressed in contractor-prepared publications in this series are not necessarily those of the NRC.

The NUREG series comprises (1) technical and administrative reports and books prepared by the staff (NUREG-XXXX) or agency contractors (NUREG/CR-XXXX), (2) proceedings of conferences (NUREG/CP-XXXX), (3) reports resulting from international agreements (NUREG/IA-XXXX), (4) brochures (NUREG/BR-XXXX), and (5) compilations of legal decisions and orders of the Commission and Atomic and Safety Licensing Boards and of Directors' decisions under Section 2.206 of NRC's regulations (NUREG-0750).

**DISCLAIMER:** This report was prepared as an account of work sponsored by an agency of the U.S. Government. Neither the U.S. Government nor any agency thereof, nor any employee, makes any warranty, expressed or implied, or assumes any legal liability or responsibility for any third party's use, or the results of such use, of any information, apparatus, product, or process disclosed in this publication, or represents that its use by such third party would not infringe privately owned rights.

# Validation of LAPUR 6.0 Code

Manuscript Completed: March 2012  
Date Published: March 2012

Prepared by:  
Oak Ridge National Laboratory  
P. O Box 2008  
Oak Ridge, TN 37831-6010

## Authors

Jose Melara, Carmen Lora (Iberdrola Ingenieria y Construccion)  
Alberto Escrivá, Jose Luis Muñoz-Cobo (Universidad Politécnica de  
Valencia)  
Manuel Albendea (Iberdrola Generación)  
Jose March-Leuba (ORNL)

Dr. Tai L. Huang, NRC Project Manager  
NRC Job Code J4430

Office of Nuclear Reactor Regulation



## ABSTRACT

The capabilities of the computer code LAPUR have been upgraded. A new version, LAPUR6 r.0, has been implemented and validated for computing friction and local losses and capabilities for modelling bundles with variable cross areas.

The previous code (LAPUR5) did not consider channels with variable areas and did not model specifically the local pressure drops due to spacers in a bundle. The only way to take into account local pressure losses and gains due to spacers and area changes in LAPUR5 was to input a friction multiplier.

This report documents a twofold validation of the new thermal-hydraulic model implemented in LAPUR6. First, a comparison of each component of the pressure drop for a single-channel model using LAPUR6 and SIMULATE-3 was performed, the result of which showed very good agreement. Slight discrepancies in void fractions between the two codes were found, but the effect on total pressure drop was negligible. In addition, the LAPUR6 void fraction model was tested against FRIGG-2 void fraction data. Void fractions predicted by LAPUR6 showed deviations similar to those of other thermal-hydraulic codes when benchmarked against FRIGG-2 experimental data.

An extensive validation comparing measured against calculated core-wide (CW) decay ratios was also conducted. A set of Average Power Range Monitor (APRM) signals were recorded at steady state during the final coastdowns for Cycles 16b and 17 and start-up for Cycles 17 and 18 in Cofrentes Nuclear Power Plant (NPP). A detailed simulation of these activities was conducted with SIMULATE-3 using cycle-specific CASMO-4 cross sections and the recorded operating data. Selected quasi-steady-state points were analyzed using noise techniques, and decay ratio values were compared to LAPUR6 results. Finally, Cycle 6 Cofrentes out-of-phase (OOP) instability was reproduced using LAPUR6, and the resulting decay ratios showed excellent agreement with the measured data.



# CONTENTS

Page

ABSTRACT.....	iii
CONTENTS.....	v
LIST OF FIGURES .....	vii
LIST OF TABLES .....	ix
ACKNOWLEDGMENTS .....	xi
1. Background.....	1
2. Scope.....	2
3. Pressure Drop Basis.....	3
3.1 Friction Pressure Drop.....	3
3.2 Local Losses.....	3
3.2.1 Spacer or Grid Losses.....	3
3.2.2 Irreversible Losses for Expansion and Contraction .....	4
3.3 Acceleration Pressure Losses.....	4
3.4 Elevation Pressure Drop .....	5
4. Generic Validation: Comparison of Pressure Drop Components for TYPE A and TYPE B .....	6
4.1 Initial Conditions.....	6
4.2 Elevation Pressure Drop .....	8
4.2.1 Elevation Pressure Drop for TYPE A.....	8
4.2.2 Elevation Pressure Drop for TYPE B.....	11
4.2.3 Conclusions of Elevation Results .....	13
4.3 Expansion and Acceleration Data .....	13
4.3.1 Expansion and Acceleration Data for TYPE A.....	13
4.3.2 Expansion and Acceleration Data for TYPE B.....	16
4.3.3 Conclusions of Expansion and Acceleration Results.....	19
4.4 Friction Pressure Drop.....	19
4.4.1 Friction Data for TYPE A .....	20
4.4.2 Friction Data for TYPE B .....	23
4.4.3 Conclusions of Friction Results .....	26
4.5 Local Pressure Drop Data .....	26
4.5.1 Local Pressure Drop Data for TYPE A.....	26
4.5.2 Local Pressure Drop Data for TYPE B.....	29
4.5.3 Conclusions of Local Losses in Pressure Drop Results .....	32
4.6 Void Fraction Data .....	32
4.6.1 Void Fraction Data for TYPE A.....	32
4.6.2 Void Fraction Data for TYPE B.....	35
4.6.3 Conclusions of Void Fraction Comparison.....	38
5. Comparison of LAPUR6 Void Fraction to FRIGG Loop Data .....	39
5.1 Experimental Conditions.....	39
5.2 Comparison of Void Fraction Results to FRIGG-2 Data.....	40
5.3 Conclusions of Void Fraction Results of LAPUR6 Compared to FRIGG-2 Data .....	40
6. Comparison of Cofrentes Nuclear Power Plant Measured Decay Ratios to LAPUR6 Results .....	44
6.1 Cofrentes Nuclear Power Plant.....	44

6.2	Stability Control in Cofrentes Nuclear Power Plant .....	44
6.3	Methodology of Calculating Decay Ratios with LAPUR6.....	45
6.4	Decay Ratio and Frequency Validation: Start-up and End-of-Cycle Coastdowns .....	46
6.4.1	Generation of SIMULATE-3 Core Configuration Data .....	48
6.4.2	Time Series Analysis of Signal for Decay Ratio Estimation .....	48
6.4.3	Results of Decay Ratio and Oscillation Frequency .....	49
6.5	Decay Ratio and Frequency Validation: Cofrentes Cycle 6 Instability.....	55
6.5.1	Event Description .....	55
6.5.2	Setup of the Core Configuration.....	55
6.5.3	LAPUR Input Data.....	55
6.5.4	LAPUR6 Results .....	56
6.5.5	Decay Ratio Values Analysis .....	57
6.5.6	APRMs Signal Analysis.....	57
6.6	LPRM and APRM Decay Ratio and Frequency Validation .....	60
6.6.1	New Data Acquisition System Test during Cycle 18 Sequence Exchanges (June 2010, September 2010) .....	62
6.6.2	Signal Analysis .....	63
6.6.3	Decay Ratio Results .....	64
6.7	LPRM Data.....	66
	CONCLUSIONS .....	68
	REFERENCES .....	70

## LIST OF FIGURES

	Page
Figure 4.1	Axial power profile used in TYPE A analyses ..... 7
Figure 4.2	Axial power profile used in TYPE B analyses ..... 7
Figure 4.3	Elevation CASE 1 TYPE A..... 8
Figure 4.4	Elevation CASE 2 TYPE A..... 9
Figure 4.5	Elevation CASE 3 TYPE A..... 9
Figure 4.6	Elevation CASE 4 TYPE A..... 10
Figure 4.7	Elevation CASE 5 TYPE A..... 10
Figure 4.8	Elevation CASE 1 TYPE B..... 11
Figure 4.9	Elevation CASE 2 TYPE B..... 11
Figure 4.10	Elevation CASE 3 TYPE B..... 12
Figure 4.11	Elevation CASE 4 TYPE B..... 12
Figure 4.12	Elevation CASE 5 TYPE B..... 13
Figure 4.13	Expansion and acceleration pressure drop for CASE 1 TYPE A ..... 14
Figure 4.14	Expansion and acceleration pressure drop for CASE 2 TYPE A ..... 14
Figure 4.15	Expansion and acceleration pressure drop for CASE 3 TYPE A ..... 15
Figure 4.16	Expansion and acceleration pressure drop for CASE 4 TYPE A ..... 15
Figure 4.17	Expansion and acceleration pressure drop for CASE 5 TYPE A ..... 16
Figure 4.18	Expansion and acceleration pressure drop for CASE 1 TYPE B ..... 17
Figure 4.19	Expansion and acceleration pressure drop for CASE 2 TYPE B ..... 17
Figure 4.20	Expansion and acceleration pressure drop for CASE 3 TYPE B ..... 18
Figure 4.21	Expansion and acceleration pressure drop for CASE 4 TYPE B ..... 18
Figure 4.22	Expansion and acceleration pressure drop for CASE 5 TYPE B ..... 19
Figure 4.23	Friction CASE 1 TYPE A ..... 20
Figure 4.24	Friction CASE 2 TYPE A ..... 21
Figure 4.25	Friction CASE 3 TYPE A ..... 21
Figure 4.26	Friction CASE 4 TYPE A ..... 22
Figure 4.27	Friction CASE 5 TYPE A ..... 22
Figure 4.28	Friction CASE 1 TYPE B ..... 23
Figure 4.29	Friction CASE 2 TYPE B ..... 24
Figure 4.30	Friction CASE 3 TYPE B ..... 24
Figure 4.31	Friction CASE 4 TYPE B ..... 25
Figure 4.32	Friction CASE 5 TYPE B ..... 25
Figure 4.33	Local CASE 1 TYPE A ..... 27
Figure 4.34	Local CASE 2 TYPE A ..... 27
Figure 4.35	Local CASE 3 TYPE A ..... 28
Figure 4.36	Local CASE 4 TYPE A ..... 28
Figure 4.37	Local CASE 5 TYPE A ..... 29
Figure 4.38	Local CASE 1 TYPE B ..... 30
Figure 4.39	Local CASE 2 TYPE B ..... 30
Figure 4.40	Local CASE 3 TYPE B ..... 31
Figure 4.41	Local CASE 4 TYPE B ..... 31
Figure 4.42	Local CASE 5 TYPE B ..... 32
Figure 4.43	Void fraction CASE 1 TYPE A..... 33
Figure 4.44	Void fraction CASE 2 TYPE A..... 33
Figure 4.45	Void fraction CASE 3 TYPE A..... 34
Figure 4.46	Void fraction CASE 4 TYPE A..... 34
Figure 4.47	Void fraction CASE 5 TYPE A..... 35
Figure 4.48	Void fraction CASE 1 TYPE B..... 36
Figure 4.49	Void fraction CASE 2 TYPE B..... 36

Figure 4.50	Void fraction CASE 3 TYPE B.....	37
Figure 4.51	Void fraction CASE 4 TYPE B.....	37
Figure 4.52	Void fraction CASE 5 TYPE B.....	38
Figure 5.1	Void fraction of FRIGG-2 Test 313009.....	39
Figure 5.2	Void fraction of FRIGG-2 Test 313014.....	40
Figure 5.3	Void fraction of FRIGG-2 Test 313016.....	41
Figure 5.4	Void fraction of FRIGG-2 Test 313018.....	42
Figure 5.5	Void fraction of FRIGG-2 Test 313020.....	42
Figure 5.6	Void fraction of FRIGG-2 Test 313024.....	43
Figure 6.1	Typical path during EOC coastdown (Cycle 16b) .....	46
Figure 6.2	Typical start-up path (Cycle 18) .....	47
Figure 6.3	Power history used for SIMULATE-3 simulation of Cycle 18 start-up.....	48
Figure 6.4	Average APRM decay ratio and frequency versus LAPUR results (EOC Cycles 16 and C17 coastdowns) .....	49
Figure 6.5	Average APRM decay ratio and frequency versus LAPUR results (Cycles 17 and 18 start-ups and coastdowns) .....	50
Figure 6.6	Decay ratio based on monitor SMART versus LAPUR .....	51
Figure 6.7	Natural frequency based on monitor SMART versus LAPUR .....	52
Figure 6.8	Comparison of Welch's method periodogram and LAPUR- calculated frequency.....	53
Figure 6.9	Welch's method periodogram at 0.1 Hz resolution.....	54
Figure 6.10	Welch's method periodogram at 0.05 Hz resolution (peak close to LAPUR frequency).....	54
Figure 6.11	APRM A 1991/01/29 Cofrentes instability event .....	58
Figure 6.12	PSD based on Welch's method periodogram (290191 Cofrentes instability) .....	58
Figure 6.13	Bode diagram of applied Butterworth filters to split up fundamental and first mode.....	59
Figure 6.14	Effect of type 1 and type 2 filtering in APRM A signal .....	60
Figure 6.15	June 2010 control sequence exchange roadmap .....	62
Figure 6.16	September 2010 control sequence exchange roadmap .....	63
Figure 6.17	Histogram of APRM-C and LPRM 22-23B with and without optoisolator .....	64
Figure 6.18	Decay ratio sample for June and September 2010 maneuvers .....	65
Figure 6.19	June and September 2010 maneuver—decay ratio comparison.....	65
Figure 6.20	June and September 2010 maneuver—frequency comparison .....	66
Figure 6.21	LPRM and APRM-C decay ratio from autocorrelation versus LAPUR decay ratio comparison—September and June 2010 sequence exchange .....	67
Figure 6.22	LPRM and APRM-C frequency autocorrelation-based versus LAPUR decay ratio comparison—September and June 2010 sequence exchange .....	67
Figure 7.1	Decay ratio autocorrelation based on LAPUR calculation .....	69
Figure 7.2	Frequency autocorrelation based on LAPUR calculation .....	69

## LIST OF TABLES

	Page
Table 4.1 TYPE A boundary conditions.....	6
Table 4.2 TYPE B boundary conditions.....	6
Table 5.1 FRIGG-2 test conditions.....	40
Table 6.1 Number of channels assigned to LAPUR for channel decay ratio calculations.....	56
Table 6.2 Number of channels assigned to LAPUR for channel decay ratio calculations.....	56
Table 6.3 Reactor conditions at the beginning of the event .....	56
Table 6.4 Simulate LAPUR pressure drops comparison.....	56
Table 6.5 Comparison of SIMULATE and LAPUR flow rate channels .....	56
Table 6.6 State point 290191 decay ratio values.....	57
Table 6.7 Filters applied to APRM signal .....	59
Table 6.8 Cofrentes 290191 instability (signal analysis results).....	61
Table 6.9 RTP2316-M input channels .....	61
Table 7.1 Cofrentes instability results.....	68



## **ACKNOWLEDGMENTS**

This research has been performed under the sponsorship of Iberdrola Generation inside the framework of the R& D project DROP (Decay Ratio On-line Predictor), which has the primary goal of developing a predictive stability tool to couple with the Core Monitoring System of a BWR.

The authors are particularly grateful to:

Marcos Rodriguez

Diego Rodriguez

Carlos Mira

Matias Urrea

Carlos Gavilan

From Cofrentes NPP, for the continuous interest and support of the Project and for the installation of needed hardware for data acquisition.



## **1. Background**

LAPUR is a computer code developed at Oak Ridge National Laboratory (ORNL) for the calculation of boiling water reactor (BWR) core stability parameters (Otaduy and March-Leuba, 1990). It uses a multinodal description of the neutron dynamics, together with a distributed parameter model of the core thermal hydrodynamics to produce a space-dependent representation of the dynamics of a BWR in the frequency domain for small perturbations around a steady-state condition. The LAPUR program consists of two autonomous modules, LAPURX and LAPURW, which are linked by means of an intermediate storage routine. The first module, LAPURX, solves the governing equations for the coolant and the fuel steady state. Maps of the core steady state are generated and stored in data files for subsequent utilization by LAPURW. The second module, LAPURW, solves the dynamic equations for the coolant, fuel, and neutron field in the frequency domain. A set of open-loop transfer functions are generated, and the stability index (decay ratio) is estimated from the closed-loop reactivity to power transfer function.

The previous LAPUR5 release 1 code (Escrivá and March-Leuba, 2000) did not consider channels with variable areas and did not distinguish specifically local pressure drop due to spacers in a bundle. The only way to take into account local pressure losses and gains due to spacers and area changes was by means of a friction multiplier, which was input. Improvements incorporated in LAPUR6 removed this deficiency.

## 2. Scope

This report documents the validation of the new thermal-hydraulic model implemented in LAPUR6 r.0 (Escrivá et al., 2008). The LAPUR6 upgrade incorporated new correlations for computing friction and local losses and capabilities for modelling bundles with variable cross areas. Additional information regarding this implementation is available in *Improvements Made in LAPUR5 to Obtain LAPUR6.0.r.0* (Universidad Politécnica de Valencia, 2006). Validation of these correlations is provided in this document. The friction and local models selected are generic and do not use any proprietary information of fuel vendors.

A comparison of pressure drop components was performed for bundles with constant (TYPE A) and variable (TYPE B) areas. LAPUR6 results were compared to results of the well-known SIMULATE-3 code (Studsvik, 2007), a reactor analysis code being used by IBERDROLA and other utilities to perform in-core fuel management studies, core design, and calculation of safety parameters. Single-channel models for each bundle design were used. Flow and power conditions for the bundles were selected to be representatives of hot channels covering real conditions on a BWR/6 power flow map. A generic single-phase friction factor was selected in order to validate exclusively the implementation of changes made to LAPUR6.

Comparisons of LAPUR-calculated void fractions to FRIGG loop data for both LAPUR5 and LAPUR6 were performed. Indirectly, this exercise showed that the LAPUR6 modifications did not affect relevant variables in LAPUR calculation process. The results of these comparisons showed that flow qualities and slip ratio are not affected by the changes in pressure drop calculation models in LAPUR6.

An extensive validation comparing measured against calculated CW decay ratios was also conducted. A set of average power range monitor (APRM) signals was recorded in steady state for the final coastdowns for Cycles 16b and 17 and start-up for Cycles 17 and 18 in Cofrentes NPP. A detailed simulation of the power, flow, and control rod sequences was carried out with SIMULATE-3 using cycle-specific CASMO-4 cross sections and the recorded operating data. Selected quasi-steady-state points were analyzed using noise techniques, and decay ratio values were compared with LAPUR6 results. Finally, Cycle 6 Cofrentes OOP instability was reproduced using LAPUR6, and the resulting LAPUR6 decay ratios showed excellent agreement with the measured data.

### 3. Pressure Drop Basis

The total pressure drop for each channel is calculated as the sum of the individual pressure drop components: friction, local (form) loss, acceleration (momentum change), and elevation. Acceleration and elevation can be evaluated once the flow quality and void fraction have been determined. The friction and local loss terms require input coefficients and models to account for two-phase effects.

#### 3.1 Friction Pressure Drop

The frictional pressure losses are correlated in terms of single-phase velocity head,

$$\Delta p_{fric} = f \frac{\Delta z}{D_h} \frac{G^2}{2 \cdot \rho_l} \phi_{2-phase\ friction}^2$$

where

$f$  = the single-phase friction factor,  
 $G$  = mass flux,  
 $\rho_l$  = liquid density, and  
 $\phi_{2-phase\ friction}^2$  = the multiplier to account for the two-phase effect. The relationship selected is the Chisholm model (FIBWR, 1981; Chisholm, 1973), which depends on flow quality, mass flux, and viscosity.

#### 3.2 Local Losses

The local pressure drop is defined as the irreversible pressure loss associated with an area change, such as an orifice, tie plate, or grid spacer. The general local pressure drop equation is similar to that for friction pressure drop.

##### 3.2.1 Spacer or Grid Losses

Considering  $K$  to be the single-phase irreversible loss for the grid or spacer, the pressure drop equation is

$$\sum_{l=1}^L \Phi_{local\ two-phase} \cdot K \cdot \frac{G^2}{2 \cdot \rho_l}$$

and

$$\Phi_{local\ two-phase} = \left[ 1 + \left( \frac{\rho_l}{\rho_g} - 1 \right) \cdot X_f \right] (\text{HEM multiplier})$$

where:

$X_f$  is the flow quality and  
 $\rho_l, \rho_g$  liquid and vapor densities.

### 3.2.2 Irreversible Losses for Expansion and Contraction

Irreversible losses for expansion have been calculated by means of the following equations:

$$DPEXP = \sum_{l=1}^L \left[ 1 + \left( \frac{\rho_l}{\rho_g} - 1 \right) \cdot X_f \right] \cdot K_{exp} \cdot \frac{G1^2}{2 \cdot \rho_l} ,$$

where

$G1$  = the upstream mass flux and  
 $K_{exp}$  = single phase irreversible loss.  
 $\rho_l, \rho_g$  = liquid and vapor densities.

Analogously,

$$DPCON = \sum_{l=1}^L \left[ 1 + \left( \frac{\rho_l}{\rho_g} - 1 \right) \cdot X_f \right] \cdot K_{con} \cdot \frac{G1^2}{2 \cdot \rho_l} ,$$

where

$K_{con}$  = single phase irreversible loss  
 $G1$  = mass flux  
 $\rho_l, \rho_g$  = liquid and vapor densities.

### 3.3 Acceleration Pressure Losses

The acceleration pressure drop includes the reversible pressure change experienced from contractions or expansions, or resulting from the acceleration of the fluid during the boiling process (density change). When two phases are present,

$$\Delta P_{acc} = \frac{2}{A_1 + A_2} \left[ \frac{1}{\rho M_2} G_2^2 - \frac{1}{\rho M_1} G_1^2 \right] ,$$

where

$$\frac{1}{\rho M} = \frac{\langle x \rangle^2}{\rho_g \langle \alpha \rangle} + \frac{(1 - \langle x \rangle)^2}{\rho l (1 - \langle \alpha \rangle)} ,$$

where

$\langle \alpha \rangle$  = void fraction  
 $\langle x \rangle$  = flow quality  
 $G_{1,2}$  = mass flux upstream and down stream, respectively.  
 $A_{1,2}$  = area upstream and downstream, respectively

### 3.4 Elevation Pressure Drop

The elevation (gravitational) pressure drop is evaluated as follows:

$$\Delta P_{elev} = \bar{\rho} \Delta z \quad ,$$

where

$$\bar{\rho} = \rho_l \bullet (1 - \langle \alpha \rangle) + \rho_g \bullet \langle \alpha \rangle \quad .$$

Note the dependence of acceleration and elevation pressure drop on void fraction.

#### 4. Generic Validation: Comparison of Pressure Drop Components for TYPE A and TYPE B

LAPUR5 release 1 code does not consider channels with variable areas and does not distinguish specifically local pressure drop due to spacers in a bundle. The only way to take into account local pressure losses and gains due to spacers and area changes is by means of a friction multiplier, which is input. This deficiency requires adjustment by input friction multipliers in order to accurately account for local and variable-area pressure effects.

In this section, validation of computing friction, local losses, and variable cross area results obtained using LAPUR6 is shown. The selection of basic models for implementation in LAPUR6 is discussed in *FIBWR: A Steady-state Core Flow Distribution Code for Boiling Water Reactors Computer Code User's Manual* (FIBWR, 1981), *RETRAN-3D—A Program for Transient and Thermal-Hydraulic Analysis for Complex Fluid Systems* (RETRAN-3D, 2006), and by Chisholm (1973). This validation was conducted by benchmarking LAPUR6 results against SIMULATE-3 single-channel results. For this comparison, the default single friction factor of SIMULATE-3 was used in both codes.

##### 4.1 Initial Conditions

Comparison of pressure drop components will be performed for bundles with constant (TYPE A) and variable area (TYPE B). Tables 4.1 and 4.2 show the conditions used.

**Table 4.1 TYPE A boundary conditions**

State point	Pressure (psi)	Inlet enthalpy (Btu/lb)	Active power (MW)	Active flow (lb/h)
1	1058.10	522.21	6.624	84366
2	1064.50	529.06	6.629	116351
3	973.5	507.62	1.908	38413
4	1005.78	500.71	4.319	42699
5	978.16	524.76	1.909	78731

**Table 4.2 TYPE B boundary conditions**

State point	Pressure (psi)	Inlet enthalpy (Btu/lb)	Active power (MW)	Active flow (lb/h)
1	1090.75	525.63	6.643	87039
2	998.40	513.27	3.189	58830
3	1031.36	508.85	4.779	56270
4	1038.24	523.46	4.784	89859
5	1097.94	531.51	6.647	110299

The power axial profiles used in verification analyses are shown in Figs. 4.1 and 4.2.

Note that the axial power profile used when performing TYPE A pressure drop comparisons is bottom peaked. However, the profile used in TYPE B is similar to a skewed cosine, with the peak at medium core height. This profile leads to elevating the boundary between bulk and subcooled boiling.

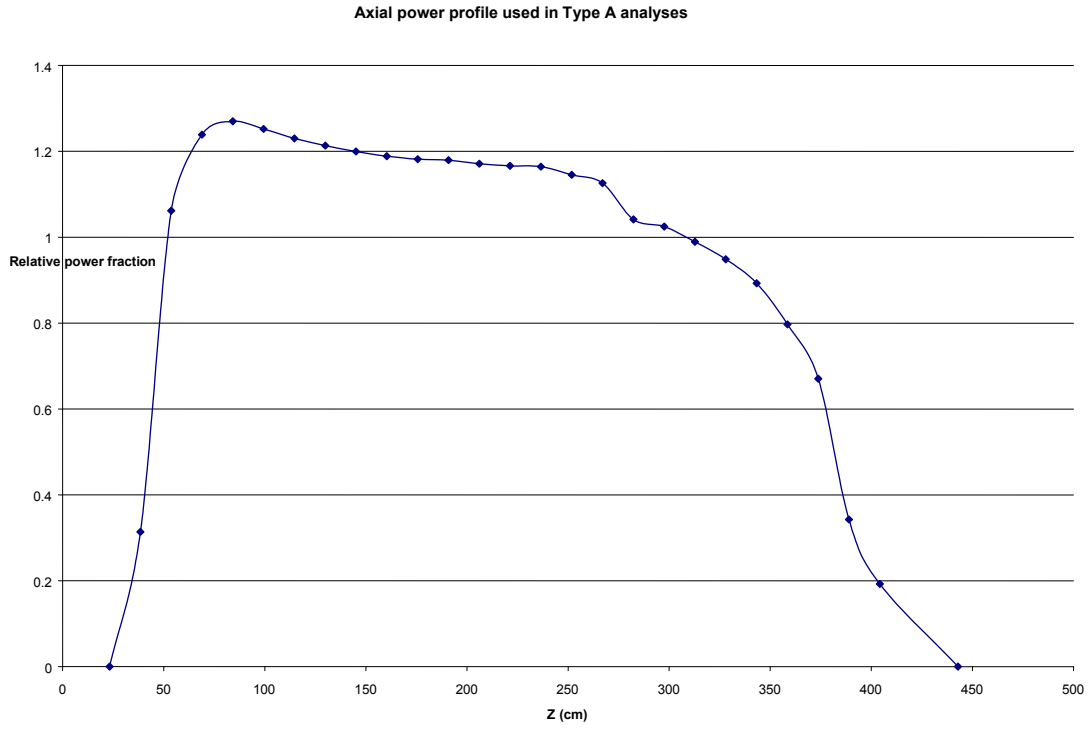


**Figure 4.1 Axial power profile used in TYPE A analyses**

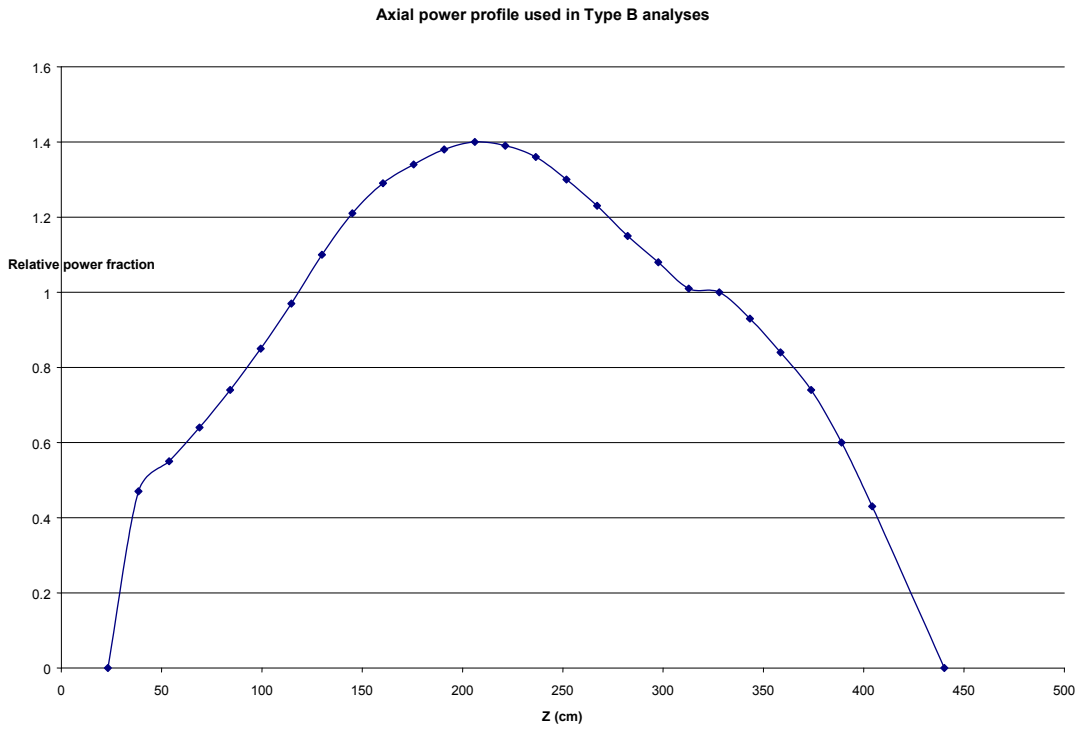


**Figure 4.2 Axial power profile used in TYPE B analyses**

## 4.2 Elevation Pressure Drop

In this section, a comparison of elevation pressure drop in LAPURX (LX) and SIMULATE-3 (S3) is provided.

### 4.2.1 Elevation Pressure Drop for TYPE A

Comparisons of elevation pressure drop for TYPE A are shown in Figs. 4.3 to 4.7.

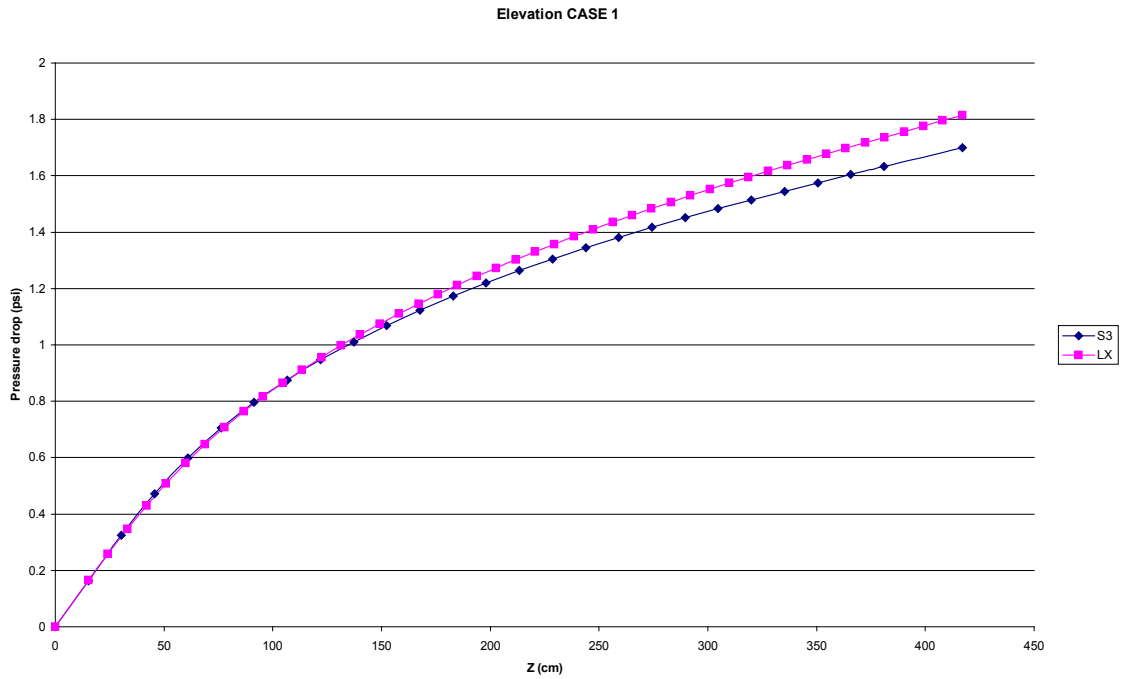
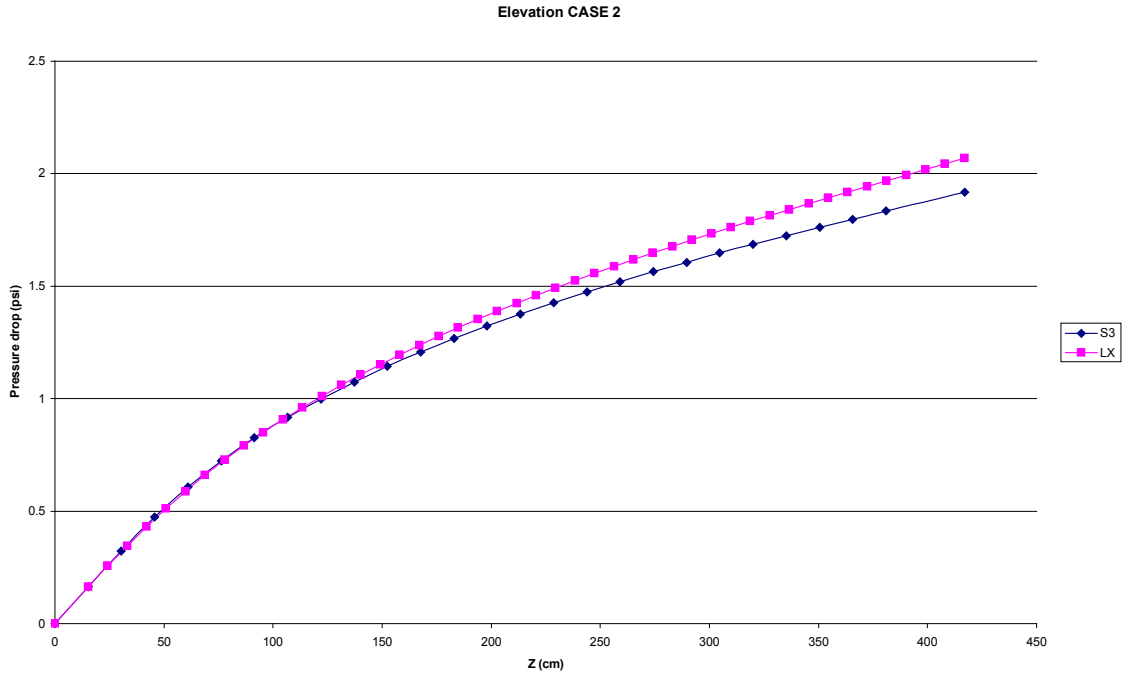
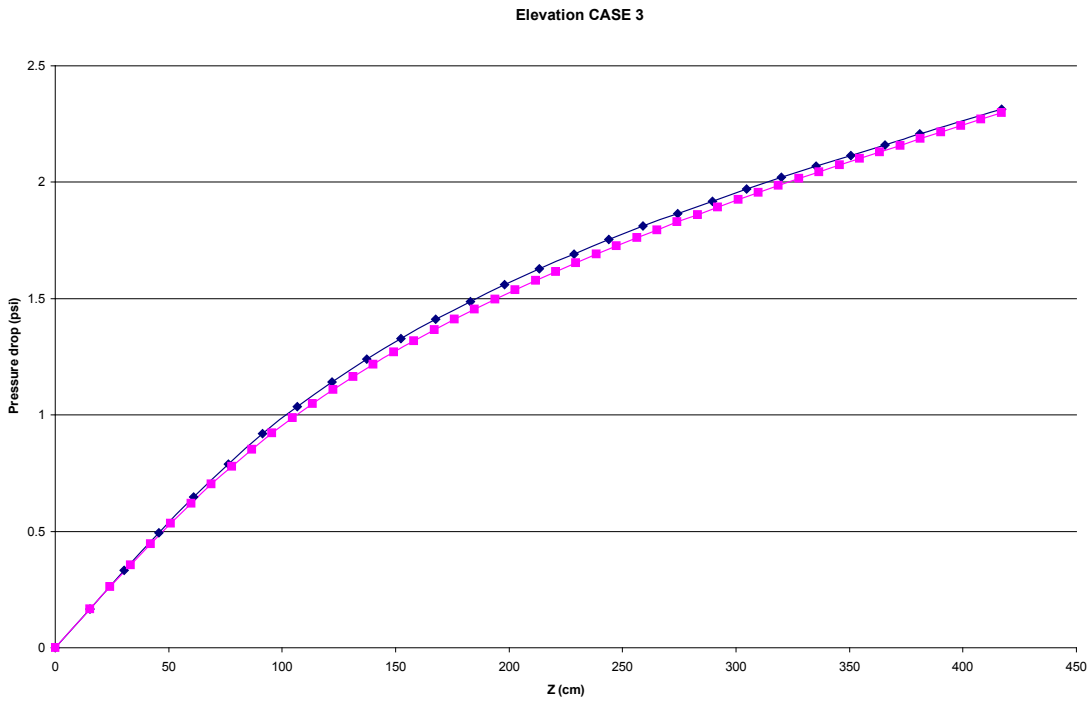


Figure 4.3 Elevation CASE 1 TYPE A



**Figure 4.4 Elevation CASE 2 TYPE A**



**Figure 4.5 Elevation CASE 3 TYPE A**

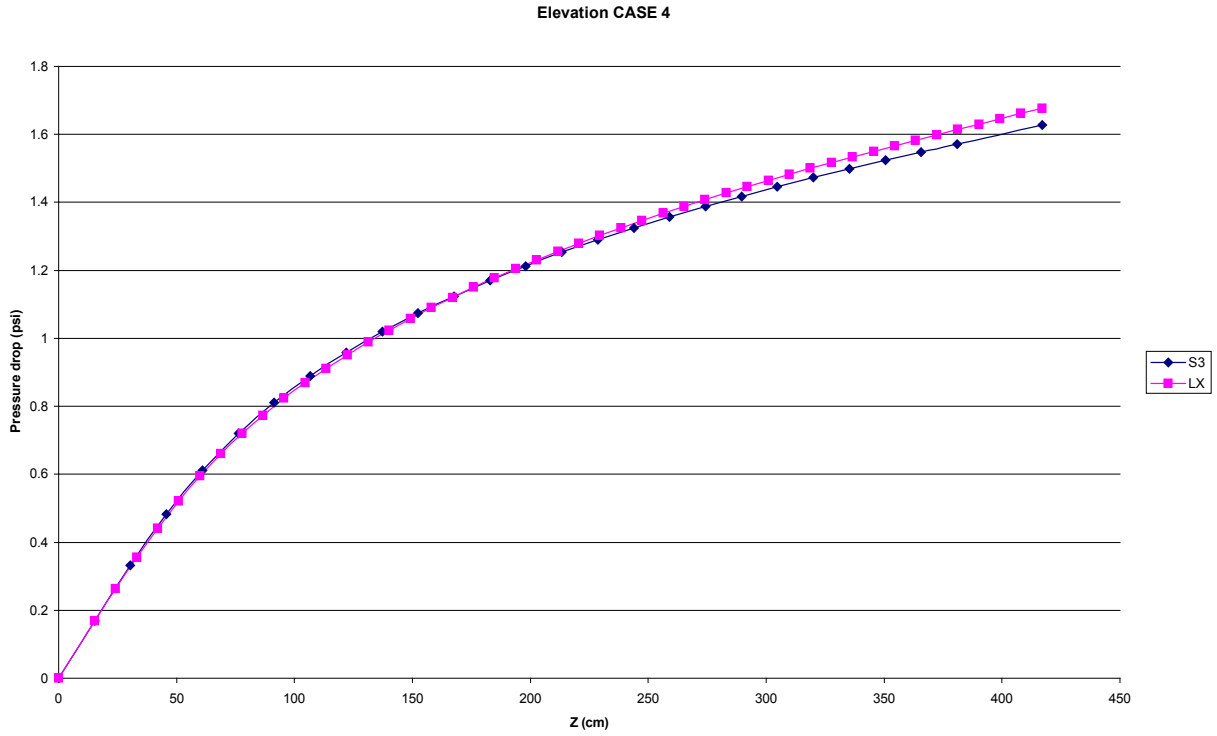


**Figure 4.6 Elevation CASE 4 TYPE A**

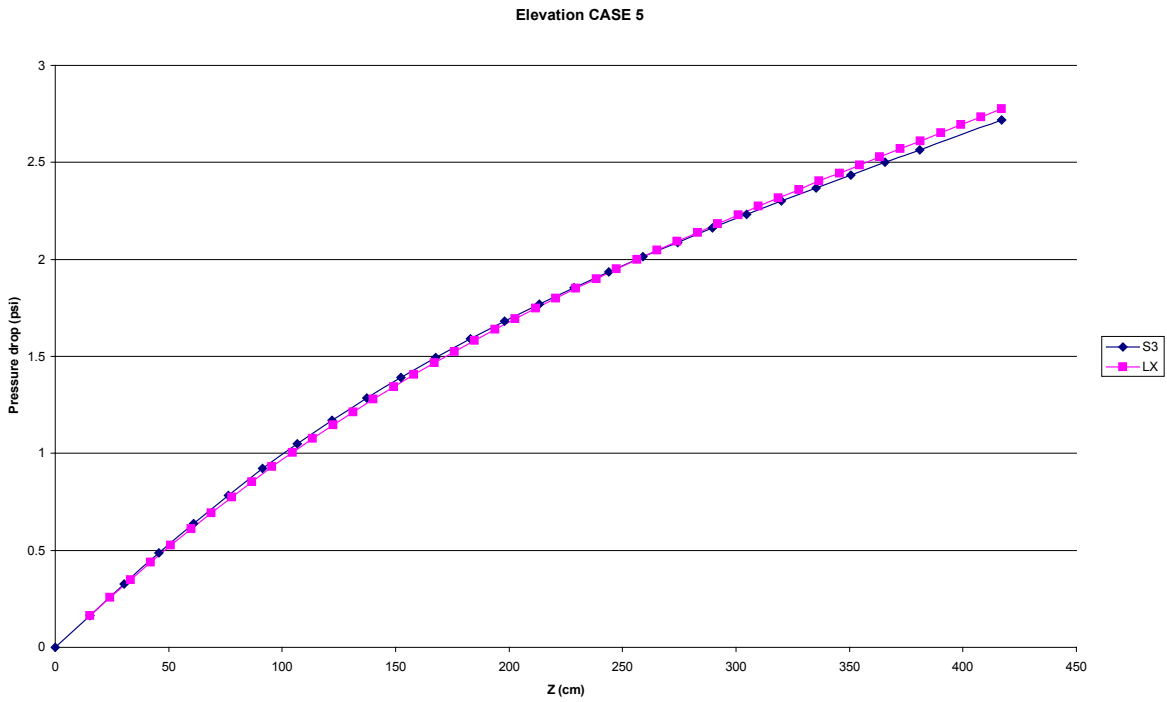


**Figure 4.7 Elevation CASE 5 TYPE A**

## 4.2.2 Elevation Pressure Drop for TYPE B

Comparisons of elevation pressure drop for TYPE B are shown in Figs. 4.8 to 4.12.

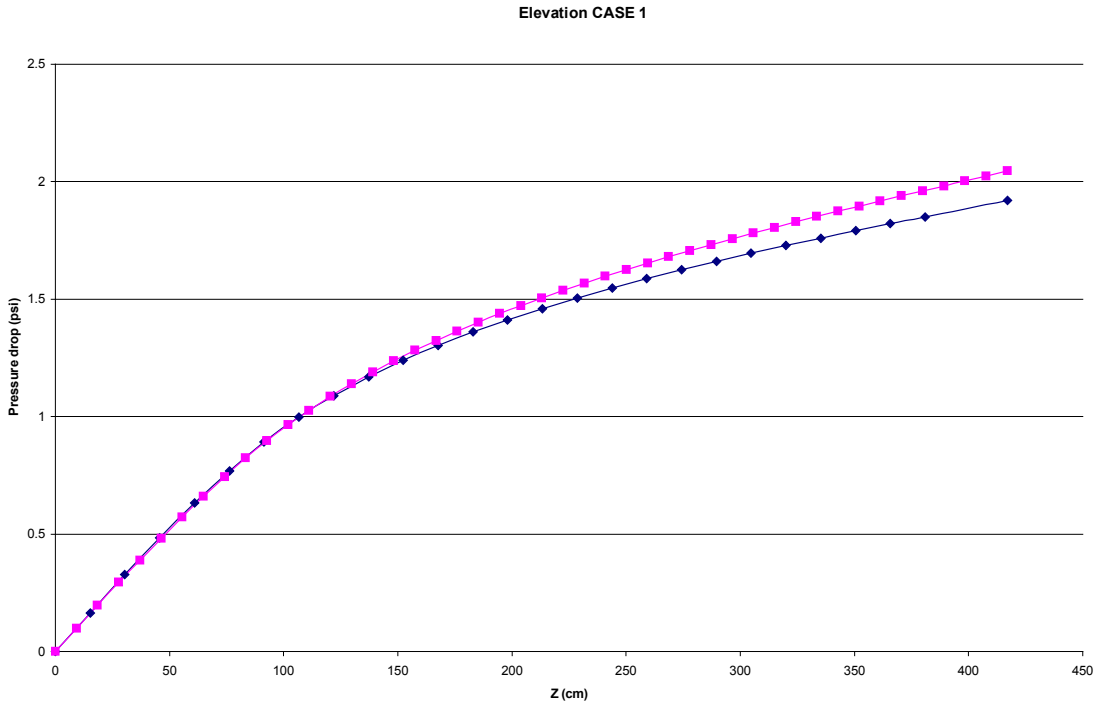


Figure 4.8 Elevation CASE 1 TYPE B

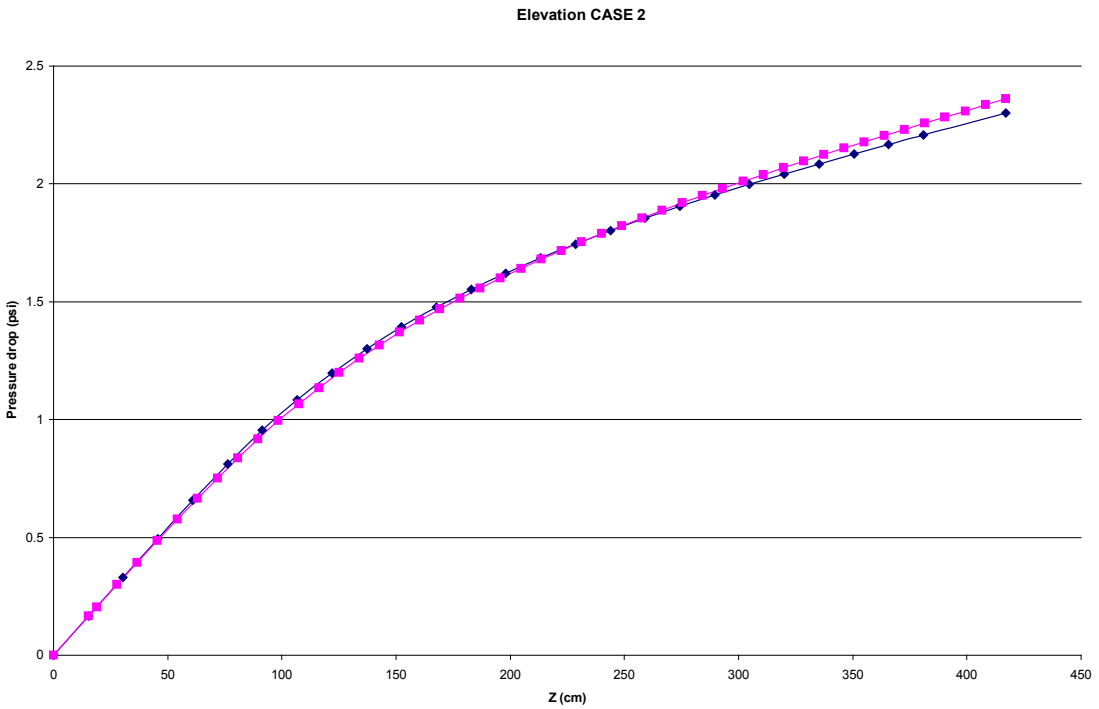
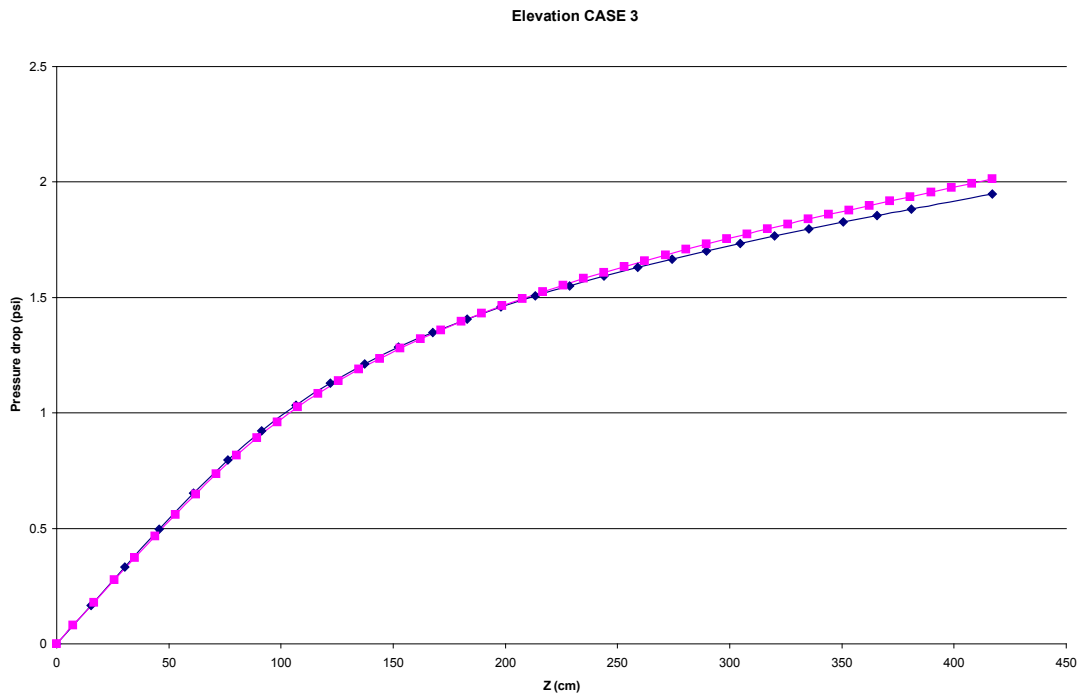
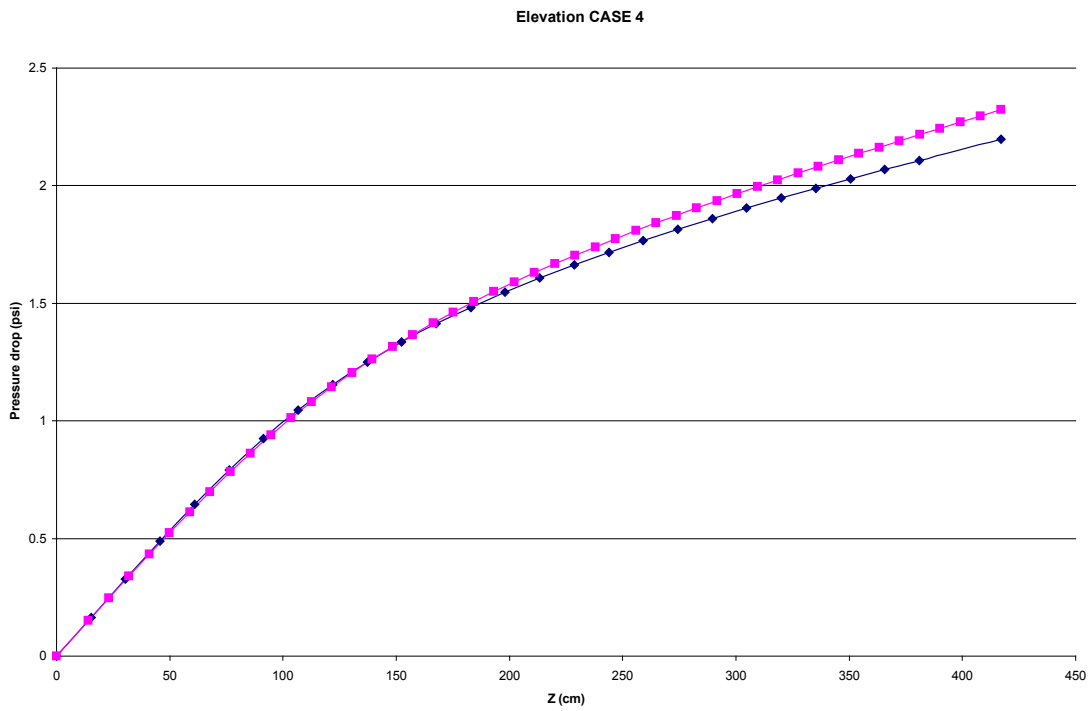


Figure 4.9 Elevation CASE 2 TYPE B



**Figure 4.10 Elevation CASE 3 TYPE B**



**Figure 4.11 Elevation CASE 4 TYPE B**

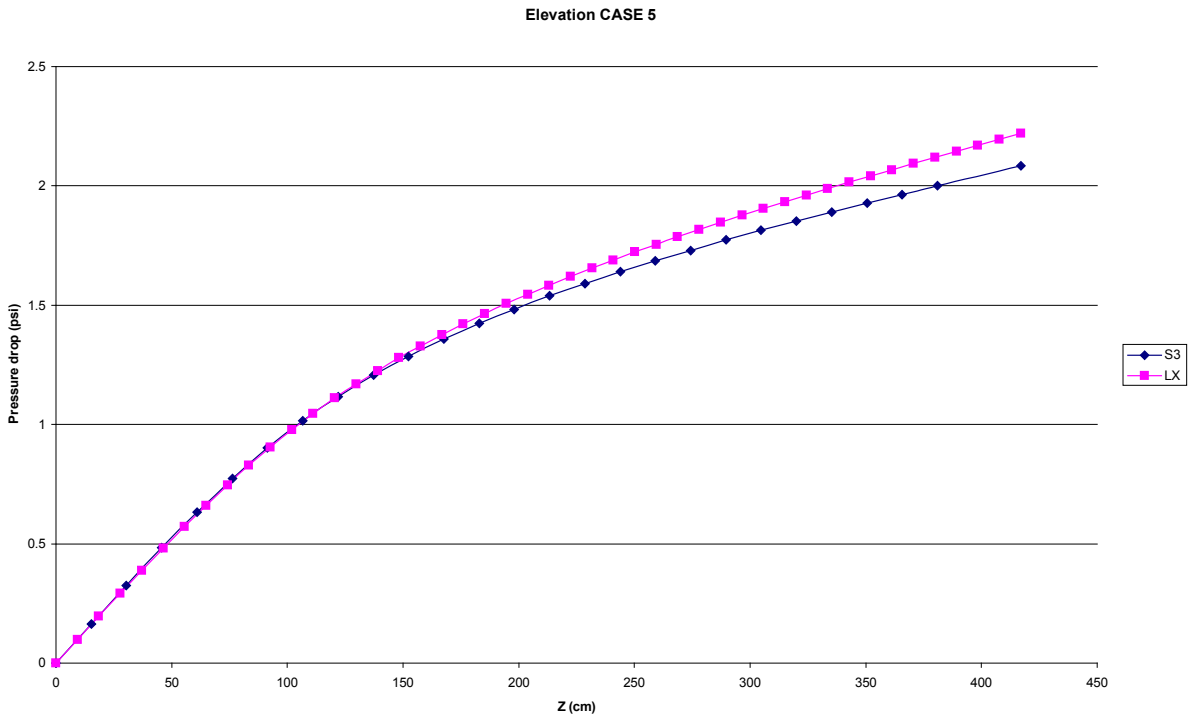


**Figure 4.12 Elevation CASE 5 TYPE B**

### 4.2.3 Conclusions of Elevation Results

LAPURX results are in good agreement with SIMULATE-3 results. However, LAPURX systematically gives an elevation pressure drop that is slightly higher than that of SIMULATE-3. This difference is the result of void fraction axial distribution discrepancies between both codes, since slip velocity correlation, subcooled flow quality model, and therefore void fraction-quality relationships are different.

The impact of total pressure drop is evident from the magnitude of its contribution. Differences are negligible.

## 4.3 Expansion and Acceleration Data

In this section, a comparison of expansion and acceleration pressure drop in LAPUR and SIMULATE-3 is provided.

### 4.3.1 Expansion and Acceleration Data for TYPE A

Comparisons of expansion and acceleration pressure drop for TYPE A are shown in Figs. 4.13 to 4.17.

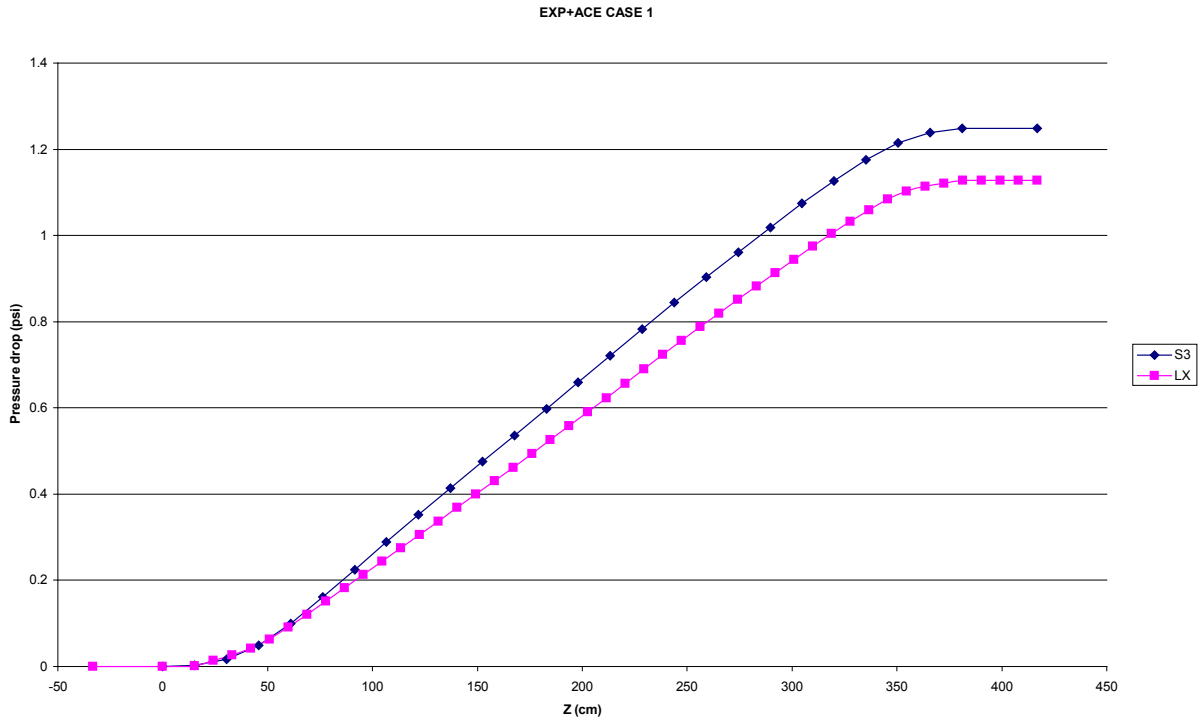


Figure 4.13 Expansion and acceleration pressure drop for CASE 1 TYPE A

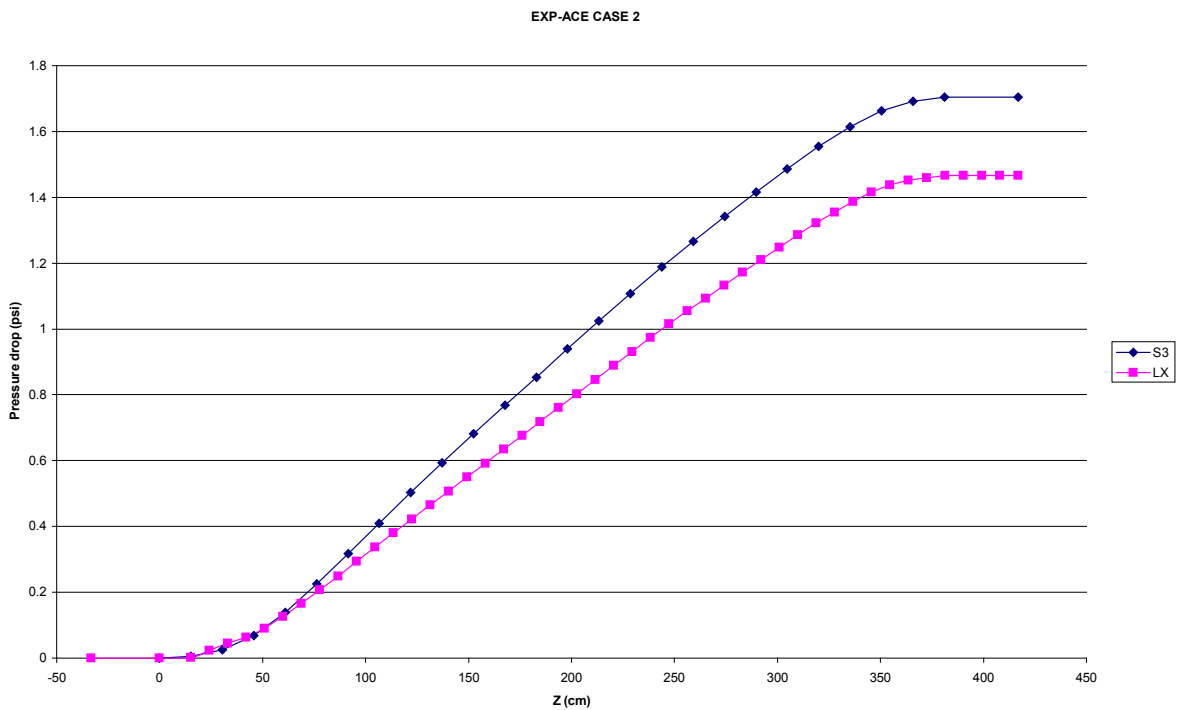
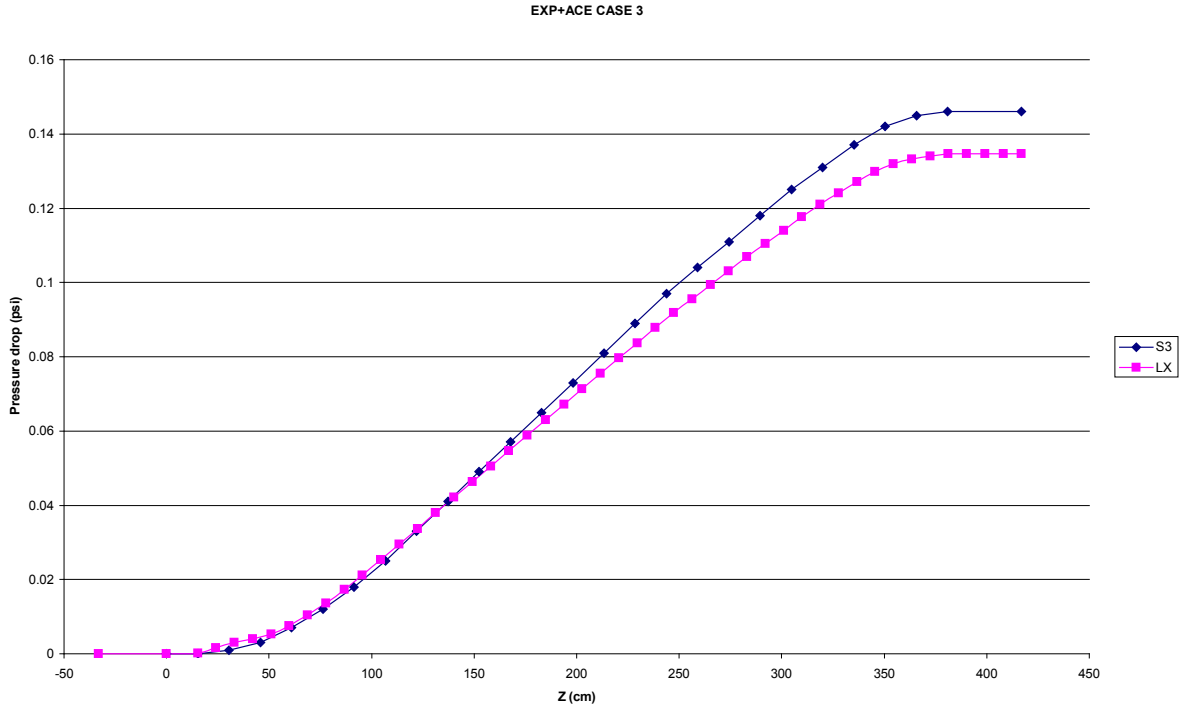
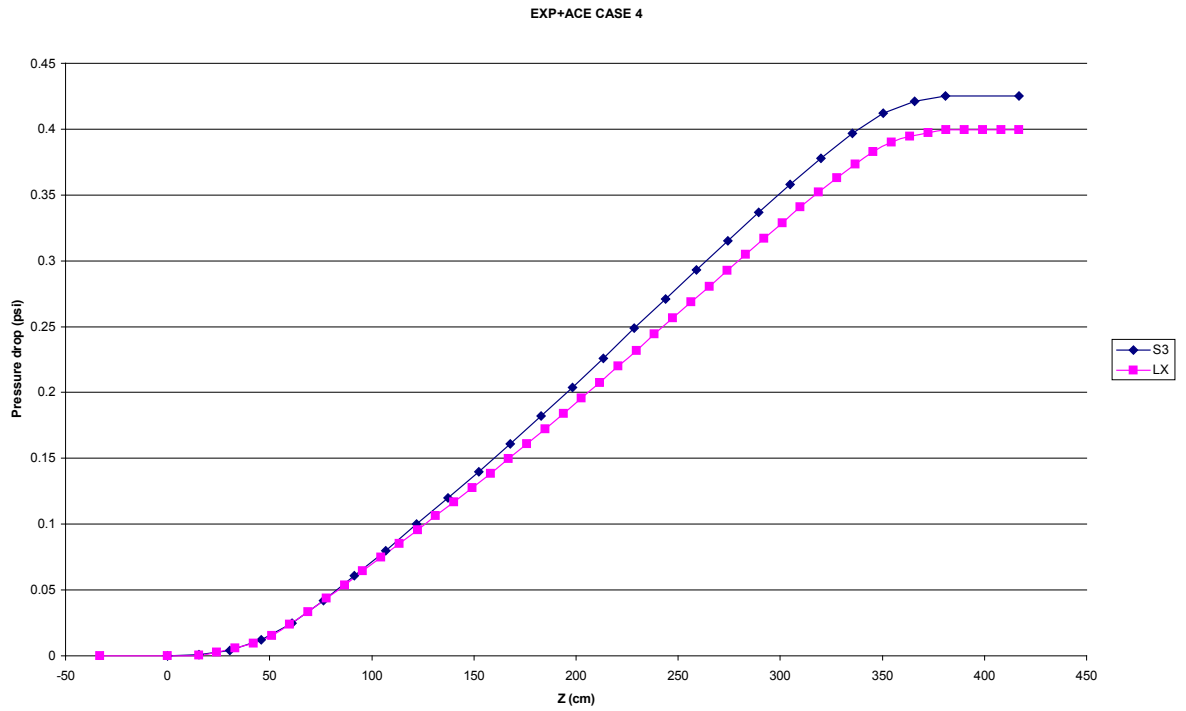


Figure 4.14 Expansion and acceleration pressure drop for CASE 2 TYPE A



**Figure 4.15 Expansion and acceleration pressure drop for CASE 3 TYPE A**



**Figure 4.16 Expansion and acceleration pressure drop for CASE 4 TYPE A**

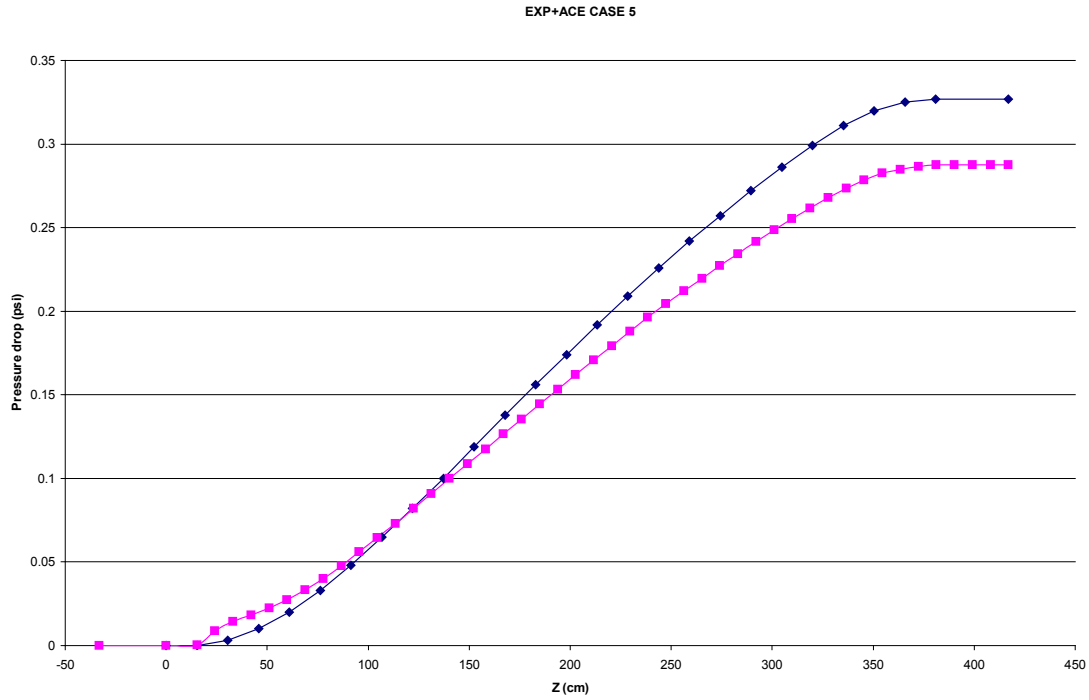


**Figure 4.17 Expansion and acceleration pressure drop for CASE 5 TYPE A**

### 4.3.2 Expansion and Acceleration Data for TYPE B

Comparisons of expansion and acceleration pressure drop for TYPE B are shown in Figs. 4.18 to 4.22.

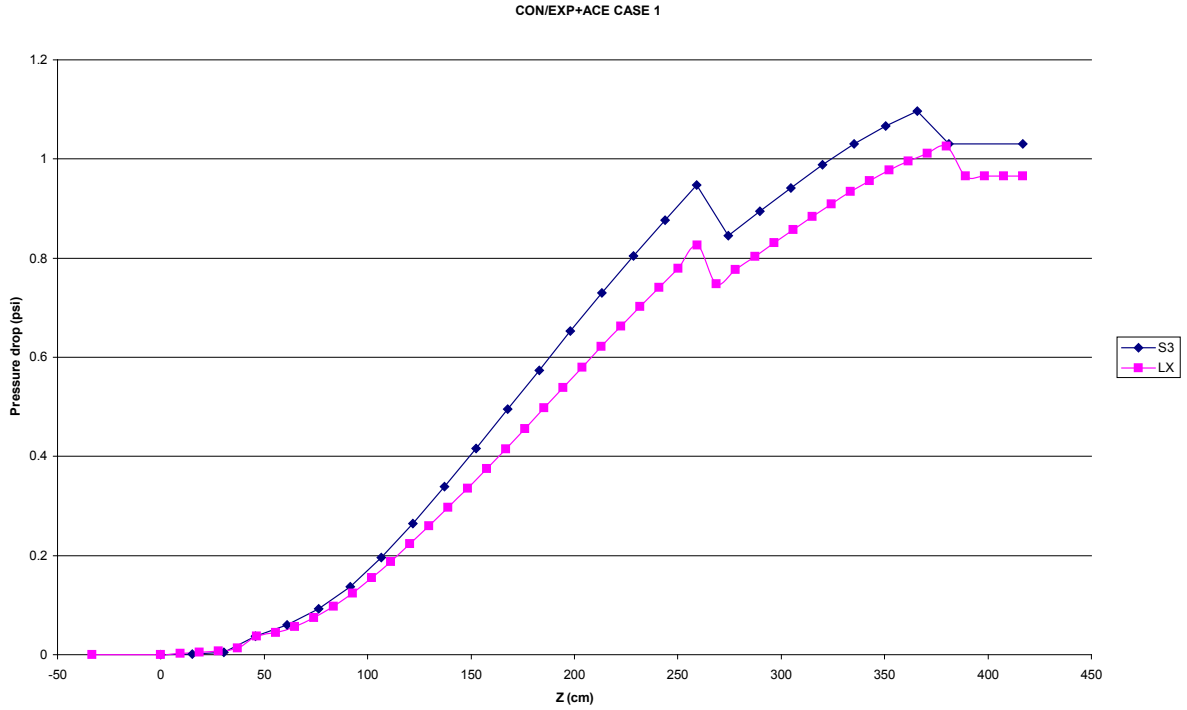


**Figure 4.18 Expansion and acceleration pressure drop for CASE 1 TYPE B**

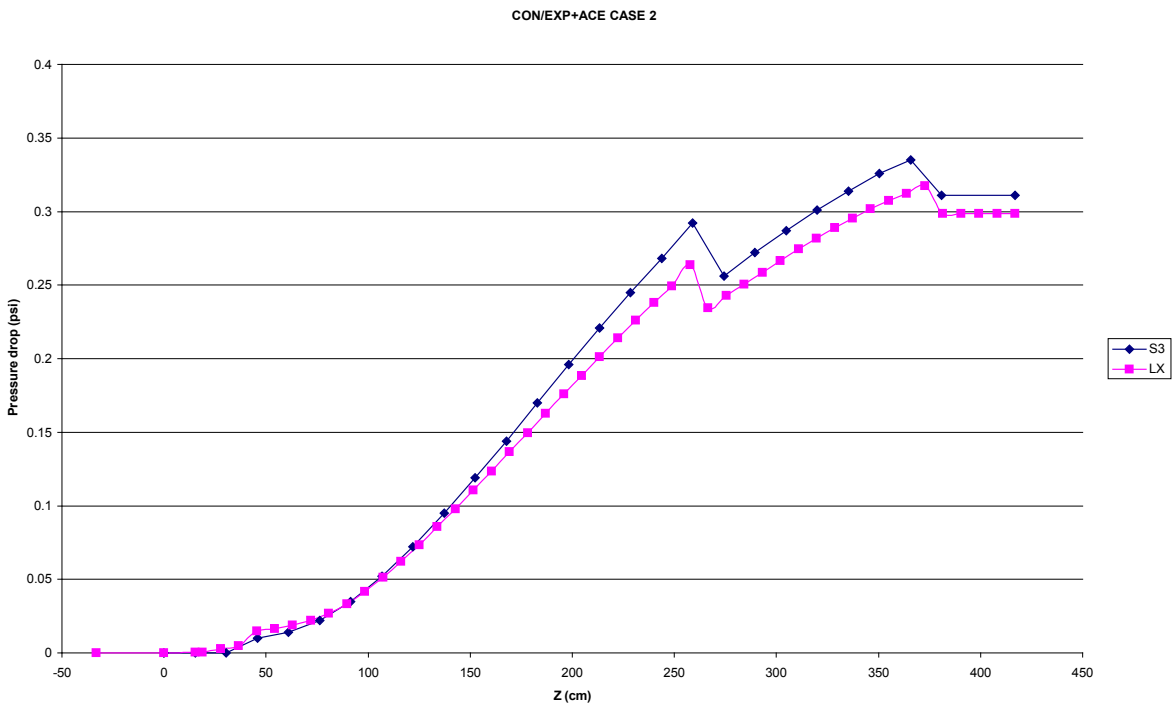


**Figure 4.19 Expansion and acceleration pressure drop for CASE 2 TYPE B**

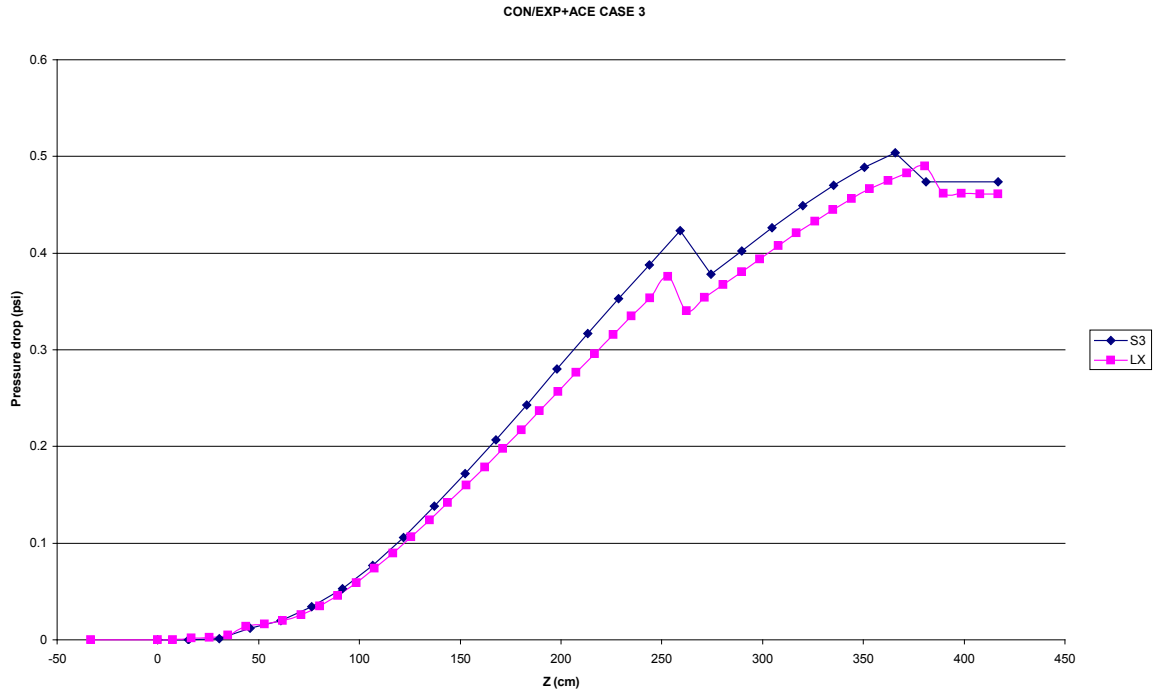


**Figure 4.20 Expansion and acceleration pressure drop for CASE 3 TYPE B**

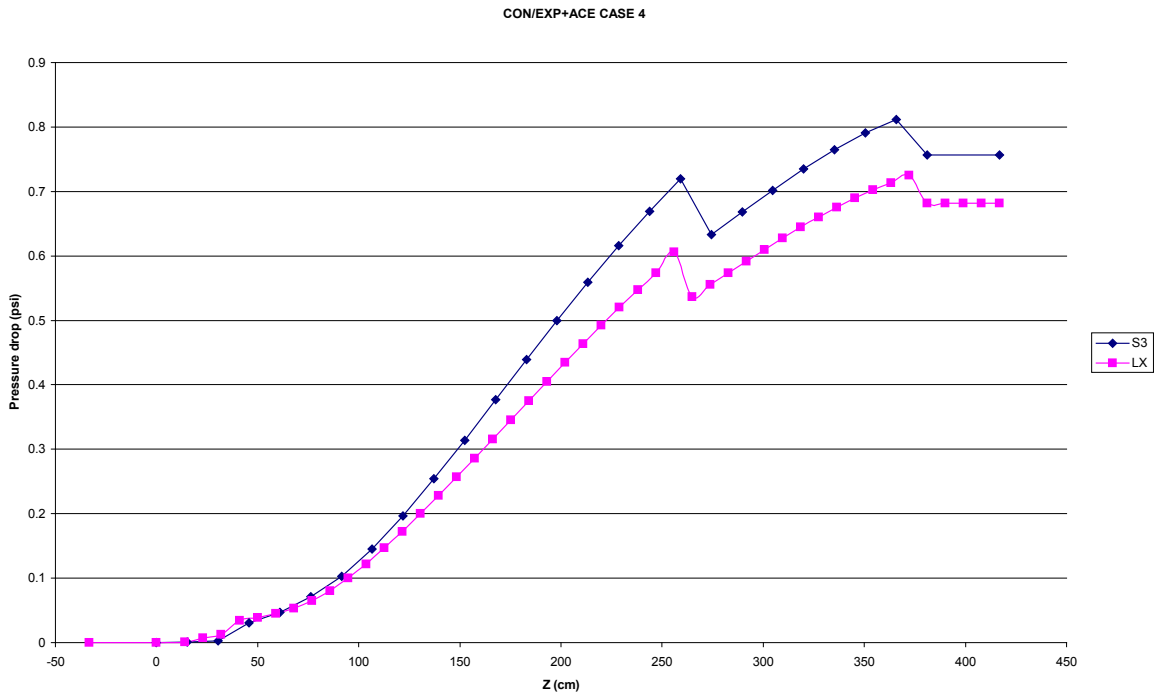


**Figure 4.21 Expansion and acceleration pressure drop for CASE 4 TYPE B**

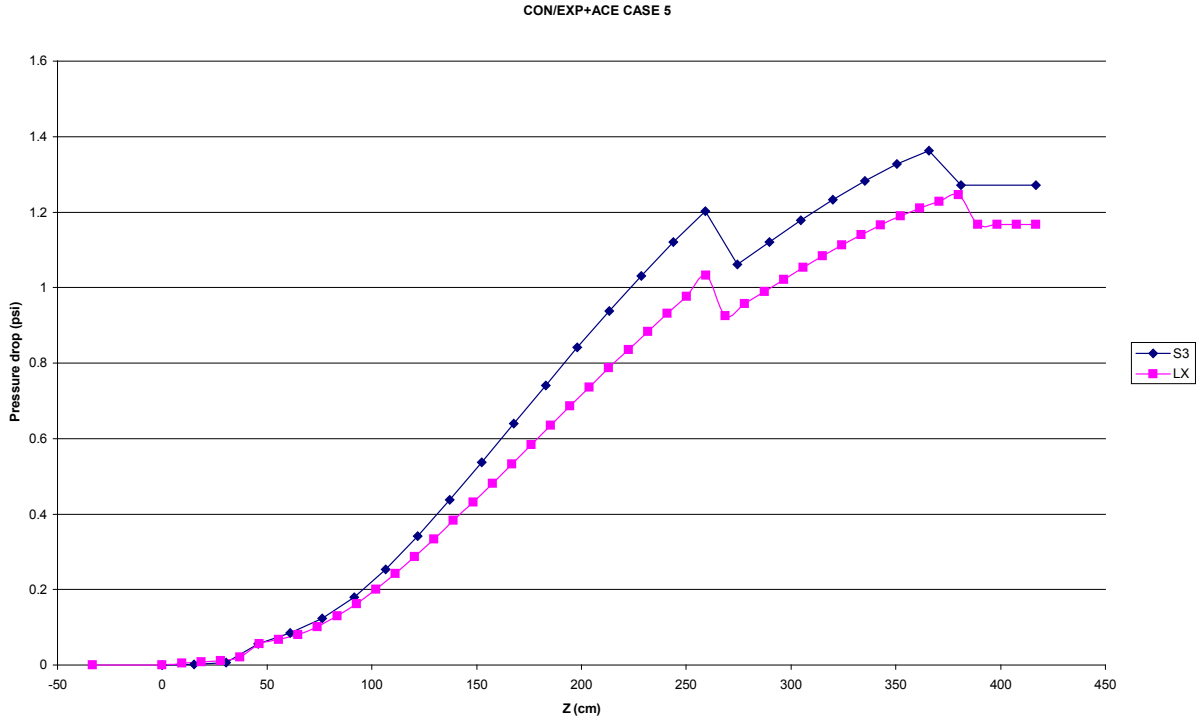


**Figure 4.22 Expansion and acceleration pressure drop for CASE 5 TYPE B**

### 4.3.3 Conclusions of Expansion and Acceleration Results

Again, the observed differences are related to the void fractions values obtained with the models of SIMULATE-3 and LAPUR. As can be seen in the figures, changes in flow area along the channel in TYPE B fuel design lead to abrupt pressure gains. The expansions are located in channel elevations with considerable void fractions (partial length rods and changes due to water rod diameter). For this reason, the comparison reveals higher values for SIMULATE-3 for this pressure drop component. A contraction occurs due to a change in water rod diameter close to lower tie plate. However, due to the low void fractions at this part of the channel, the effect in pressure is negligible and the agreement between codes is good. On the other hand, TYPE A is a fuel design with a constant flow area and no contraction and expansion exist along the channel length. Pressure drop due to acceleration shows the same discrepancies as in TYPE B due to void fraction differences in both codes.

The impact in the total pressure drop is evident from the magnitude of its contribution. Differences are negligible.

### 4.4 Friction Pressure Drop

In this section, a comparison of one of the dominant contributors to the pressure drop between LAPUR and SIMULATE-3 is provided.

### 4.4.1 Friction Data for TYPE A

Comparisons of the friction component of pressure drop for TYPE A are shown in Figs. 4.23 to 4.27.

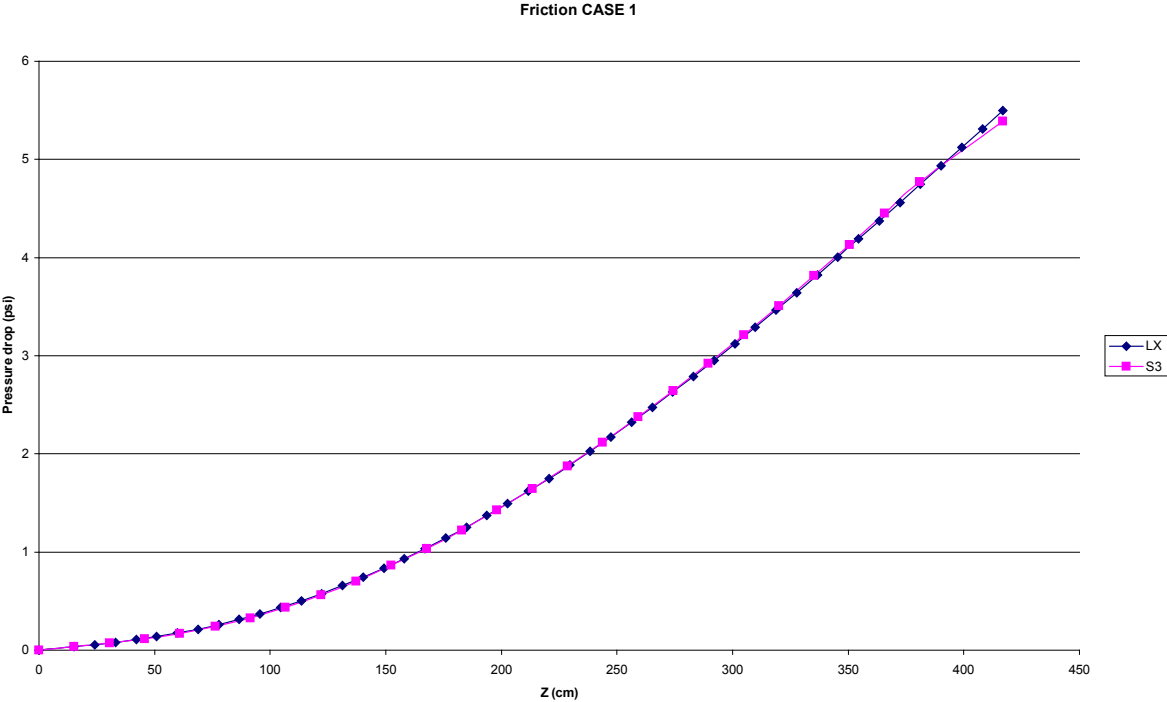
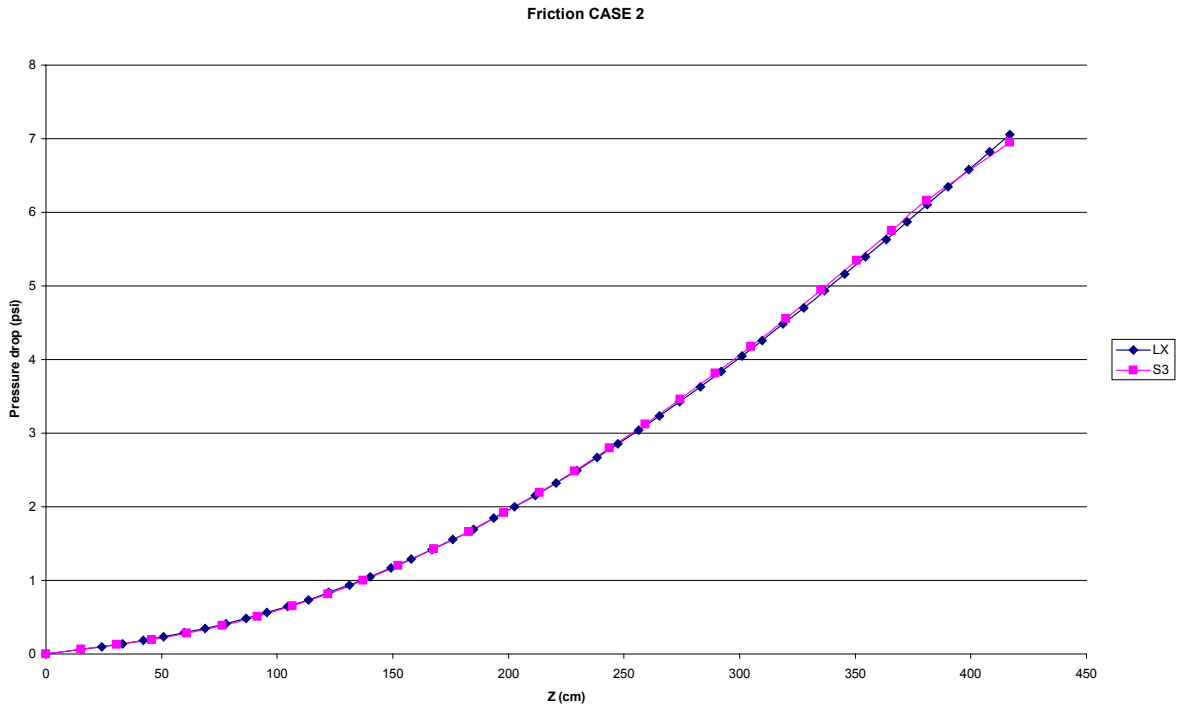
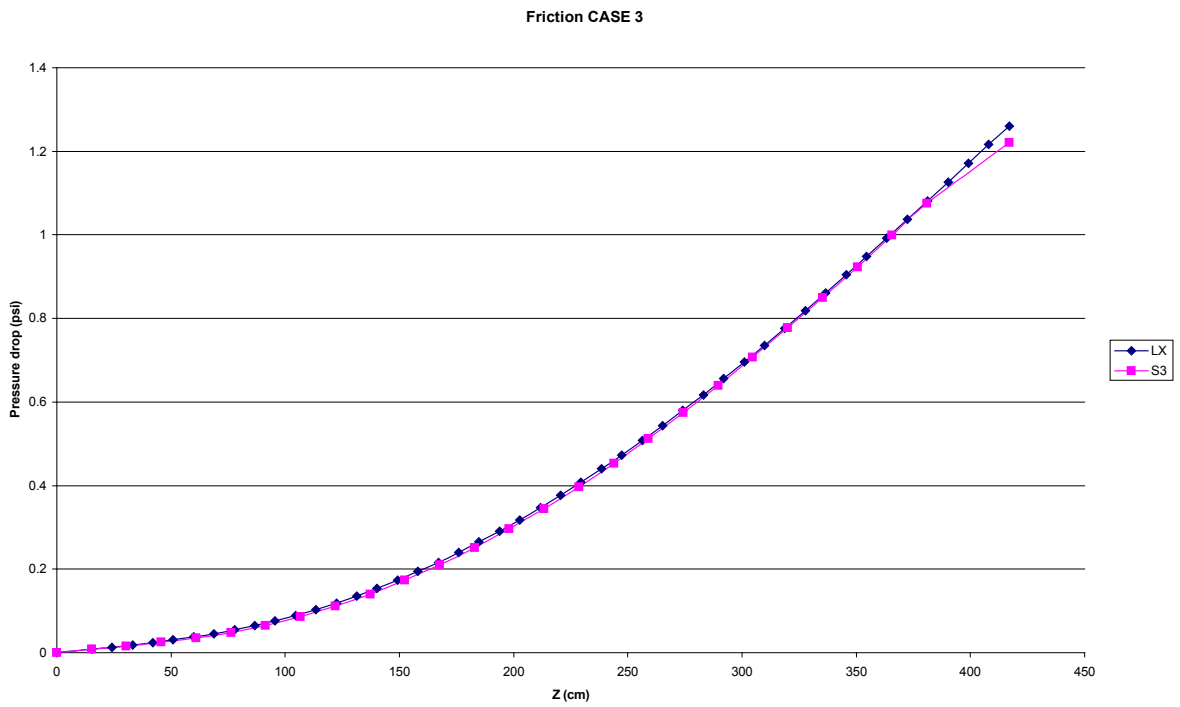


Figure 4.23 Friction CASE 1 TYPE A



**Figure 4.24 Friction CASE 2 TYPE A**



**Figure 4.25 Friction CASE 3 TYPE A**

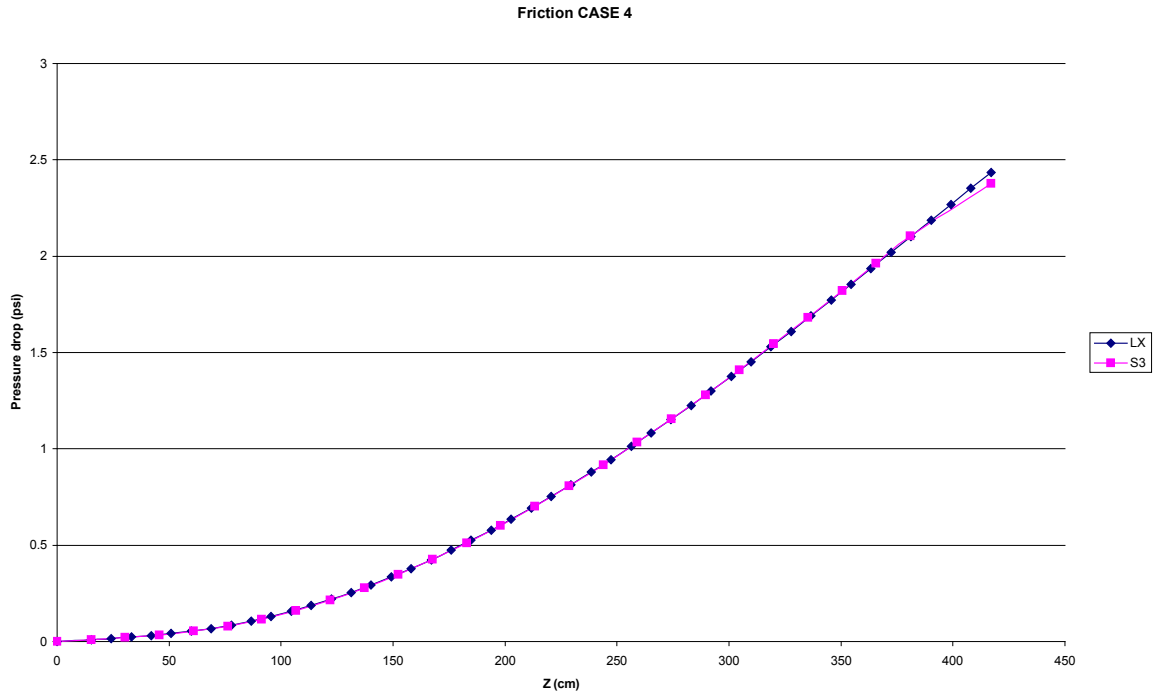


**Figure 4.26 Friction CASE 4 TYPE A**

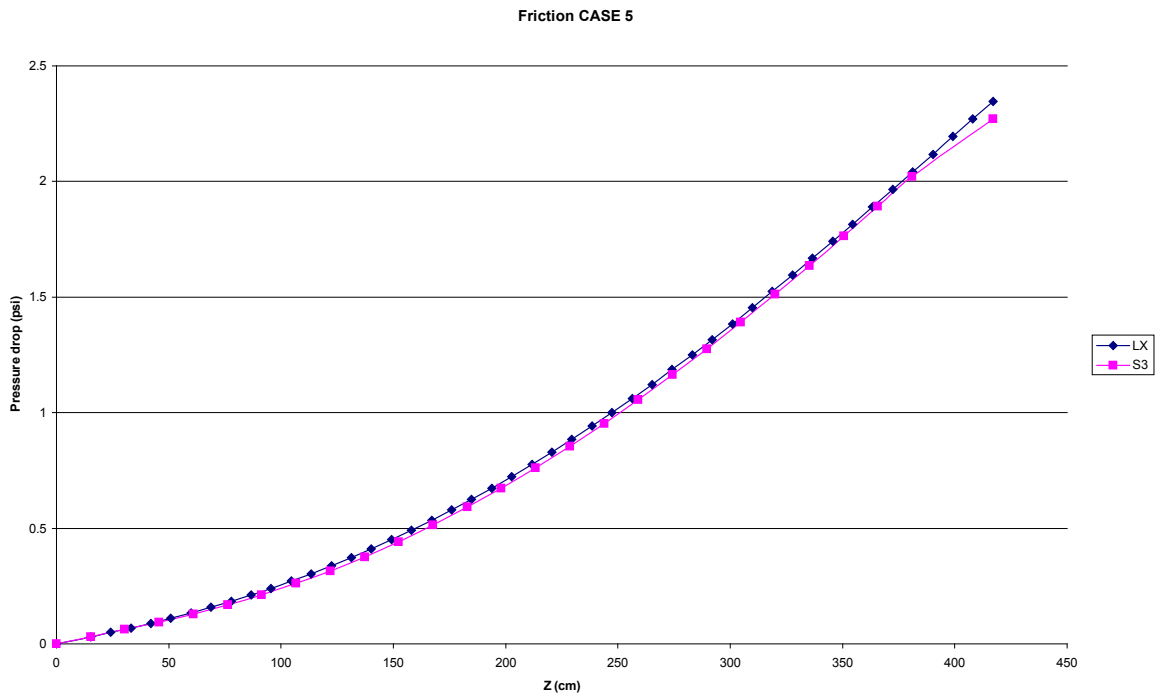


**Figure 4.27 Friction CASE 5 TYPE A**

#### 4.4.2 Friction Data for TYPE B

Comparisons of the friction component of pressure drop for TYPE B are shown in Figs. 4.28 to 4.32.

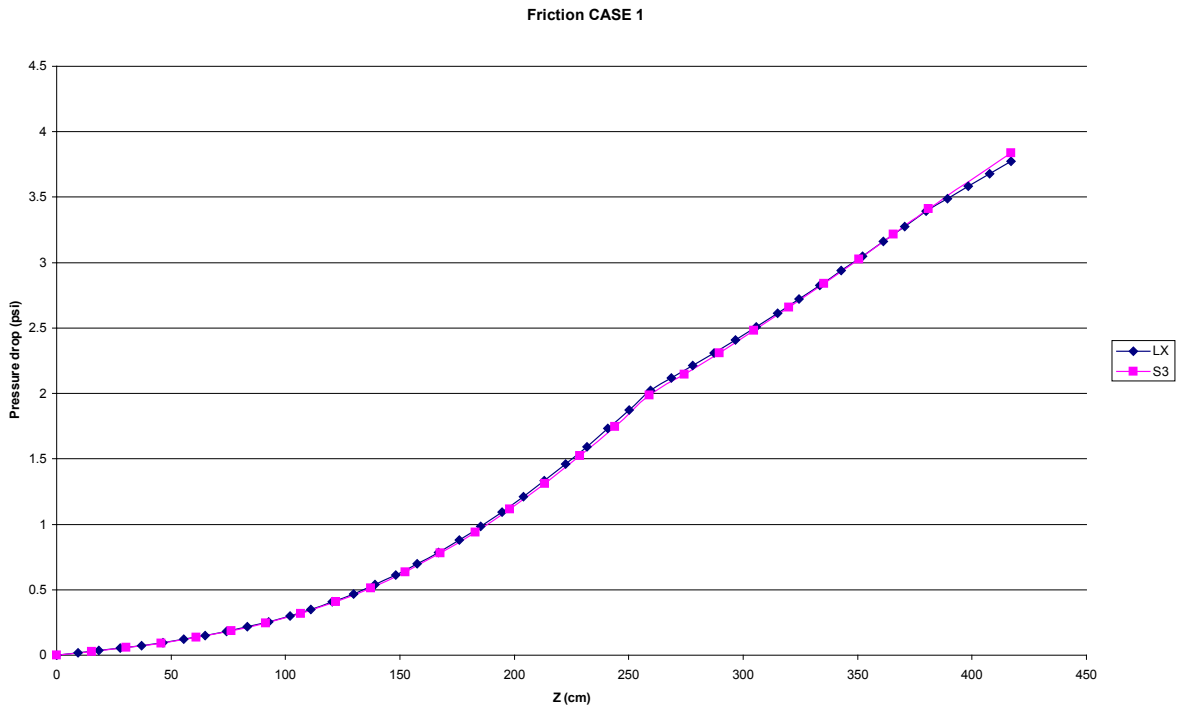
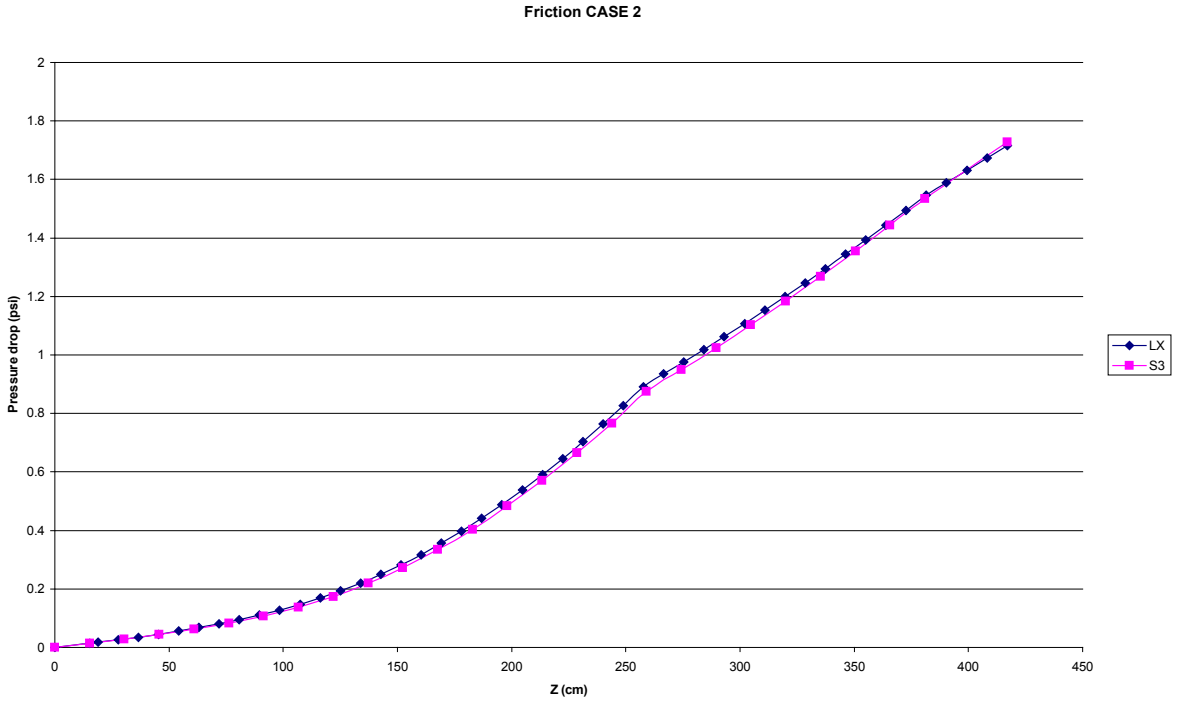
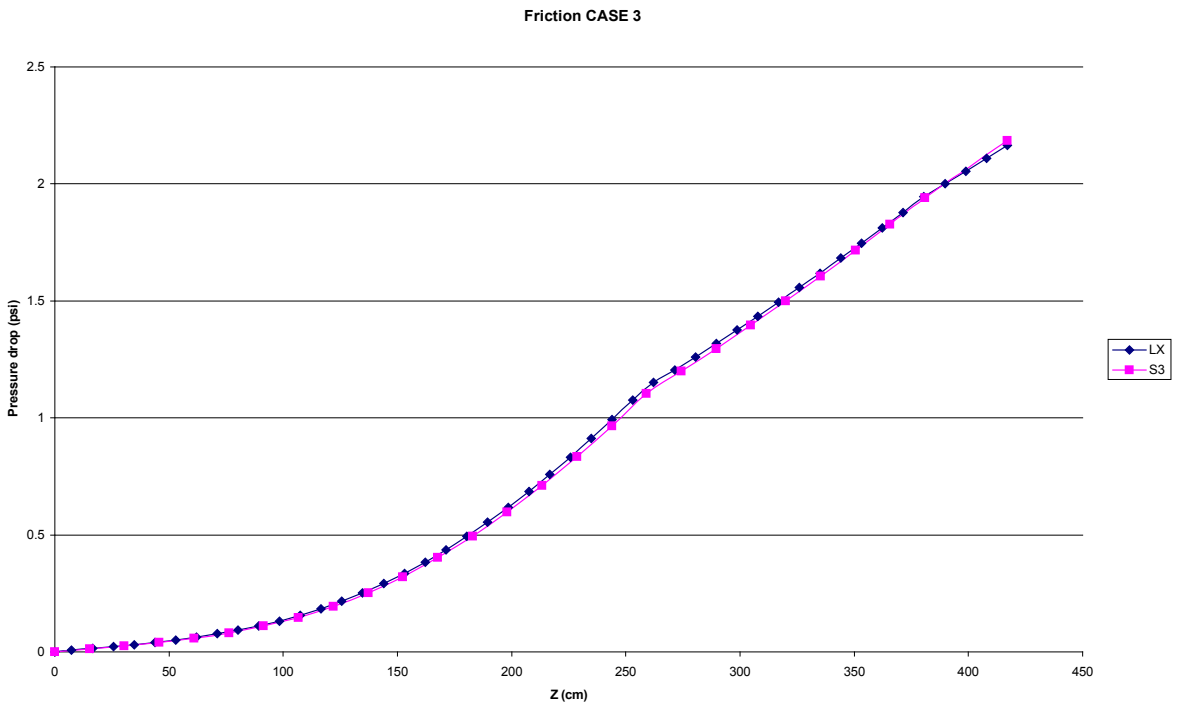


Figure 4.28 Friction CASE 1 TYPE B



**Figure 4.29 Friction CASE 2 TYPE B**



**Figure 4.30 Friction CASE 3 TYPE B**

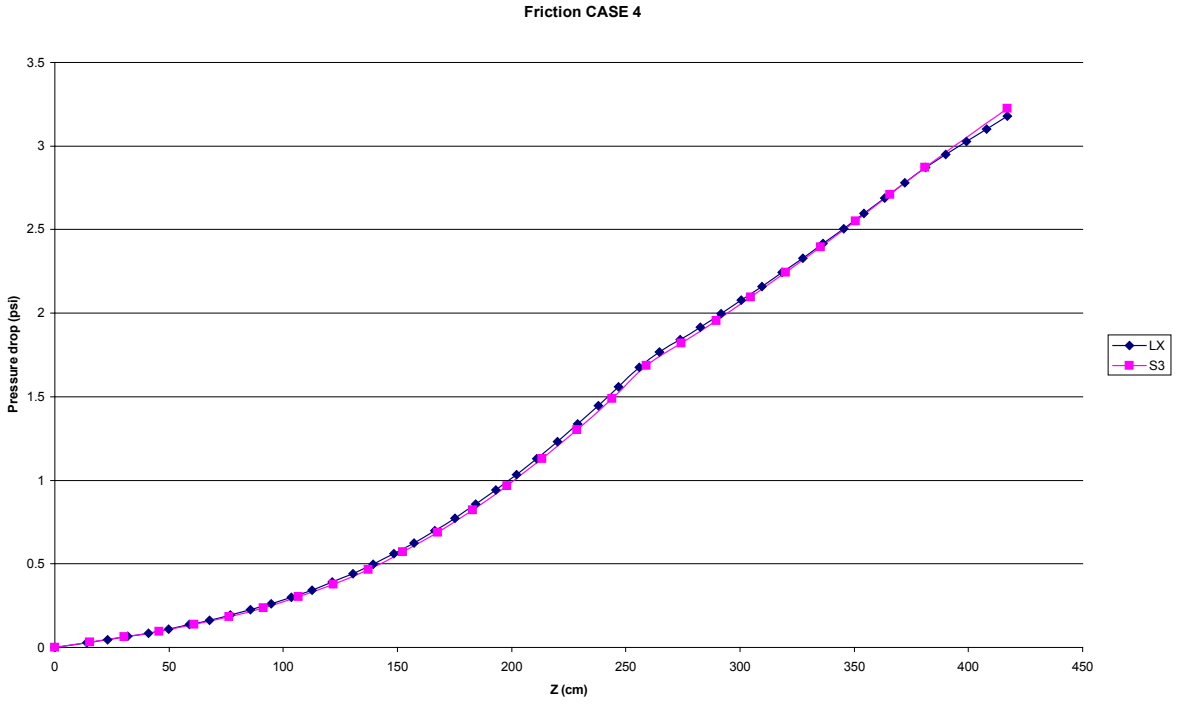


**Figure 4.31 Friction CASE 4 TYPE B**

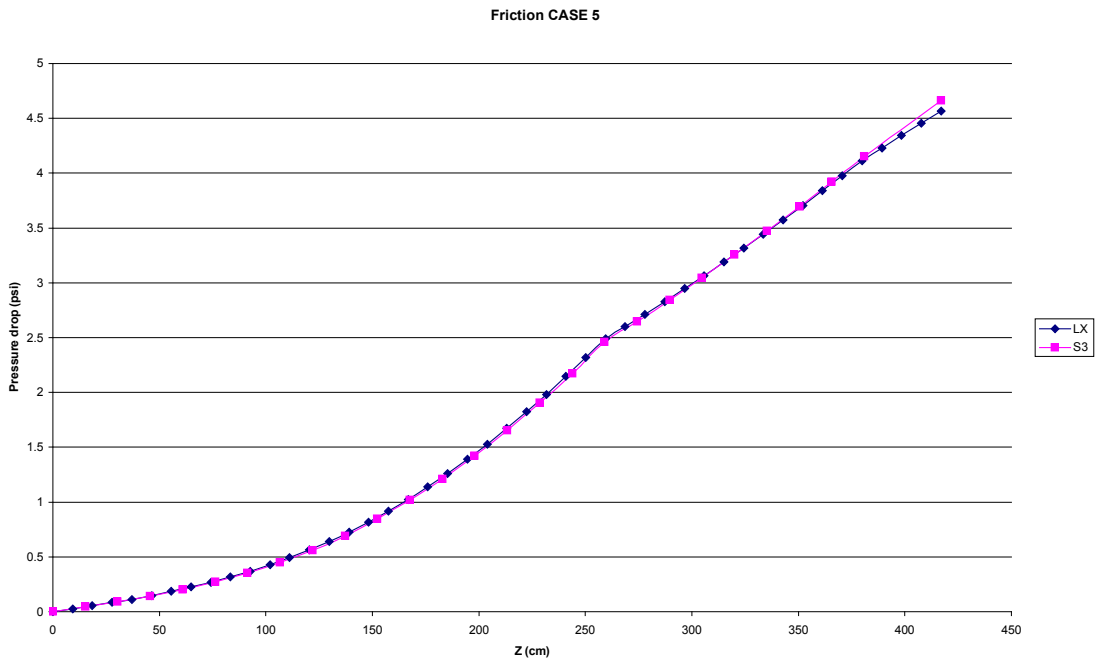


**Figure 4.32 Friction CASE 5 TYPE B**

### **4.4.3 Conclusions of Friction Results**

According to Sect. 3, two-phase friction is accounted for by means of a two-phase multiplier, which depends on flow quality. Friction pressure drop results for both codes are in very good agreement. Differences occur only in values corresponding to last node of SIMULATE-3. These differences can be attributed to (1) friction in SIMULATE taking into account exit water rod flow rate mixing and (2) friction between upper tie plate and channel exit considering only unrodded channel flow area. Changes in area in the channel length from the top of active fuel to the upper tie plate are not considered in computing friction pressure drop in this node.

It can be shown that flow quality is equivalent to flow thermodynamic quality in the bulk boiling region. However, in the subcooled boiling region, a correlation is used to obtain the “real” flow quality in this region, due to equal temperature assumption of the conservation equations. Correlations for computing real flow quality are different in LAPUR and SIMULATE-3, and flow quality results are slightly different between the two codes. The integral effect in friction is negligible, as shown in the figures.

### **4.5 Local Pressure Drop Data**

In this section, a comparison of other dominant contributors to the pressure drop in LAPUR and SIMULATE-3 is provided.

#### **4.5.1 Local Pressure Drop Data for TYPE A**

Comparisons of the component of pressure drop due to local obstructions (spacers and tie plates) for TYPE A are shown in Figs. 4.33 to 4.37.

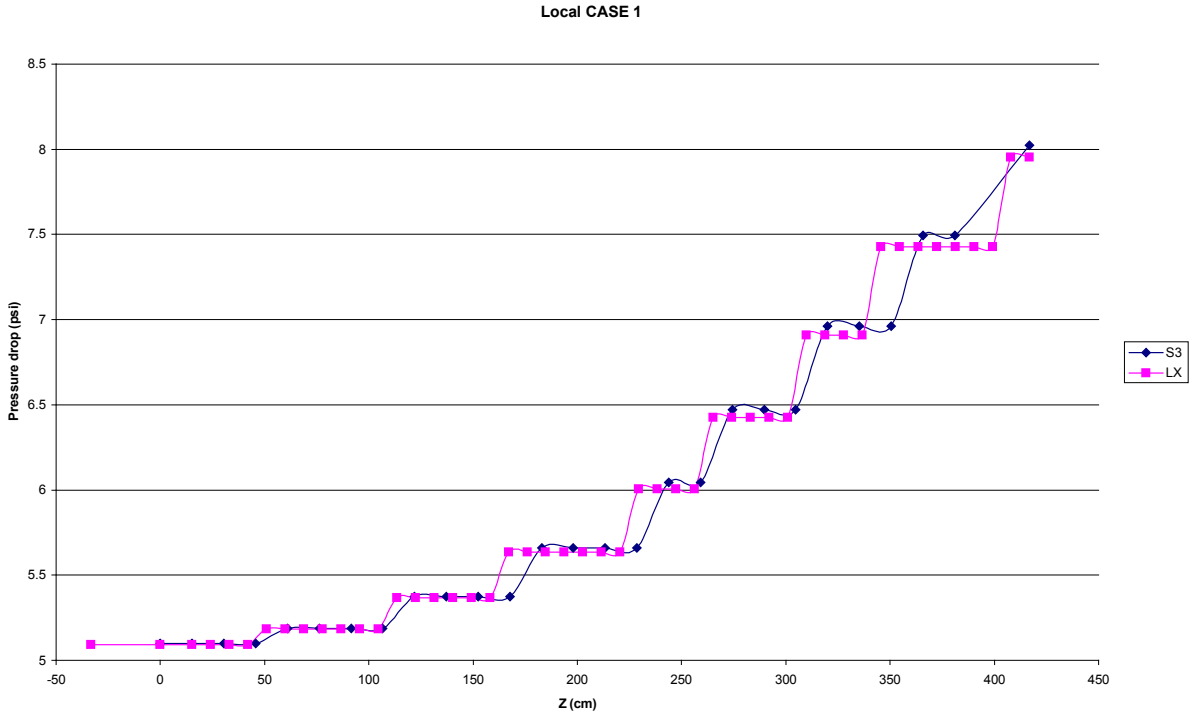


**Figure 4.33 Local CASE 1 TYPE A**

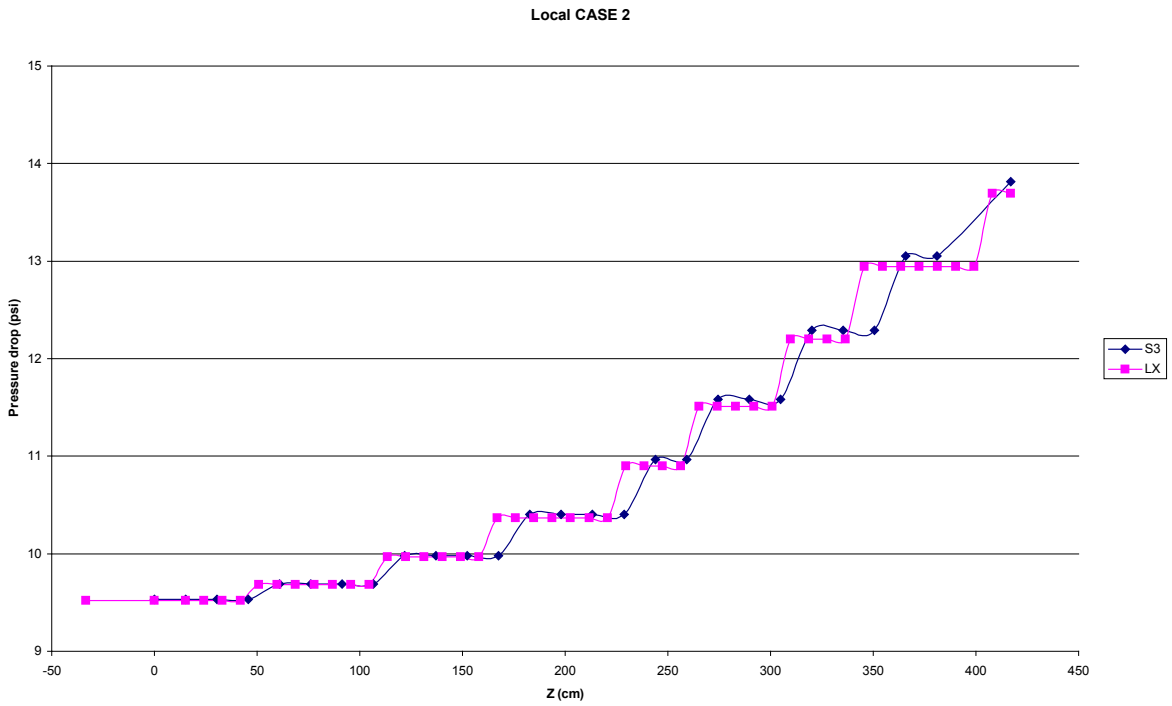


**Figure 4.34 Local CASE 2 TYPE A**

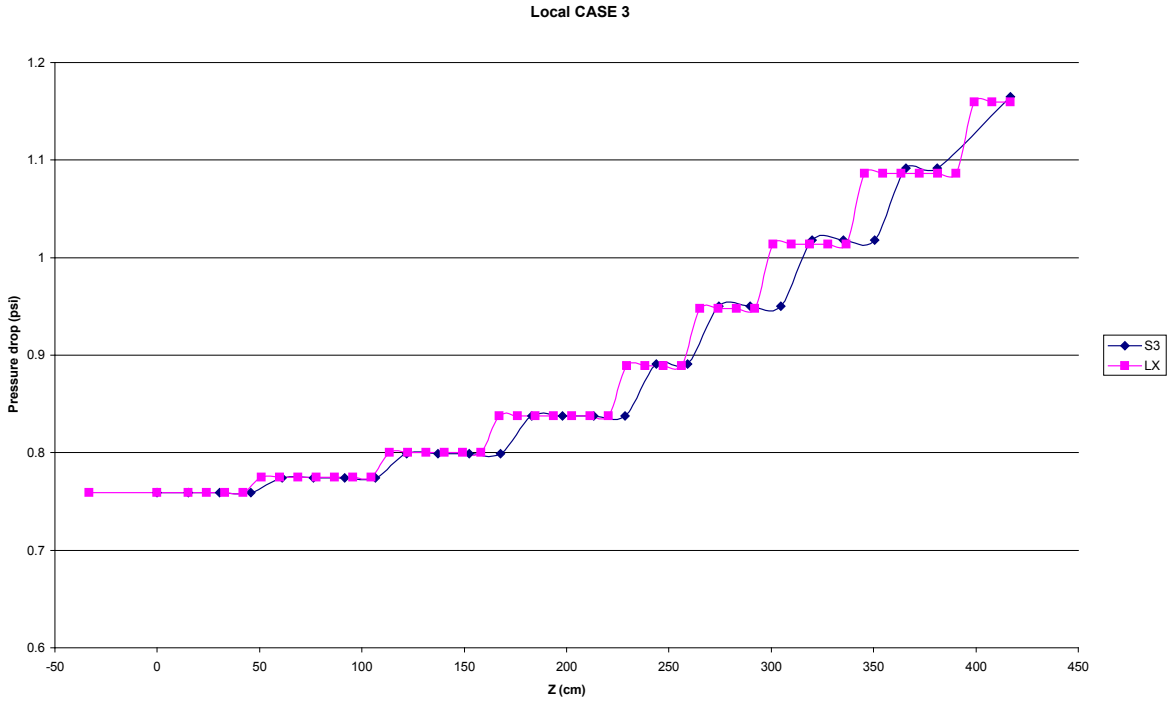


**Figure 4.35 Local CASE 3 TYPE A**

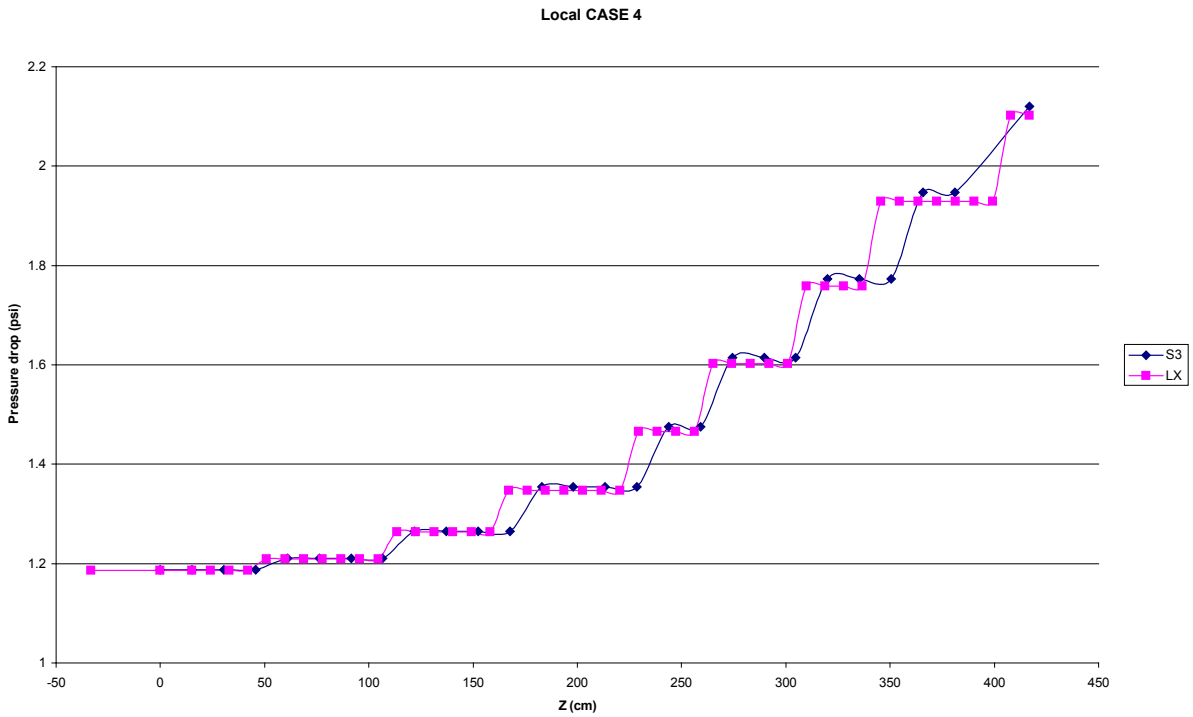


**Figure 4.36 Local CASE 4 TYPE A**

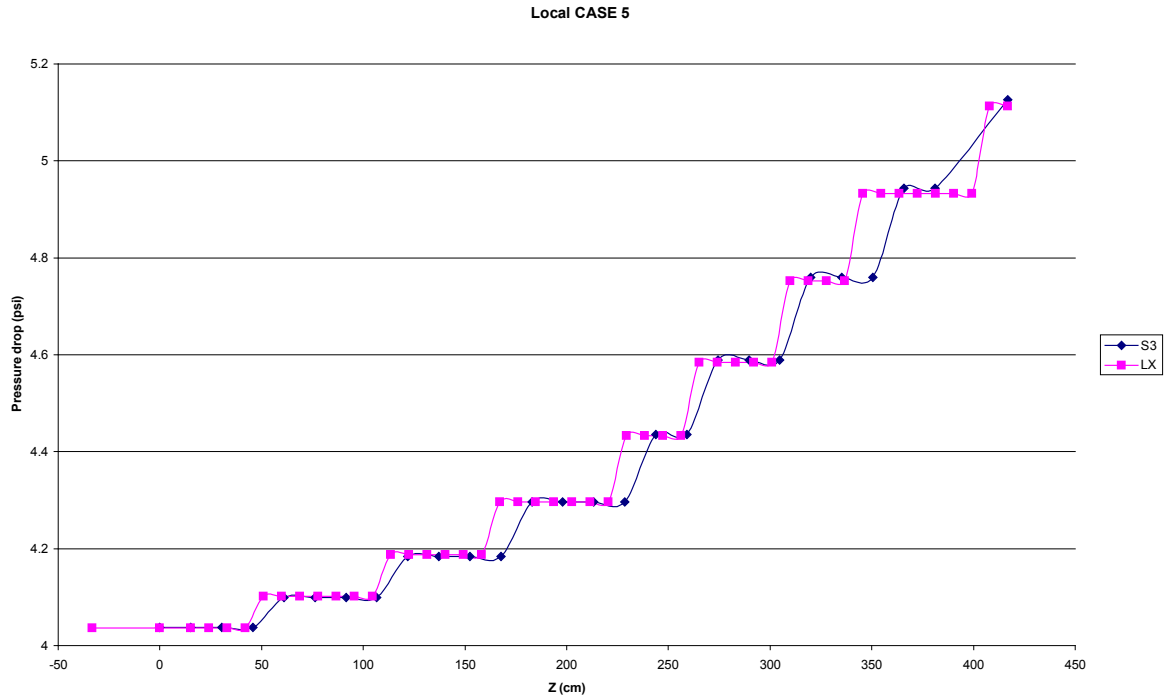


**Figure 4.37 Local CASE 5 TYPE A**

#### 4.5.2 Local Pressure Drop Data for TYPE B

Comparisons of the component of pressure drop due to local obstructions (spacers and tie plates) for TYPE B are shown in Figs. 4.38 to 4.42.

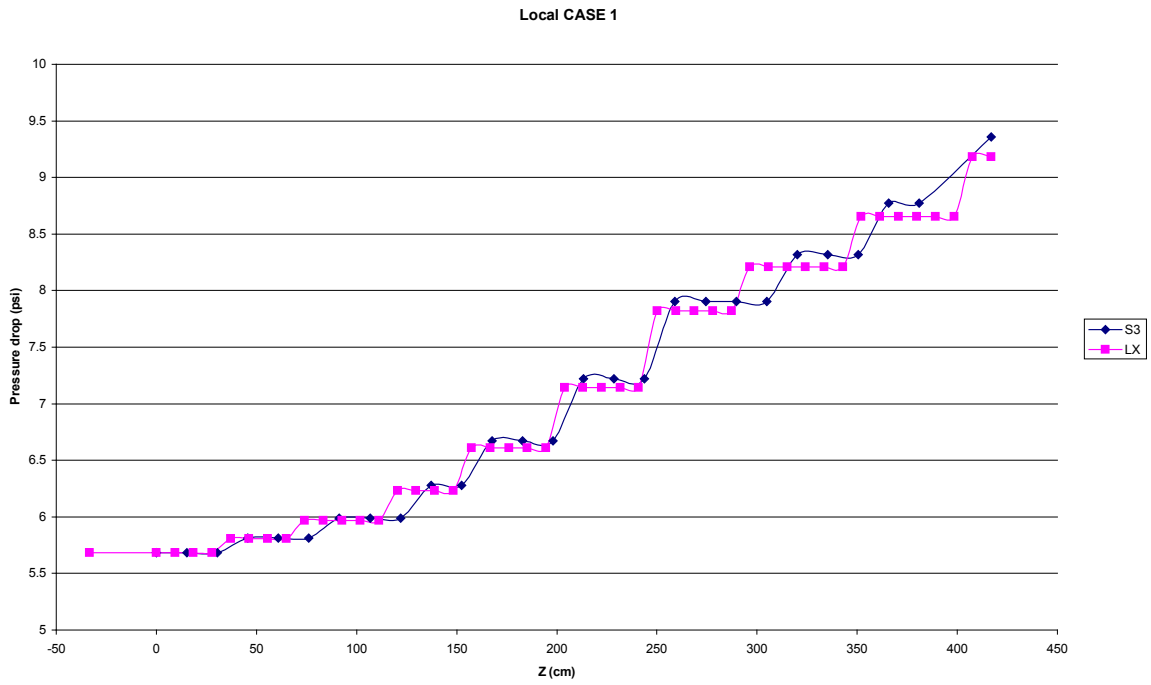


**Figure 4.38 Local CASE 1 TYPE B**

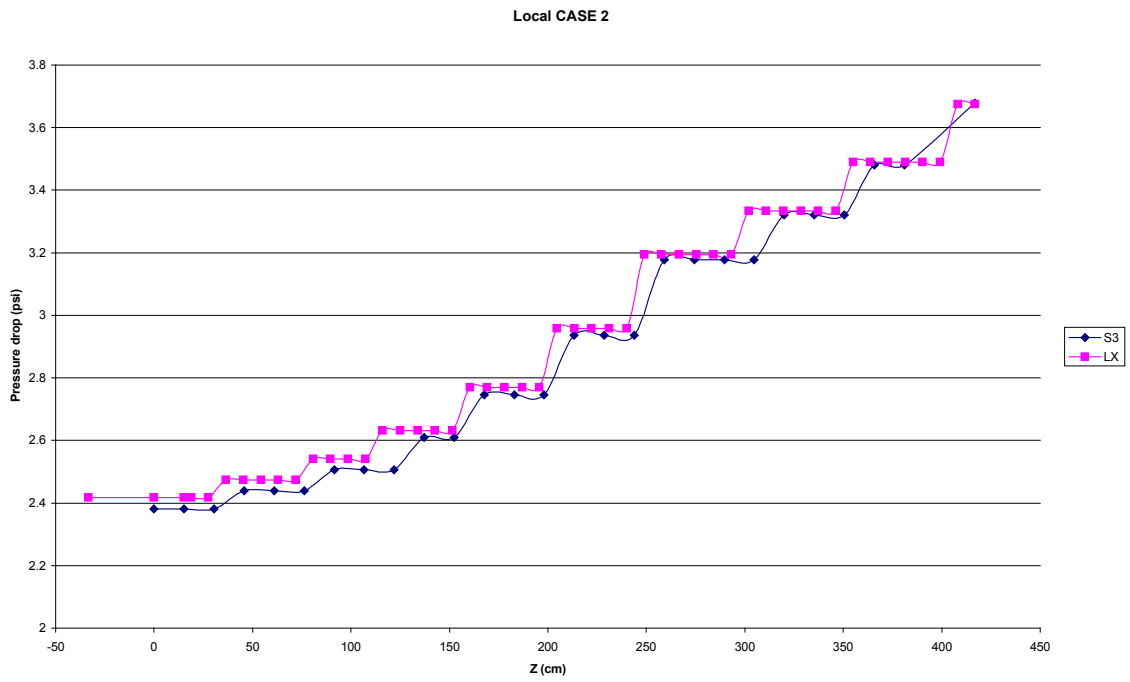


**Figure 4.39 Local CASE 2 TYPE B**

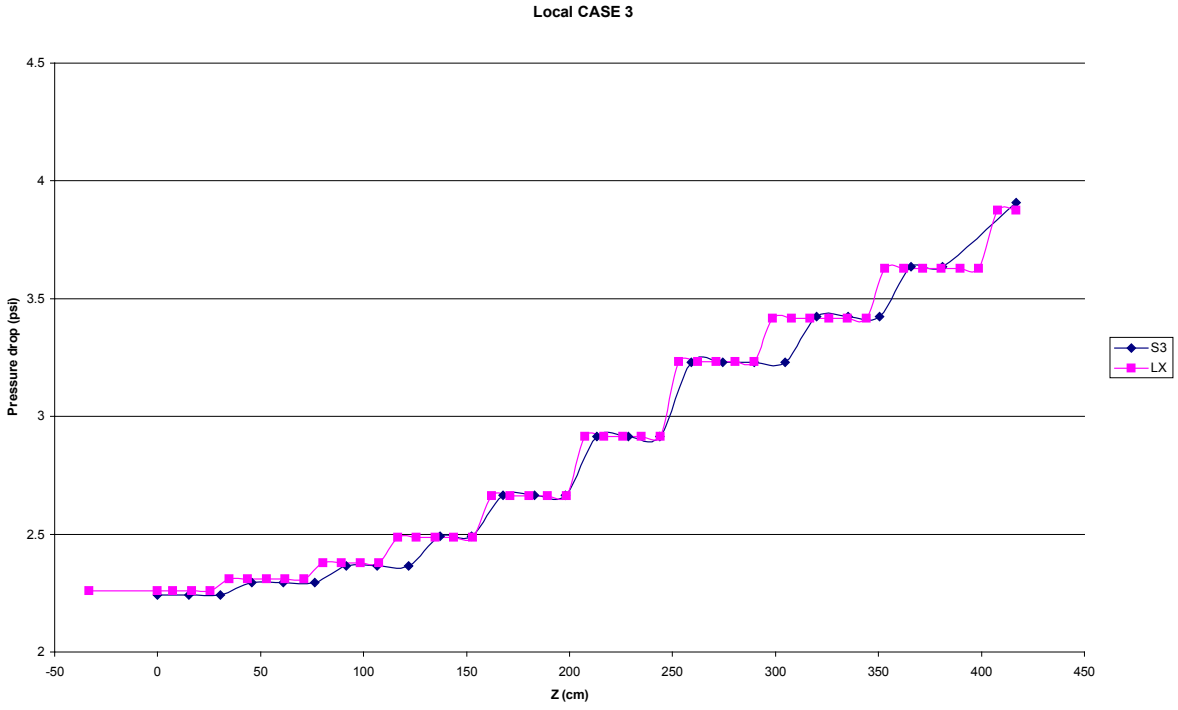


**Figure 4.40 Local CASE 3 TYPE B**

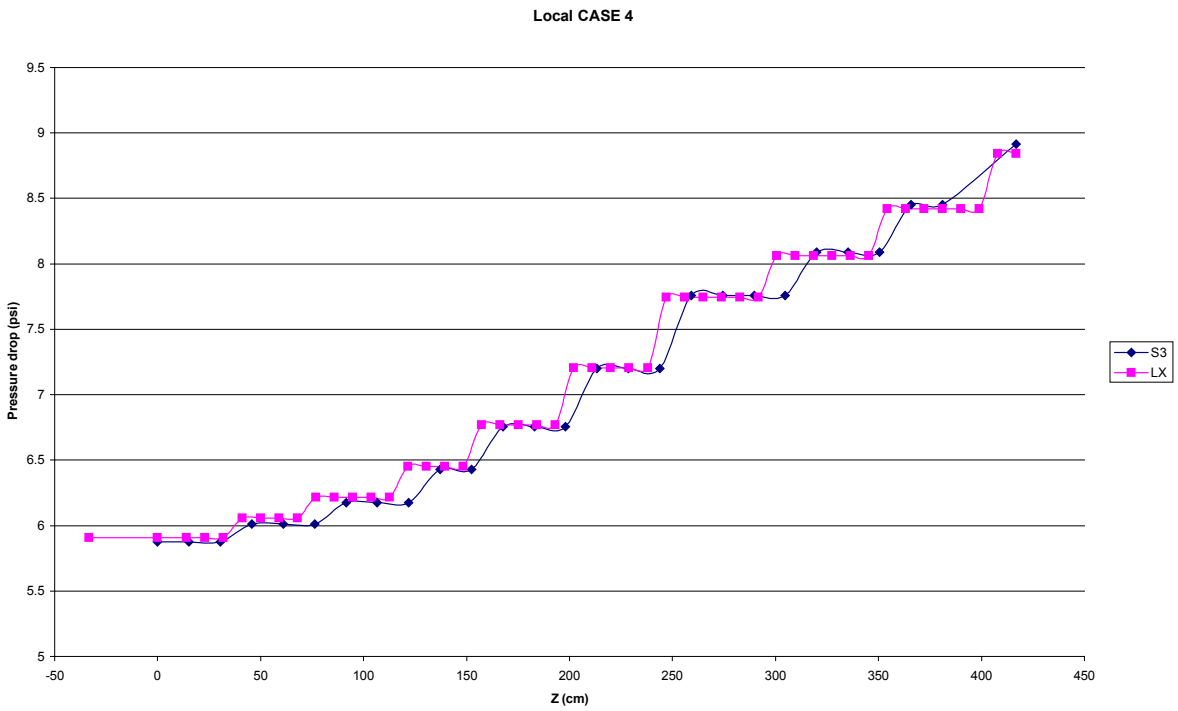


**Figure 4.41 Local CASE 4 TYPE B**

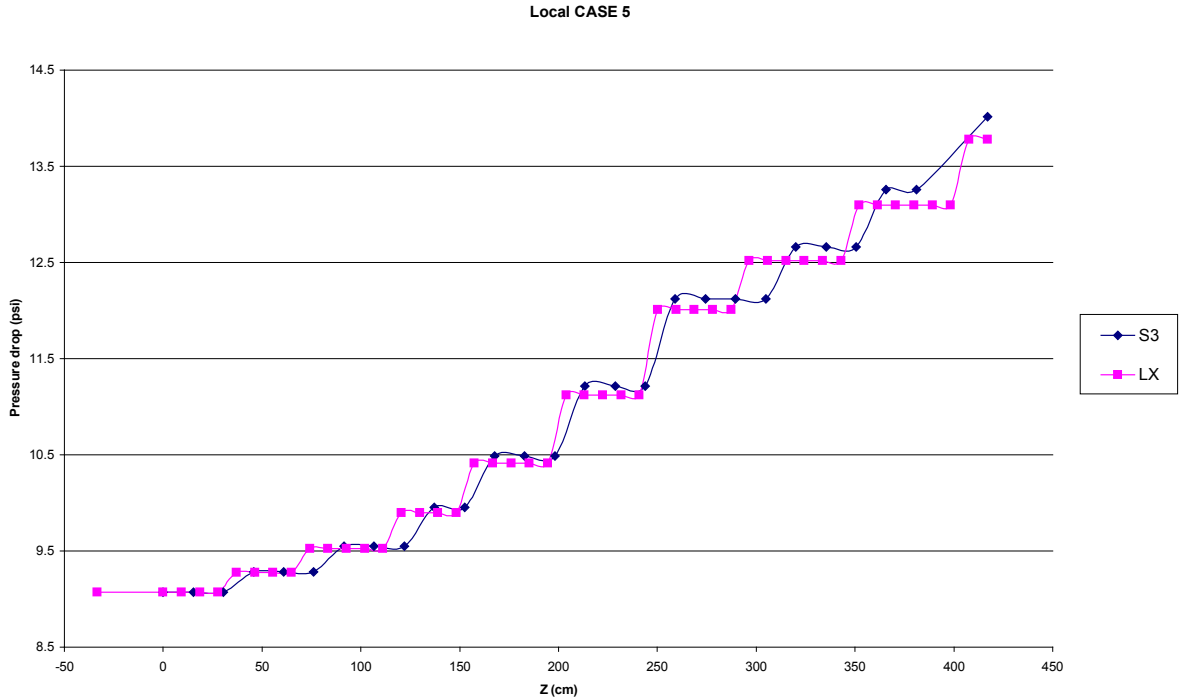


**Figure 4.42 Local CASE 5 TYPE B**

### 4.5.3 Conclusions of Local Losses in Pressure Drop Results

The two-phase effect is accounted for by calculating local pressure drop by means of a homogeneous multiplier, as shown in Sect. 3. Due to the different number of nodes used in the LAPUR and SIMULATE-3 applications (45 nodes in boiling region for LAPUR and 25 fixed nodes for SIMULATE-3), the flow quality used in the calculation for local pressure drop is slightly different. As shown in the figures, the discrepancies are small and less than a 2% of the total local losses in pressure drop for TYPE B. Results for TYPE A type fuel are in better agreement possibly caused by compensation of errors in the pressure drops, spacer by spacer. The quality profile for both cases is different because the power profile used for TYPE B and TYPE A are different. However, overall the results show excellent agreement.

### 4.6 Void Fraction Data

In this section, a comparison of the void fraction predicted for LAPUR and SIMULATE-3 is provided.

#### 4.6.1 Void Fraction Data for TYPE A

Void fraction data for TYPE A test cases are shown in Figs. 4.43 to 4.47.

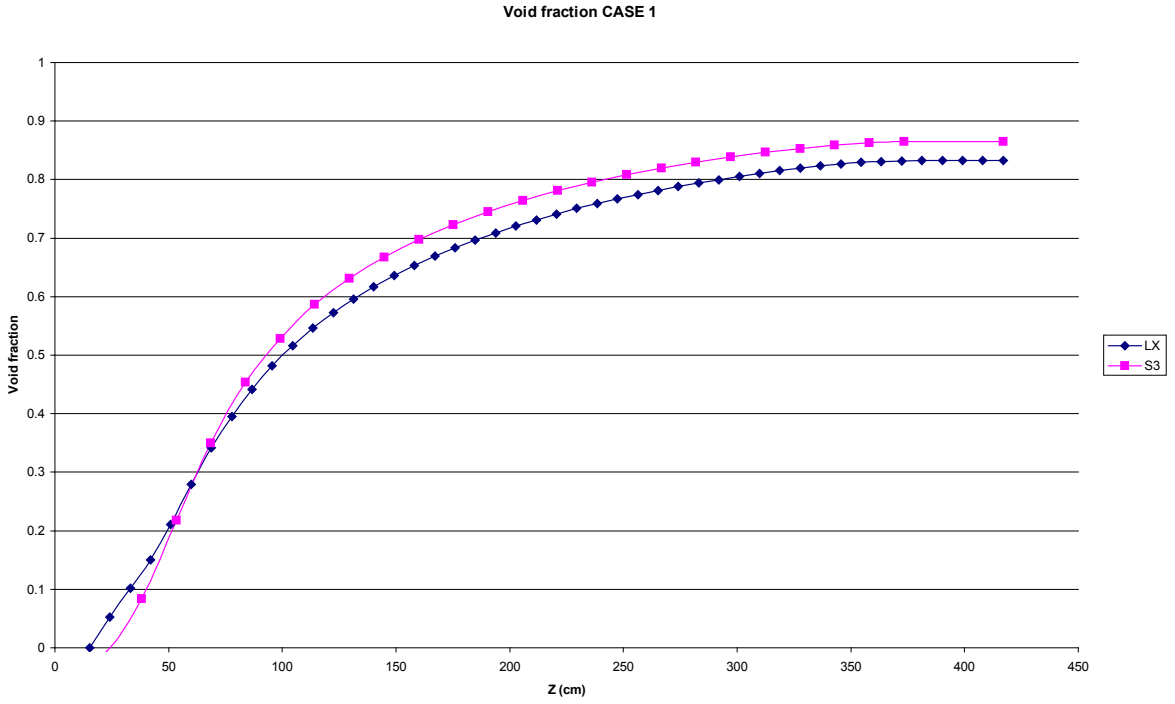


**Figure 4.43 Void fraction CASE 1 TYPE A**

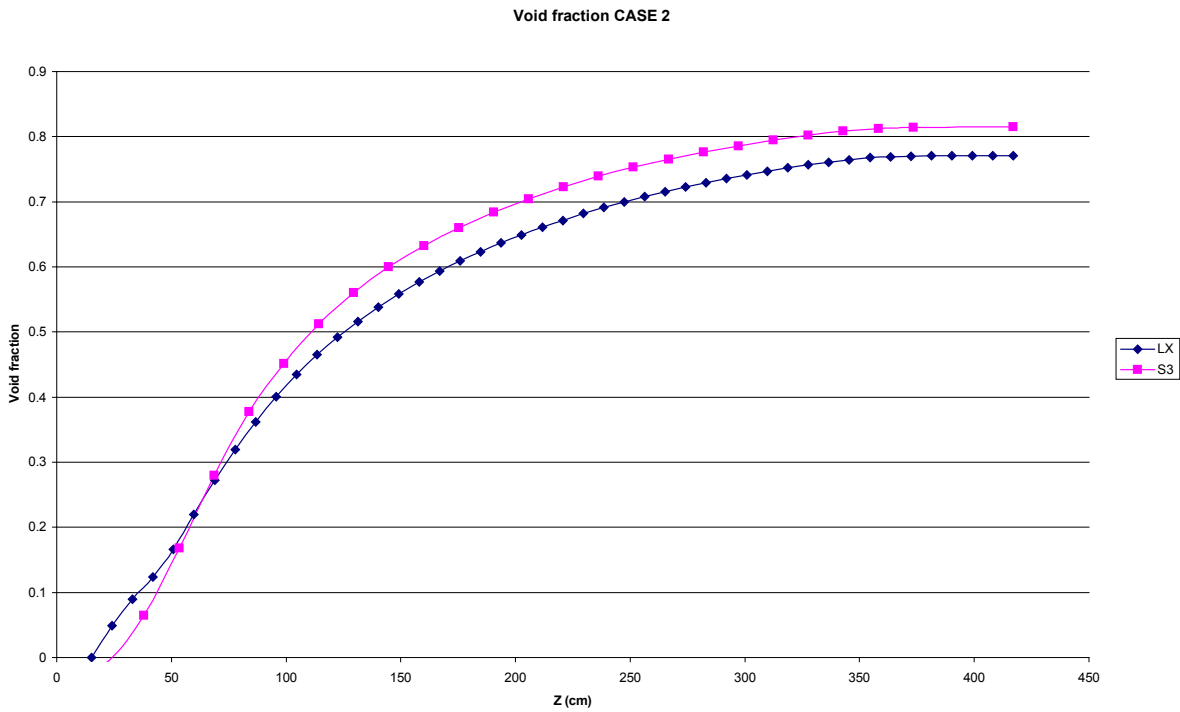


**Figure 4.44 Void fraction CASE 2 TYPE A**

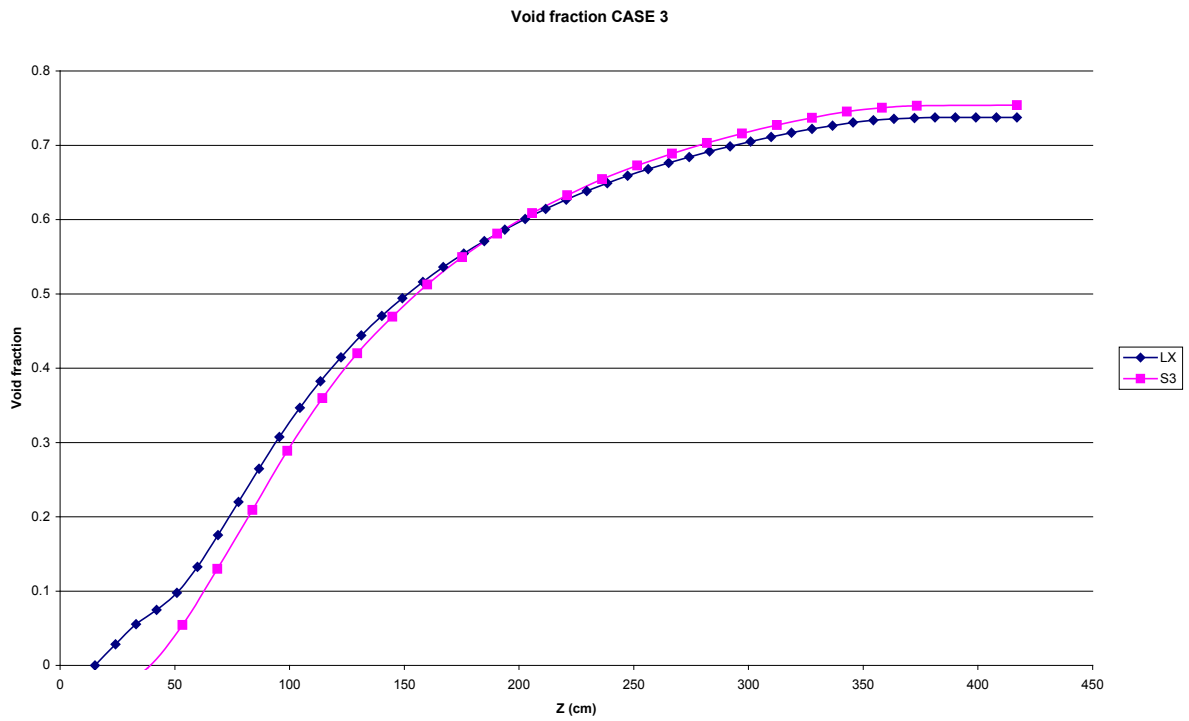


**Figure 4.45 Void fraction CASE 3 TYPE A**

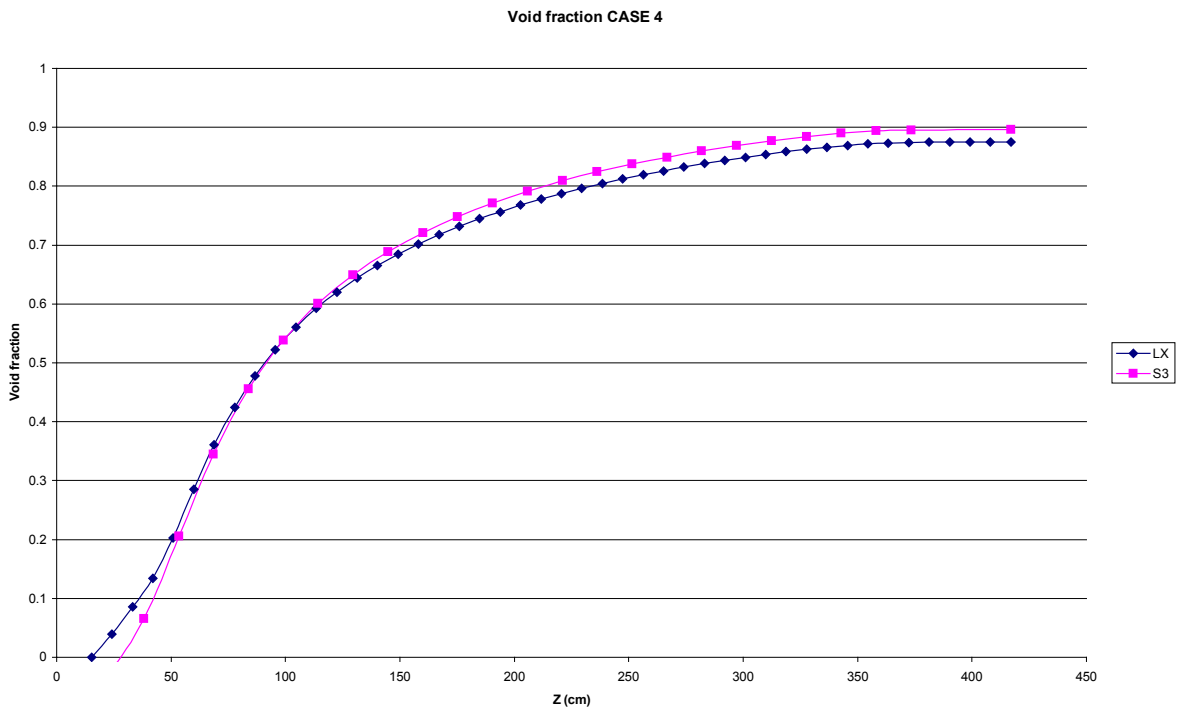


**Figure 4.46 Void fraction CASE 4 TYPE A**

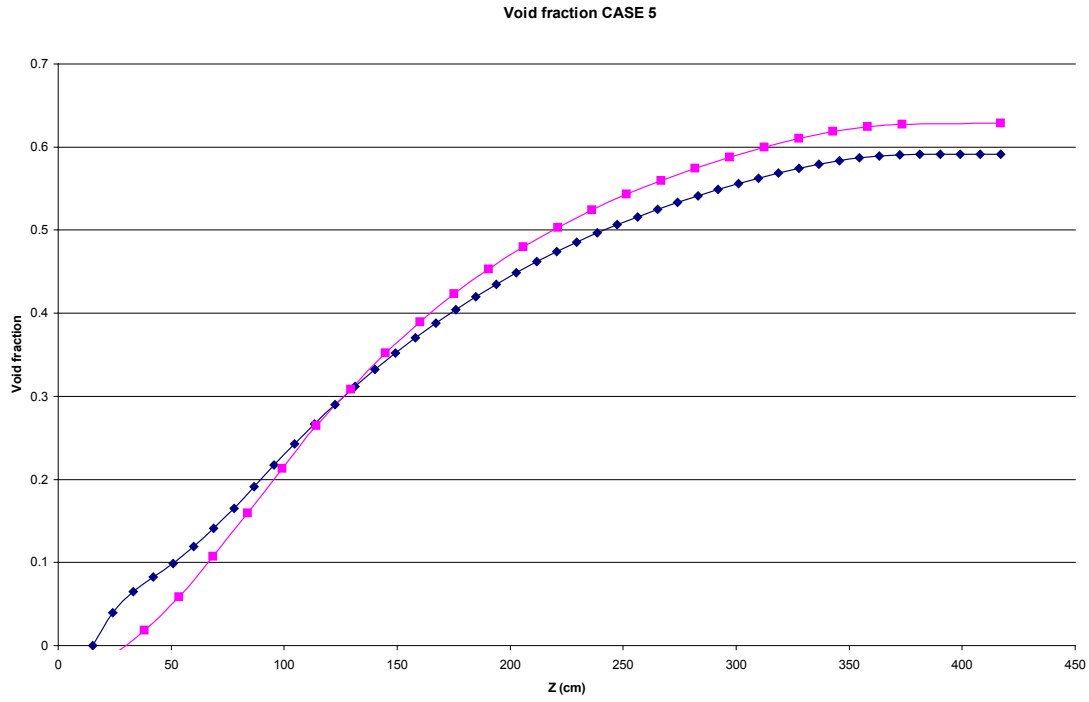
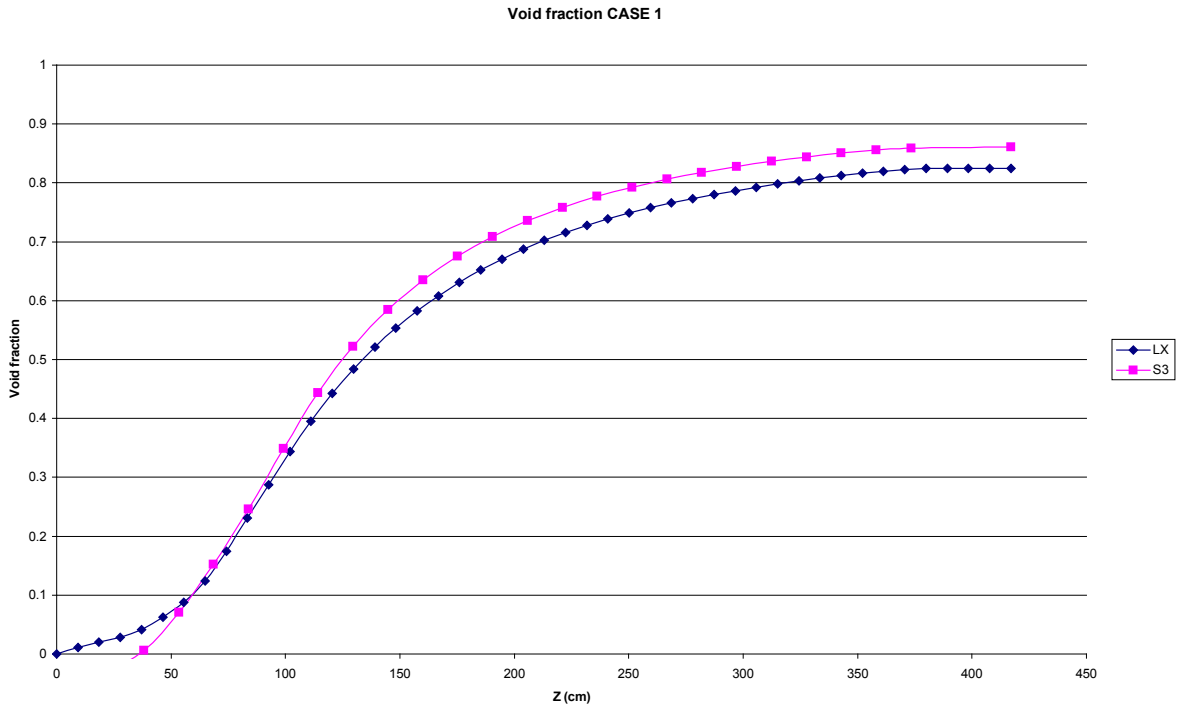


Figure 4.47 Void fraction CASE 5 TYPE A

#### 4.6.2 Void Fraction Data for TYPE B

Void fraction data for TYPE B test cases are shown in Figs. 4.48 to 4.52.



**Figure 4.48 Void fraction CASE 1 TYPE B**

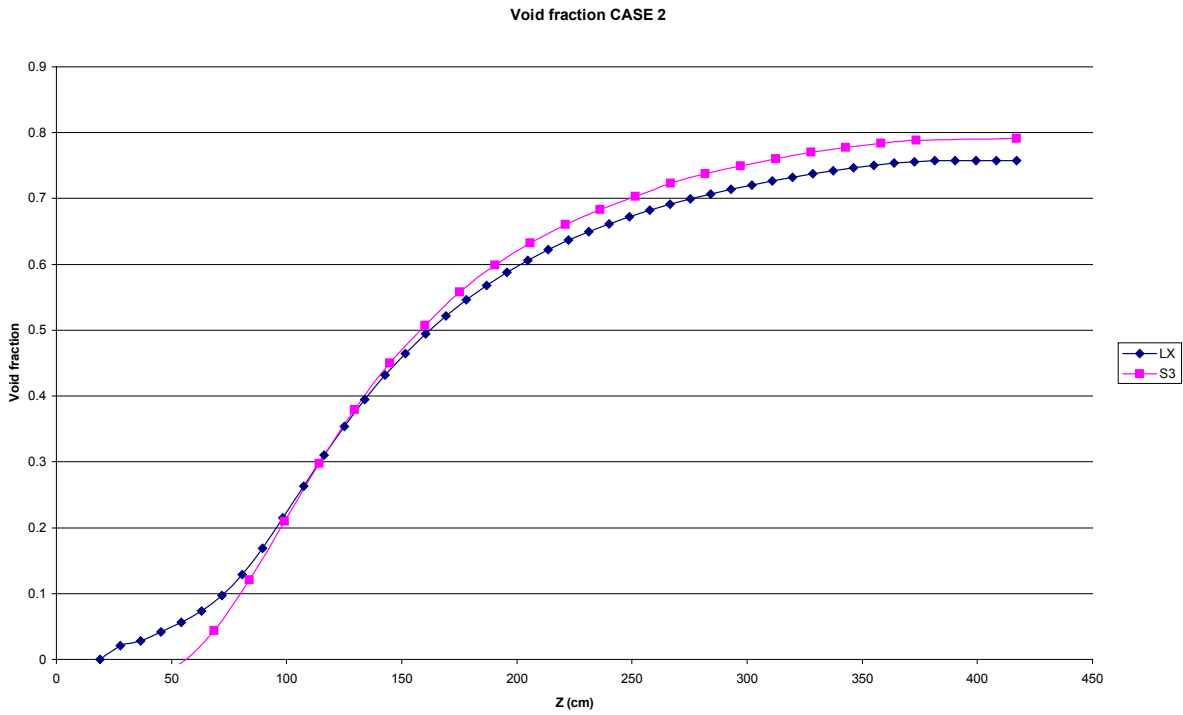


**Figure 4.49 Void fraction CASE 2 TYPE B**

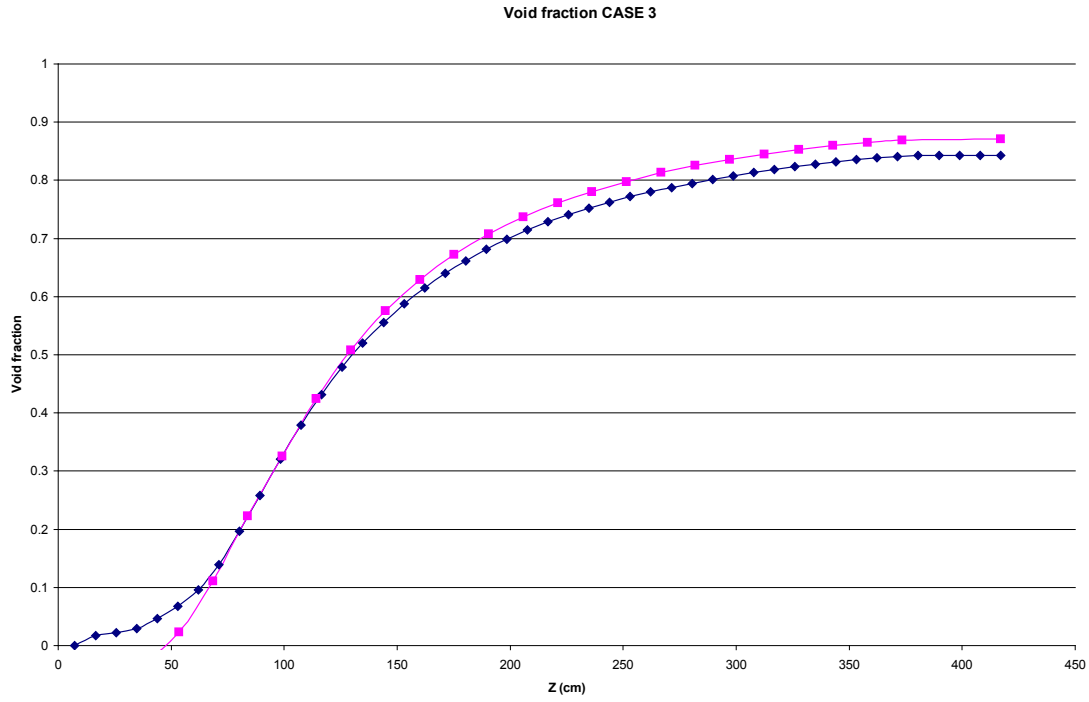


**Figure 4.50 Void fraction CASE 3 TYPE B**

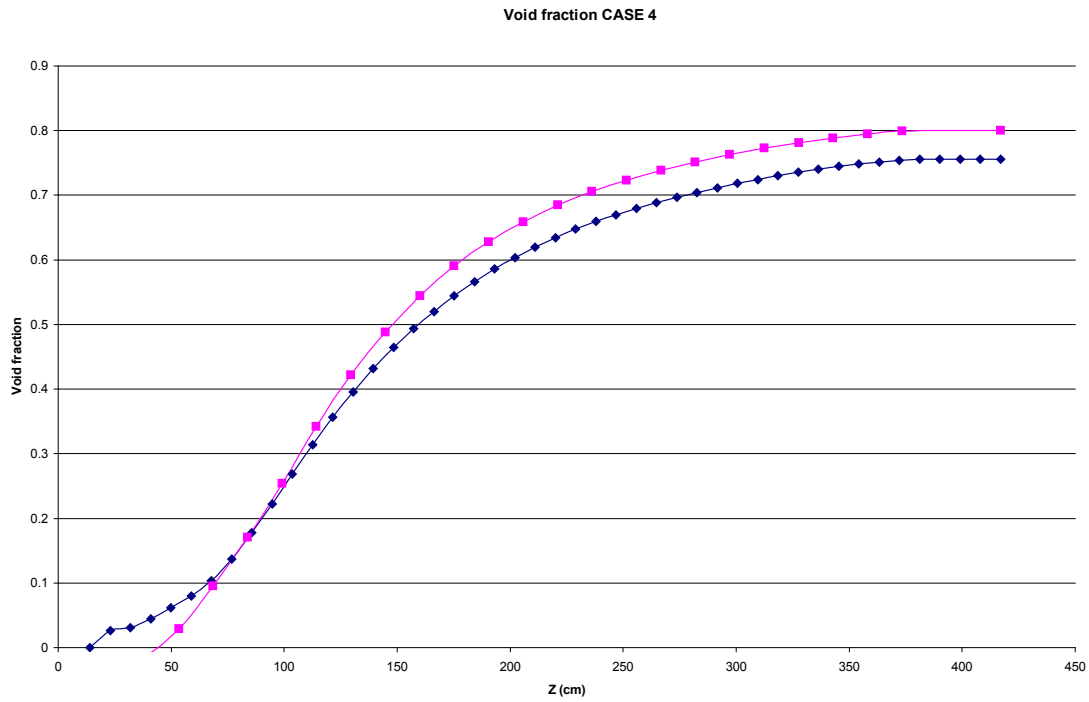


**Figure 4.51 Void fraction CASE 4 TYPE B**

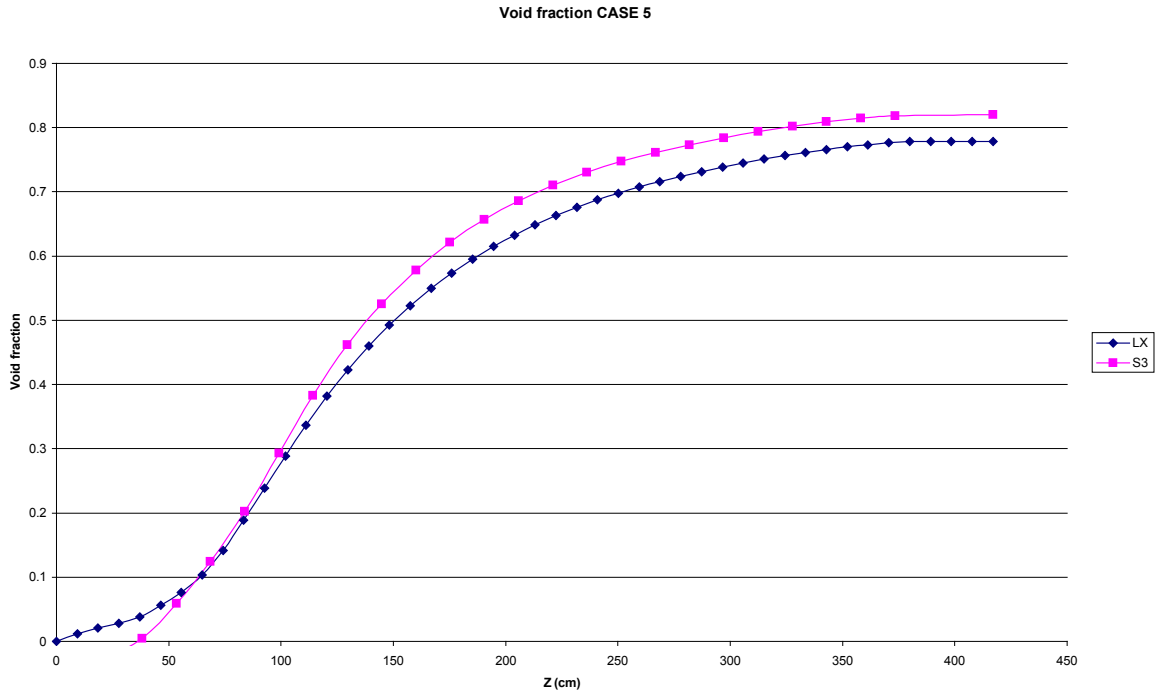


**Figure 4.52 Void fraction CASE 5 TYPE B**

### 4.6.3 Conclusions of Void Fraction Comparison

Slight differences in the void fraction calculated by SIMULATE and LAPUR were identified. The impact on the total pressure drop was negligible; however, comparisons of void fraction calculated with LAPUR to experimental data are not readily available. The following section compares void fractions to FRIGG loop data.

## 5. Comparison of LAPUR6 Void Fraction to FRIGG Loop Data

Void fraction results of LAPUR6 and LAPUR5.1 release 1 are provided in this section. Indirectly, this study demonstrated that the modifications made did not affect the independent void fraction calculation process in LAPUR. These results show that flow qualities and slip ratio are not affected by changes in pressure drop calculation models. Runs were performed with LAPUR5.1 and LAPUR6, and the void fractions were practically the same (1% of maximum differences). The results of LAPUR6 are represented as LAPURX in Figures 5.1 to 5.2.

### 5.1 Experimental Conditions

The FRIGG-2 experiments that were analyzed involved a steady-state flow test in 36-rod, electrically heated rod bundles. Subcooled liquid was introduced at the bundle inlet, and both axial and radial void fractions were obtained. Data from other experiments included mass flow rate, wall heat flux, and exit pressure values. The average bundle void fraction data were compared with LAPUR-calculated results. Table 5.1 shows input data selected from FRIGG loop (RETRAN-3D, 2006)

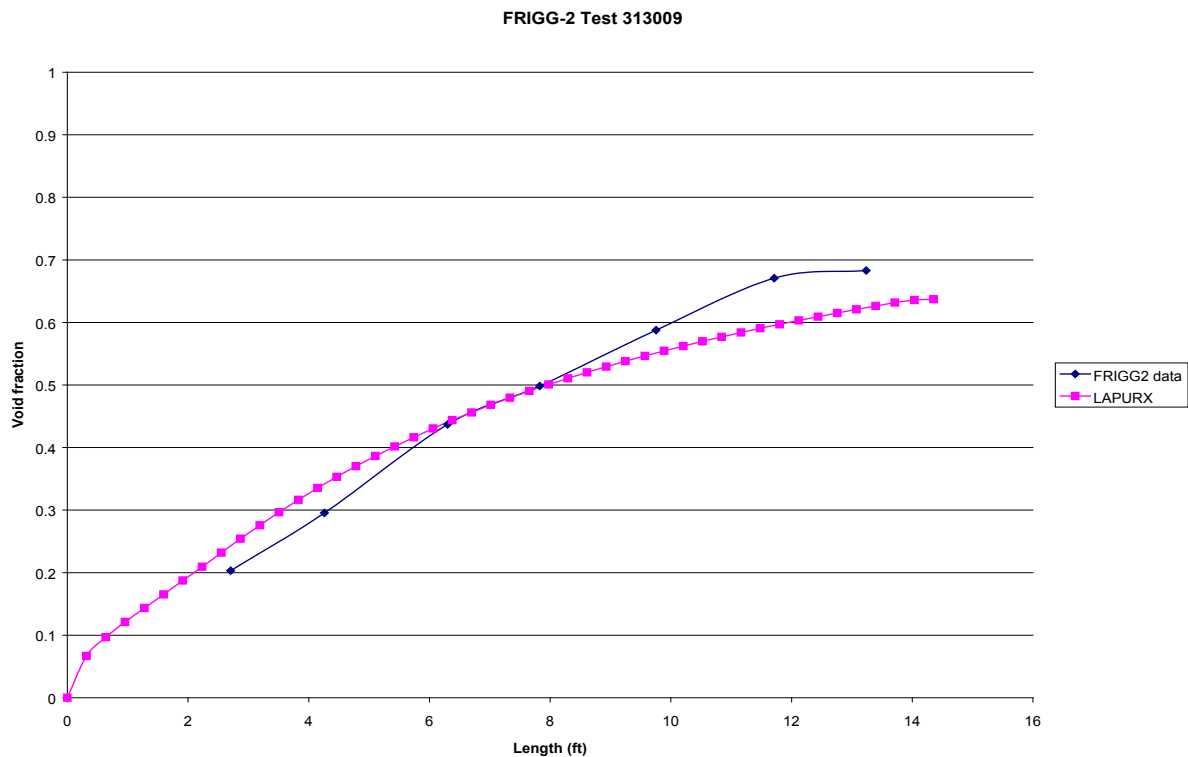


Figure 5.1 Void fraction of FRIGG-2 Test 313009

FRIGG-2 Test 313014

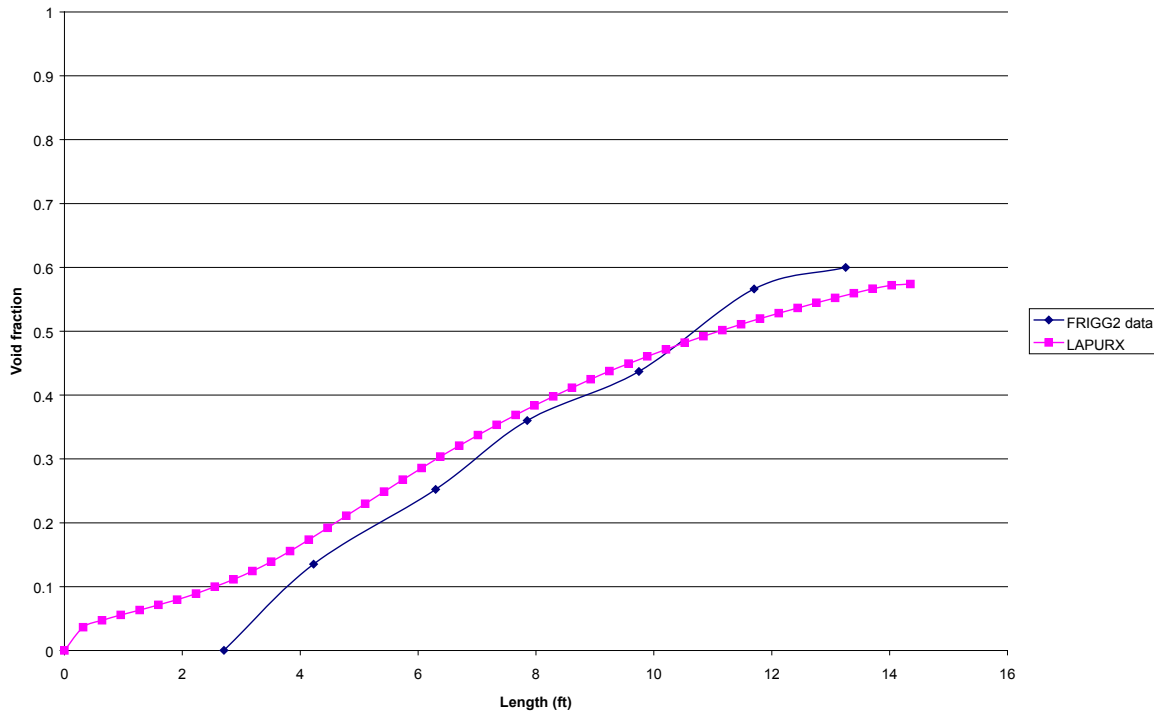


Figure 5.2 Void fraction of FRIGG-2 Test 313014

Table 5.1 FRIGG-2 test conditions

Test	Pressure (psia)	Inlet enthalpy (Btu/lb)	Power (Mw)	Flow rate (lb/s)
313009	725.00	487.05	2.978	34.856
313014	720.65	472.07	2.930	36.619
313016	719.20	454.55	2.909	38.036
313018	720.65	487.53	4.392	35.391
313020	720.65	448.44	4.412	34.493
313024	720.65	486.46	1.475	27.016

## 5.2 Comparison of Void Fraction Results to FRIGG-2 Data

Average bundle void fraction data are compared with LAPUR6 calculated results in Figs. 5.1 to 5.6.

## 5.3 Conclusions of Void Fraction Results of LAPUR6 Compared to FRIGG-2 Data

Void fraction results and FRIGG-2 data were in reasonably good agreement. The highest deviations were similar to those of other models with three equation models and algebraic slip (RETRAN-3D, 2006). However, void fractions obtained with LAPUR6 are practically the same as those of previous version, LAPUR5.1 release 1. Logically, changes in pressure drop

calculations do not affect slip and void fraction calculations because they are independent calculations.

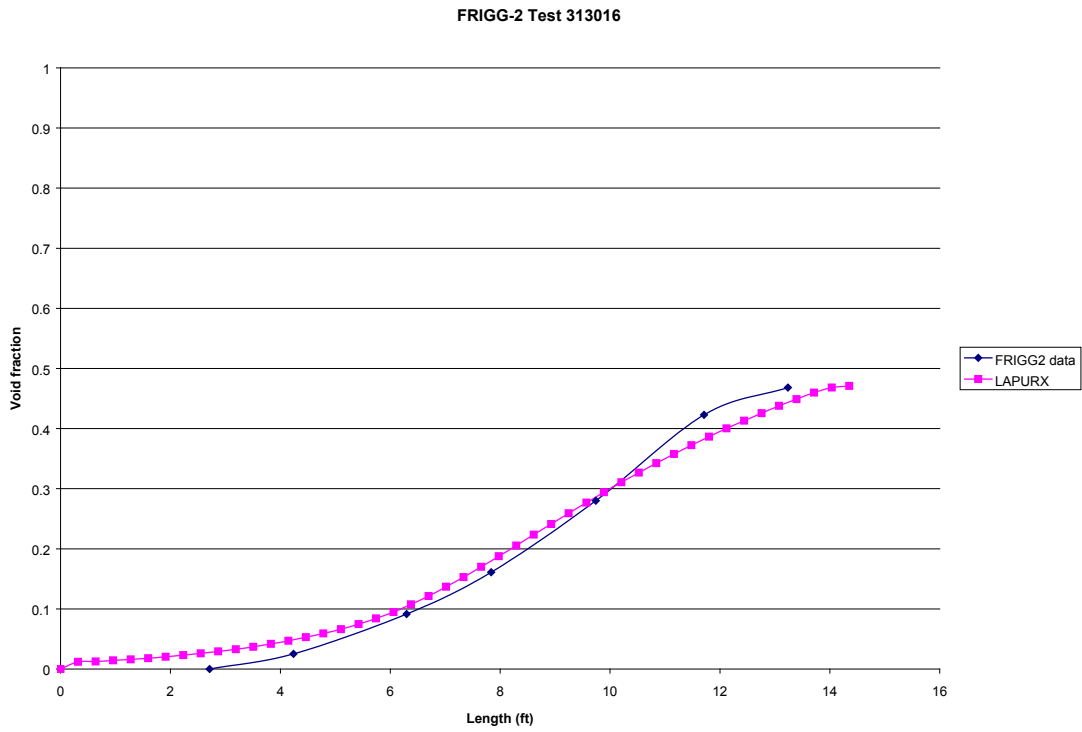


**Figure 5.3 Void fraction of FRIGG-2 Test 313016**

FRIGG-2 Test 313018

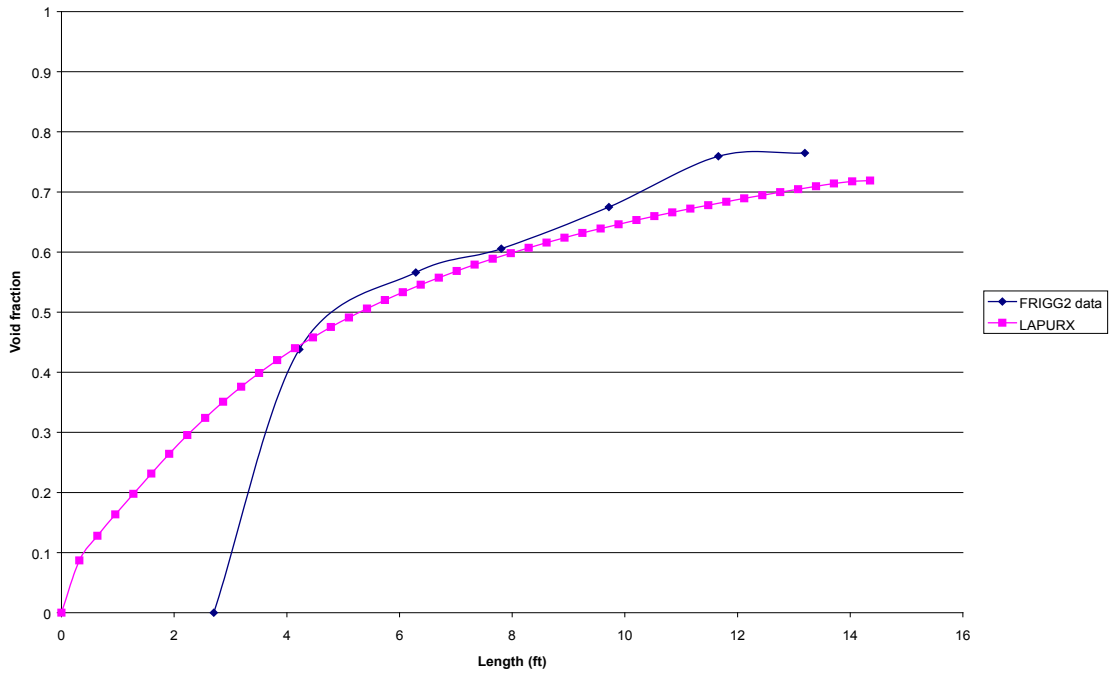


Figure 5.4 Void fraction of FRIGG-2 Test 313018

FRIGG-2 Test 313020

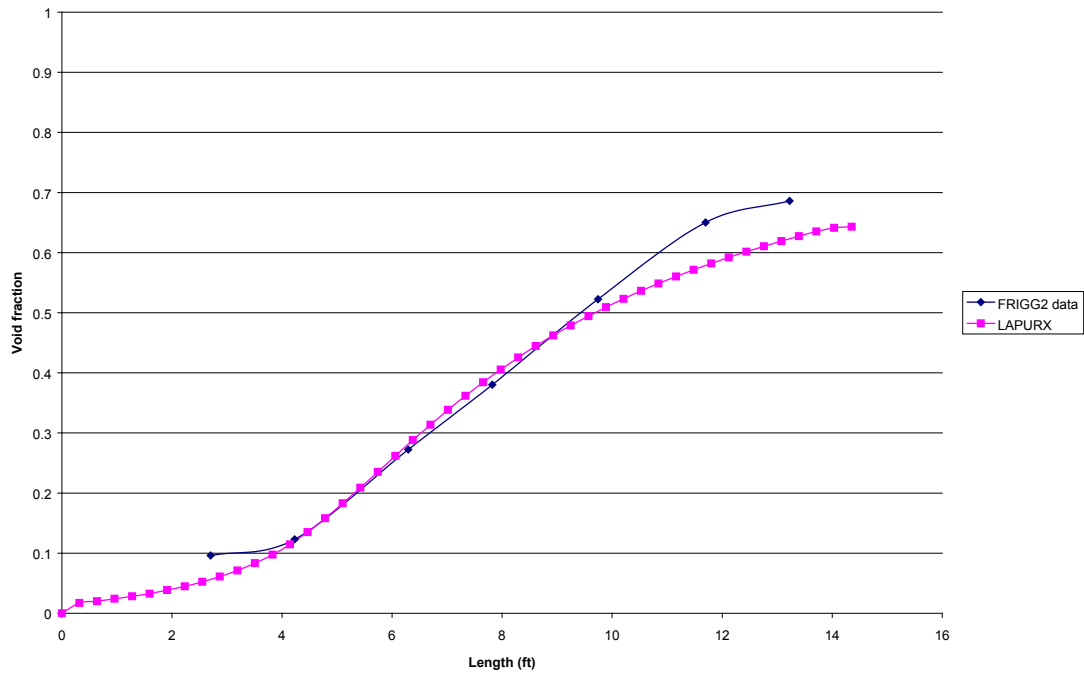


Figure 5.5 Void fraction of FRIGG-2 Test 313020

FRIGG-2 test 313024

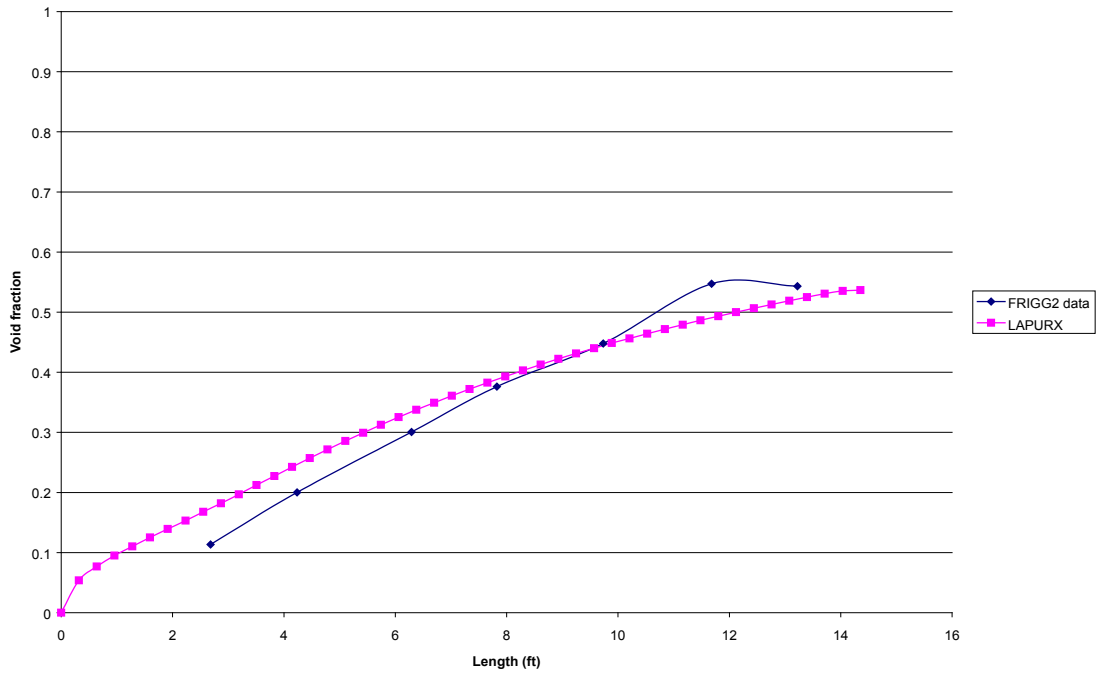


Figure 5.6 Void fraction of FRIGG-2 Test 313024

## **6. Comparison of Cofrentes Nuclear Power Plant Measured Decay Ratios to LAPUR6 Results**

### **6.1 Cofrentes Nuclear Power Plant**

The Cofrentes NPP is located 2 kilometers from the village of Cofrentes, in the province of Valencia, on the right bank of the river Júcar, very close to the Embarcaderos reservoir, which serves as a cooling source for the plant.

The plant is equipped with a General Electric BWR/6-type boiling water reactor, with a thermal power level of 3,237 MW and an electrical output of 1,092 MW. Plant cooling is accomplished by means of two natural draught cooling towers, each with a capacity of 50%. The total surface area of the site is 300 Ha.

The construction permit for the Cofrentes NPP was granted in 1975, and the plant was connected to the national grid 9 years later, in October 1984.

### **6.2 Stability Control in Cofrentes Nuclear Power Plant**

The Enhanced Option I-A E1A stability solution has been adopted by IBERDROLA as a long-term strategy for stability control of the Cofrentes NPP. Enhanced Option I-A E1A, developed by General Electric Company (GE) and BWR Owners Group, complies with General Design Criterion 12 of 10CFR50.55 Appendix A through the use of licensing features that prevent reactor instabilities from occurring under operating conditions that can be reasonably anticipated.

A design philosophy of progressive protection is coupled with a conservative approach by means of stability regions boundaries and mandated operator actions. The Exclusion Region is analytically defined to be that area of the licensed core power and flow operating domain where the reactor is susceptible to coupled neutronic/thermal-hydraulic instability. The reactor is automatically prevented from operating in this excluded region by the APRM flow-biased reactor trip function of the Neutron Monitoring System (NMS).

The Restricted Region of E1A is defined to be that area of the licensed core power and flow operating domain where the reactor is susceptible to coupled neutronic/thermal-hydraulic instability without regard to core void distributions. Automatic controls such that E1A APRM control-rod block set points, as well as administrative controls (boiling boundary), are implemented to prevent entry into the Restricted Region during scheduled reactor operation. Anticipated transients that originate outside the Restricted Region and terminate inside the Restricted Region are not expected to result in reactor instability. However, continued operation inside the Restricted Region is not permitted without putting in place specified administrative controls.

The Monitored Region is defined as that area of the core power and flow operating domain where the reactor may be susceptible to reactor instabilities *under conditions exceeding* the licensing basis of the current reactor system. This defense-in-depth feature is provided to preclude reactor instability even under unanticipated conditions. Continued operation within the Monitored Region boundary requires the presence of an automatic stability detection system. Defense-in-depth features are incorporated into the solution to improve overall reactor safety.

The E1A methodology application process is designed such that the E1A stability methodology can be implemented in any GE design BWR using qualified stability analytical tools. Decay ratio calculations form the framework for the generation and validation of the stability region boundaries.

The qualified stability analytical tool used in the E1A Cofrentes application is LAPUR6. A methodology for calculating decay ratios using LAPUR6 has been developed (Methodology, 2006) in which a validation matrix is defined against analytical and plant-measured decay ratios. The methodology application is designed to perform the Generation and Validation evaluations of E1A Regions for Cofrentes based on decay ratio calculations.

Decay Ratio On-line Predictor (DROP) is a research and development project being carried out by IBERDROLA jointly with the Polytechnic University of Valencia. The purpose of the DROP project is to develop a predictor-monitor system for computing the stability margin in BWRs based on LAPUR6 frequency domain code. One of the tasks for the DROP project has been the validation of LAPUR6 presented in this document.

### **6.3 Methodology of Calculating Decay Ratios with LAPUR6**

The methodology is based on an automated procedure for generation of LAPUR6 input and for checking the consistency of LAPUR6 results. Core channels will be grouped according to the number of LAPUR thermal-hydraulic regions necessary to take into account the core radial power distribution.

The grouping criteria is based on

- relative power fraction,
- different fuel designs mixed in the core, and
- peripheral or non-peripheral channel. Peripheral channels have a bottom entry orifice (BEO) instead of a side entry orifice (SEO). Peripheral channels are typically collapsed into a single LAPUR-averaged channel for each type.

In order to ensure the quality of the process, the following set of internal validations has been defined.

- Consistency of collapsed LAPUR6 radial and axial power thermal-hydraulic regions with SIMULATE power radial and axial peaking factors
- coherence of LAPUR6 flow distribution and core pressure drop with SIMULATE output

The following chain of codes is used.

- The SIMULATE (Studsvik, 2007) computer code is the 3D core simulator used to calculate the core detailed hydraulic and neutronic configuration of the different state points for analysis. The Cofrentes NPP core monitoring system, CAPRICORE, is based on SIMULATE (Albendea and Crespo, 2000) and can configuration data for LAPUR6 either to predict stability margins on-line or to perform stability licensing calculations off-line.
- PAPU (UPV, 1998) is a post-processor used to obtain Doppler and reactivity density coefficients from the perturbation calculations performed by SIMULATE around the base case.

- LIP pre- and post-processor (Tofiño, 2004; IT-COSNU-260, 2006) extracts from the SIMULATE summary and output file a database for all core assemblies classified according to type in different output files and generates the complete input data for LAPUR. The process is completely automated and can use LAPUR6 to either predict stability margins on-line or to perform stability licensing calculations off-line.

#### 6.4 Decay Ratio and Frequency Validation: Start-up and End-of-Cycle Coastdowns

The purpose of this validation set was to qualify LAPUR6 as a stability on-line predictor; therefore, the same automated procedure (CC-COSNU-445, 2006) was followed for all decay ratio calculations.

Average Power Range Monitor (APRM) and Local Power Range Monitor (LPRM) data were collected during the Cofrentes NPP Cycles 16b and 17 coastdown and Cycles 17 and 18 start-up (summer 2007 and November 2009). Cycle 16 is split up in two periods (16a and 16b) due to a fuel failure in mid-cycle, and Cycle 16b corresponds with the Cycle 16 End of Cycle (EOC) after discharging the failed fuel in a mid-cycle outage. The signals were analyzed with noise techniques, and the experimental decay ratios were compared against LAPUR6 calculations.

The data acquisition system used is the standard of the plant. A sampling rate of 20 Hz for 10 minutes was recorded for each state point in a typical Tabular Trend Report.

Figure 6.1 shows a typical EOC coastdown. The plant is operating in Final Feedwater Temperature reduction operation mode (FFWTR). For the shutdown, the operating crew restores feedwater heaters to increase feedwater temperature. The negative reactivity insertion helps to shut down the reactor. Control rod insertion and core flow decrease allow downshift of the recirculation pumps and uncoupling of the generator, which finally leads the reactor to cold shutdown.

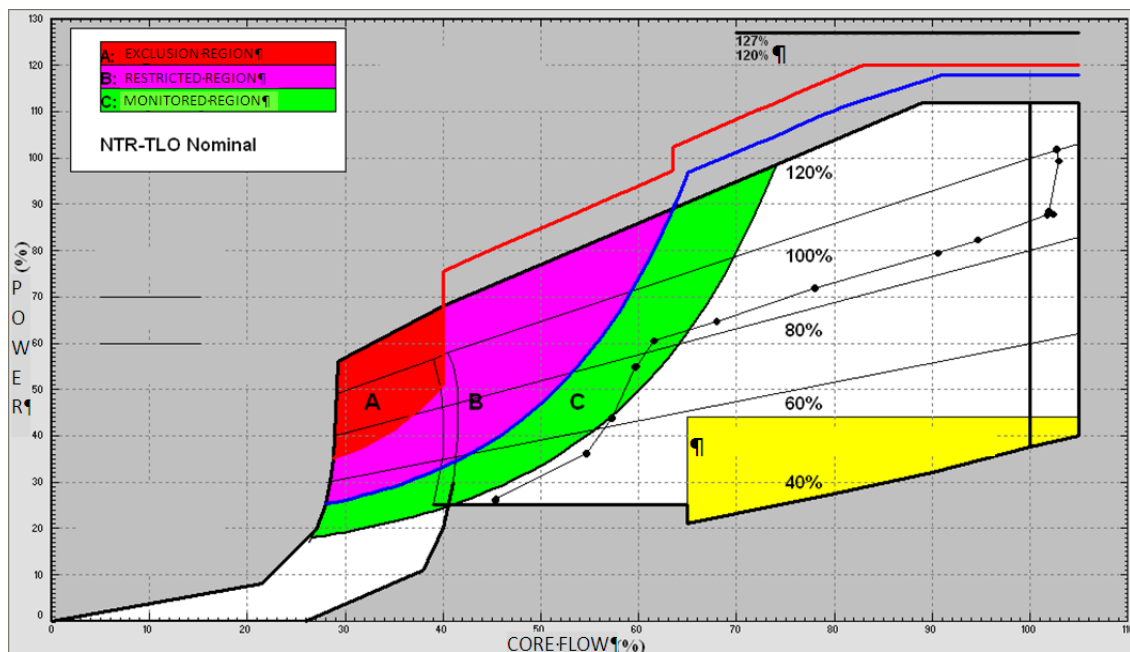


Figure 6.1 Typical path during EOC coastdown (Cycle 16b)

At EOC, the void coefficient reaches the maximum absolute value, and higher decay ratios than at the Beginning of Cycle (BOC) are expected. APRM and LPRM data were taken at power levels close to 90%, 80%, 70%, 50%, and 40% for EOC Cycles 16b and 17. Two additional state points close to 30% and 20% were taken for EOC Cycle 17. During 16b and 17 coastdowns, a total of 12 recordings of 10 minutes were taken.

Figure 6.2 shows the typical path during a start-up. For low-power conditions, a GE-BWR-6 operates with recirculation pumps at low speed and the FCVs close to 50%. When the power is above 25% and before the upshift, entry in Region B is required for a period, and E1A average boiling boundary control above 4 ft (the lowest one-third of the core) using a shallow control rod pattern is mandatory. With a fraction of core boiling boundary (FCBB) greater than 1, that is, a core boiling boundary above 4 ft, Restricted Region FCTR control rod block set points are switched to setup mode to allow entry in this region (blue arrow number 1 in Figure 6-2). During the maneuver, the FCV position has to be less than 5% to avoid a high peak of neutron flux (blue arrow number 2 in Figure 6-2). From this last state point and power above 25%, the cavitation interlock allows upshift recirculation pumps to operate at high speed (blue arrow number 3 in Figure 6-2). After the upshift, withdrawal of the required control rods in order to reach full power has to be performed out of the Restricted Region because simultaneous boiling boundary control and rod withdrawal is not possible. In order to withdraw enough control rods to reach the target rod pattern, the power ascension is performed inside the Monitoring Region but not too far out of the Restricted Region Boundary.

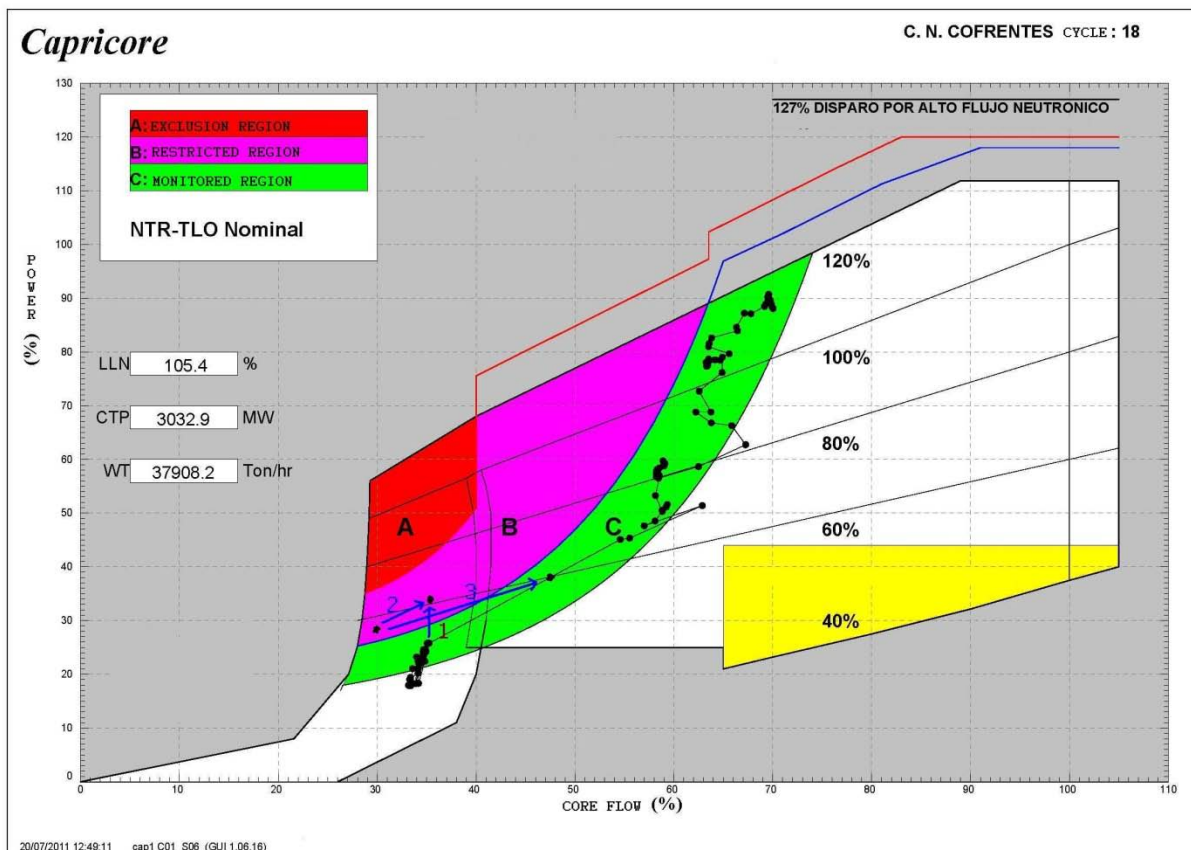


Figure 6.2 Typical start-up path (Cycle 18)

### 6.4.1 Generation of SIMULATE-3 Core Configuration Data

As described previously, SIMULATE-3 (Studsvik, 2007) is the nodal simulator used by IBERDROLA for core following and design. It is also the calculation engine for the core monitoring system CAPRICORE ( Albendea and Crespo, 2000). Using real data from the core monitoring system, start-ups and coastdowns are simulated taking into account enough steps to reasonably follow the xenon transient. In Figure 6.3, each marked diamond is a step in the Cycle 18 start-up power history. The black continuous line represents one real state point taken into account in the SIMULATE-3 start-up simulation.

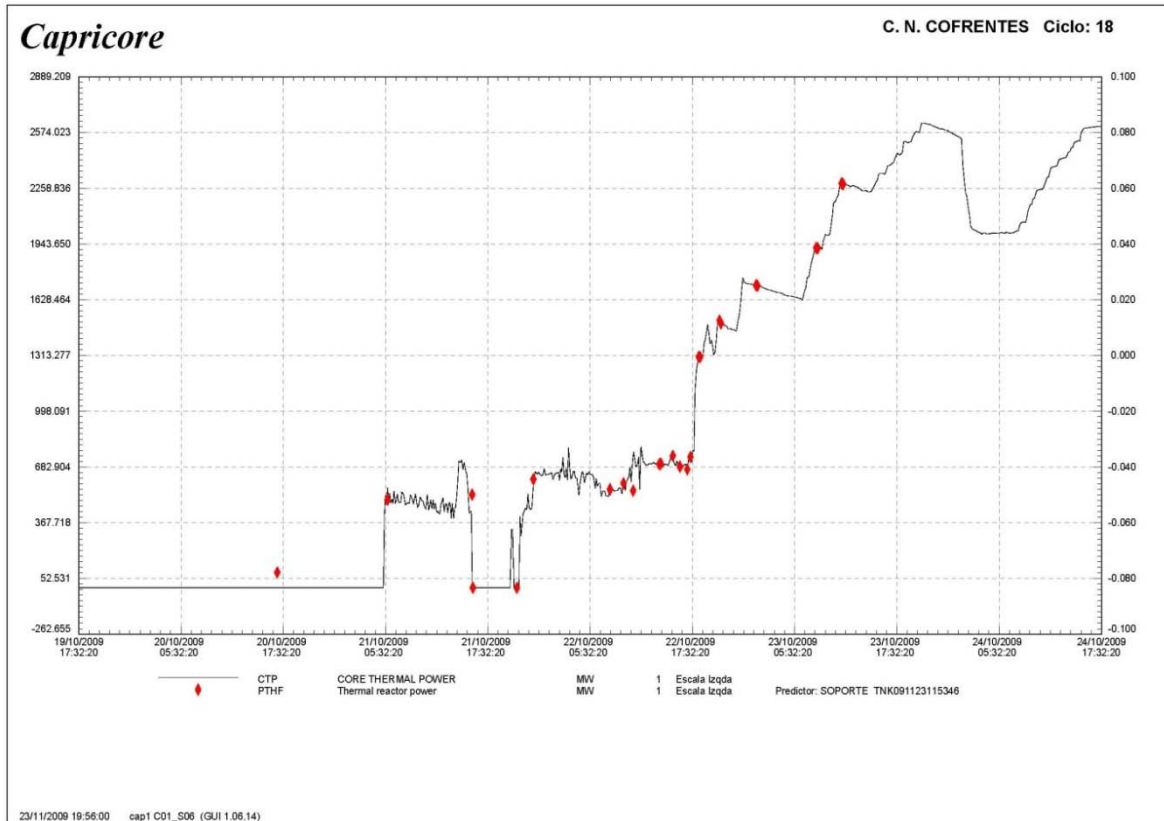


Figure 6.3 Power history used for SIMULATE-3 simulation of Cycle 18 start-up

### 6.4.2 Time Series Analysis of Signal for Decay Ratio Estimation

Different signal time series analysis methods can be used for decay ratio estimation (Verdu et al., 2001; March-Leuba, 1984). After a detailed review of the different time series analysis methods, a method based on the interpolation of an autocorrelation function was selected. The robustness of this method was tested over a full range of decay ratios values using analytical and real signal analysis. A decay ratio monitor called SMART has been developed by the Universidad Politécnic de Valencia (Spain) jointly with IBERDROLA (Montesinos et al., 2010). The SMART stability monitor, which was developed with MATLAB, will be used for autocorrelation-based decay ratio estimation.

### 6.4.3 Results of Decay Ratio and Oscillation Frequency

According to the procedure described previously, decay ratios from the APRM's autocorrelation function, natural frequency, and the equivalent from LAPUR were estimated.

In Figure 6.4, averaged APRM versus LAPUR results are shown. As can be seen, the frequency trend is consistent. The decay ratio values are very low, mainly because at end of the cycle the axial power profile is top peaked, which has a stabilizing effect. The state points analyzed appear along the Monitoring Region boundary (green line), which is the locus of a 0.4 decay ratio value. Values obtained were well below Monitoring Region criteria, which indicates the degree of conservatism of the E1A methodology.

Figure 6.5 shows slightly lower values in BOC start-ups when compared with EOC coastdown. Because the reactor power was close to 25% thermal power and 35% core flow for 12 h due to typical tuning problems during the first start-up after the outage, four sets of 10 minute data were taken during this 12 h interval to account for the xenon effect.

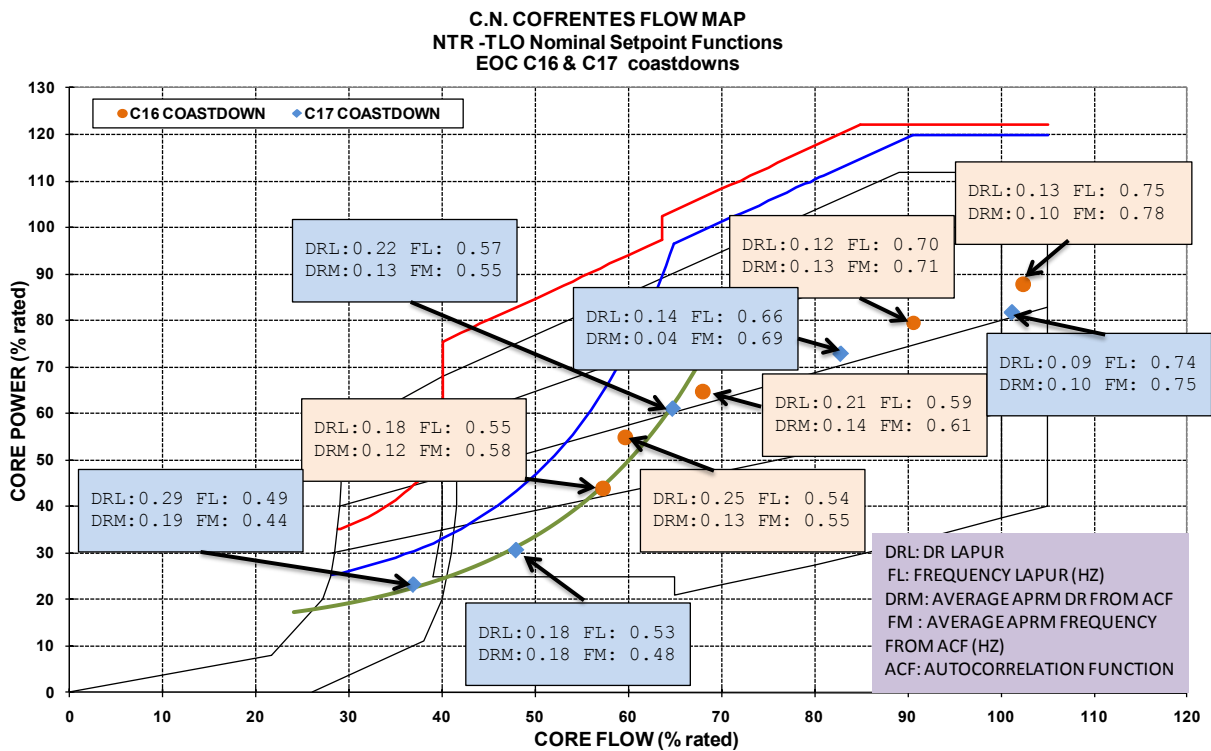
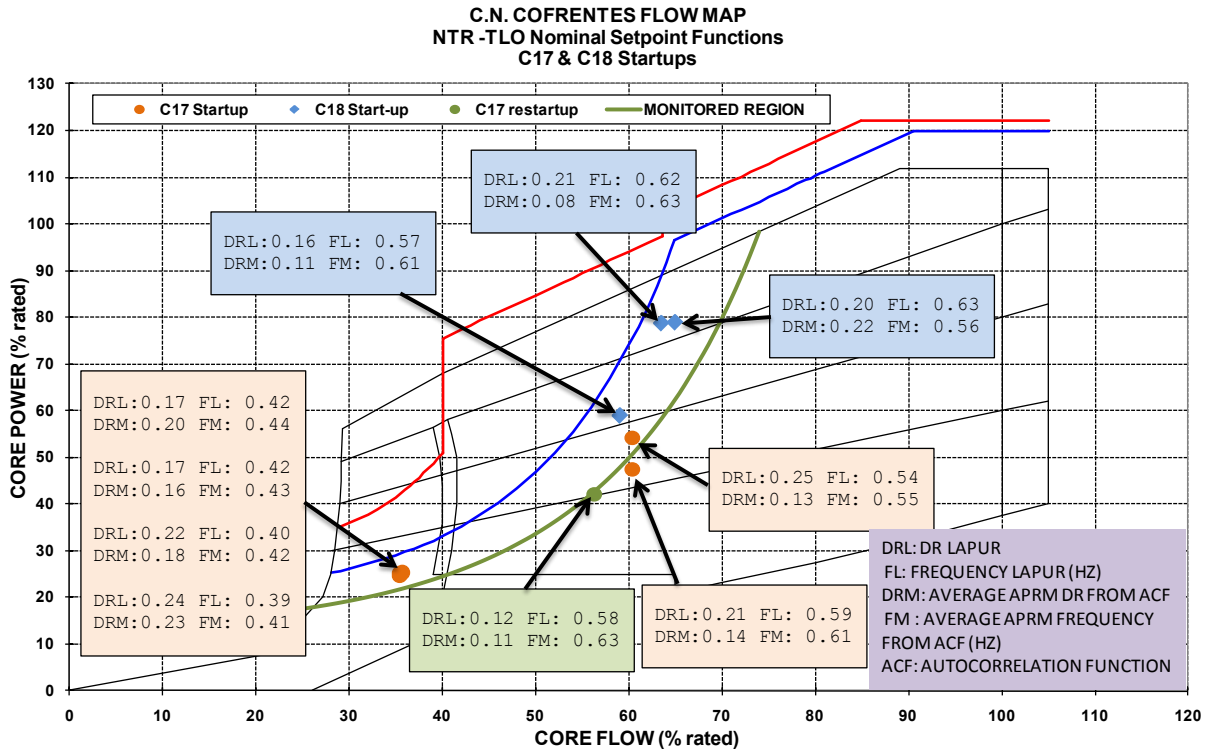


Figure 6.4 Average APRM decay ratio and frequency versus LAPUR results (EOC Cycles 16 and C17 coastdowns)



**Figure 6.5 Average APRM decay ratio and frequency versus LAPUR results (Cycles 17 and 18 start-ups and coastdowns)**

The values obtained in the four sets of LAPUR calculations are very similar. Decay ratios were obtained at the highest flow rate between 55 and 65%, core flow was around 0.2, and natural frequency was around 0.55–0.63 Hz. Decay ratios were lower in comparison with decay ratio criteria of the Monitoring Region.

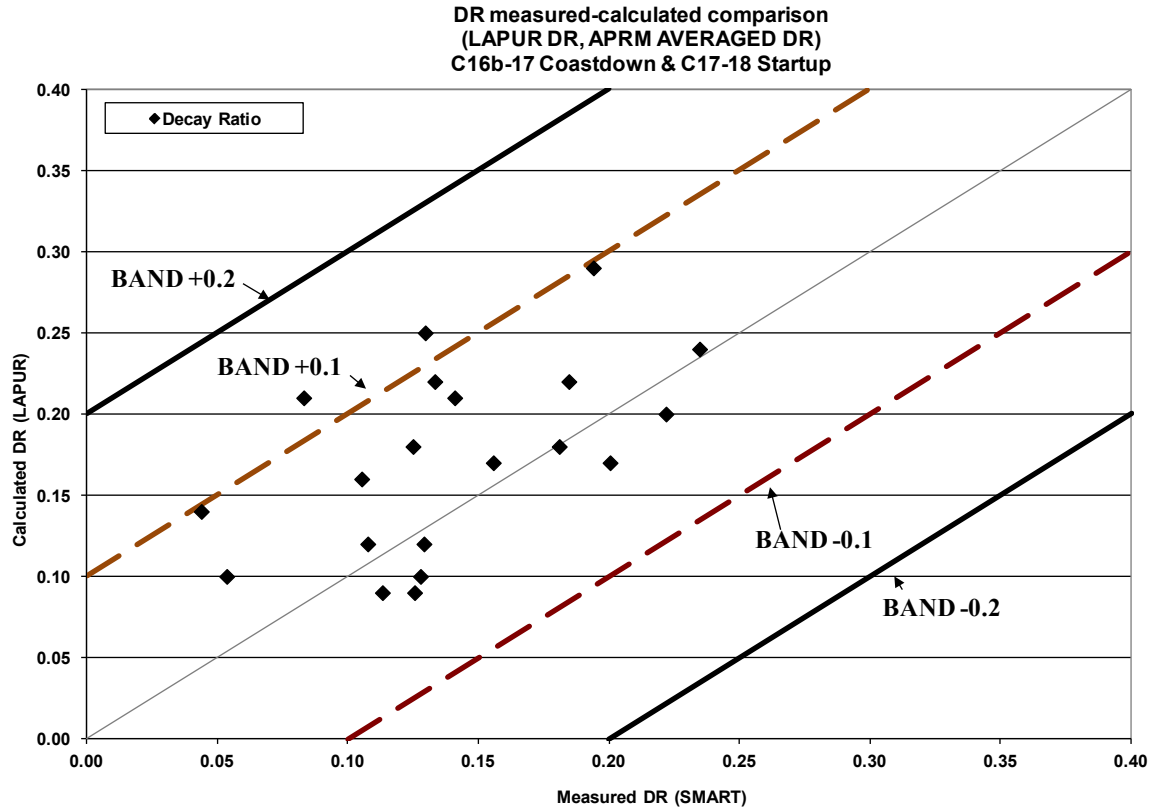
The hottest channel decay ratio for each fuel design was isolated in a LAPUR channel, and exclusive thermal-hydraulic (without neutronic feedback) decay ratio calculations were simultaneously performed for each hot channel. Hot channel decay ratio was close to zero for all of state points.

Obtaining decay ratios from LPRM data was not possible because the signal to noise level was not sufficient to obtain consistent results.

#### 6.4.3.1 Analysis of data

Estimated decay ratio and natural frequency based on autocorrelation function are in good agreement with LAPUR results.

The results shown in Figure 6.6 are in the  $\pm 0.1$  band, with noticeably good agreement for the low decay ratios.



A bias of 0.3 was obtained by subtracting the SMART decay ratio from the average of LAPUR decay ratio and shows a slightly conservative trend in LAPUR predictions. The sample standard deviation is 0.05, which shows a very reasonable dispersion.

Figure 6.7 shows the natural frequency agreement between LAPUR and SMART. A bias of 0.0 Hz was obtained by subtracting the SMART frequency from the average LAPUR frequency, with a sample standard deviation of 0.04, which shows a very low dispersion of frequency prediction. LAPUR predicts very accurately natural frequency in the 0.40–0.80 Hz.

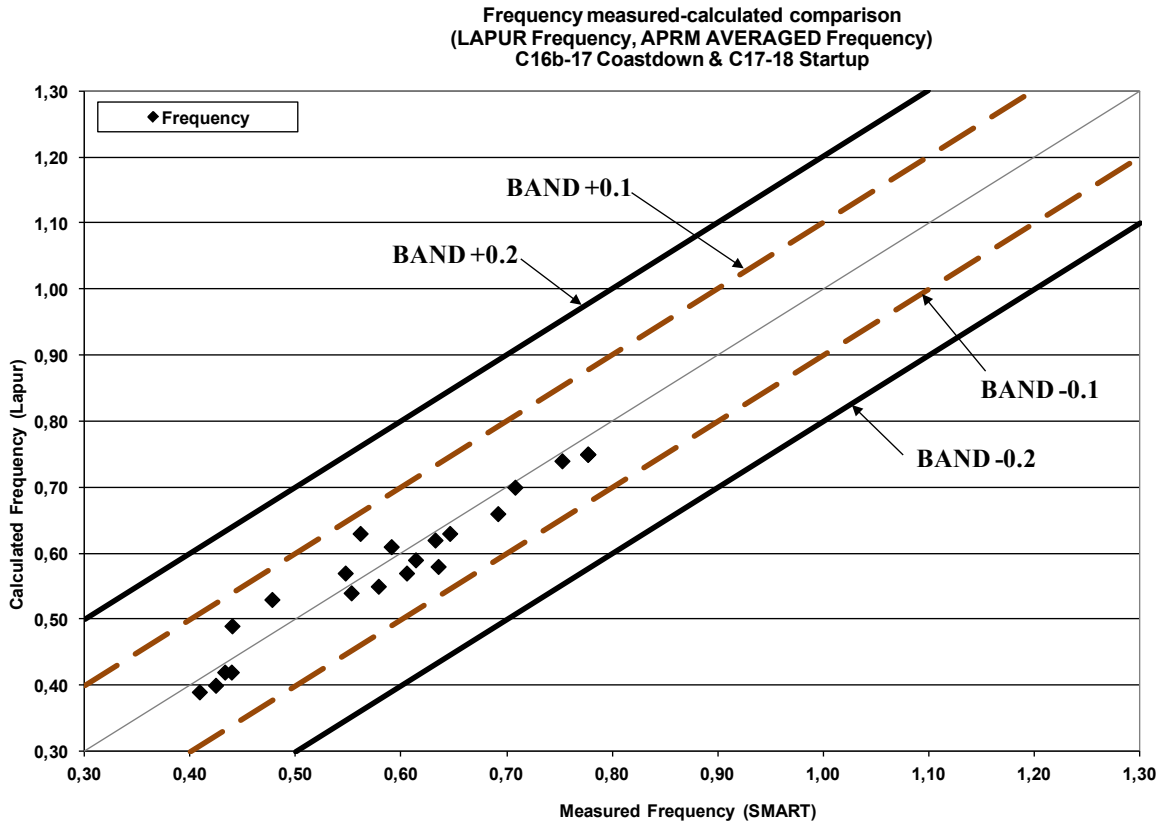


**Figure 6.7 Natural frequency based on monitor SMART versus LAPUR**

### 6.4.3.2 Comparison of SMART frequency and power spectral density peaks

In this section, SMART natural frequency based on autocorrelation function is compared with the resonance peaks of a non-parametric spectrum estimation based on Welch's method and a Hanning window (Proakis and Manolakis, 1998), with a segment window length to obtain a resolution of 0.1 Hz. Figure 6.8 compares LAPUR-calculated frequency to the closest frequency peak of Welch's method spectrum estimation. The periodogram is composed of several peaks. The three highest peaks are extracted, and the closest to autocorrelation-based frequency is plotted against LAPUR-calculated frequency. Due to the low energy of the peaks that is consistently obtained with low decay ratios, a few frequency results are inconsistent, but the majority are reasonably consistent, as shown in the figure.

For the frequency comparison which is out +0.2 band (0.34 PSD, 0.63 LAPUR) when a 0.05 Hz resolution periodogram is obtained, there is a peak close to LAPUR frequency. Figures 6.9 and 6.10 show periodograms with two different resolutions.

Because the decay ratio is very low, the PSD peaks have very low energy, as shown in Figs. 6.9 and 6.10.

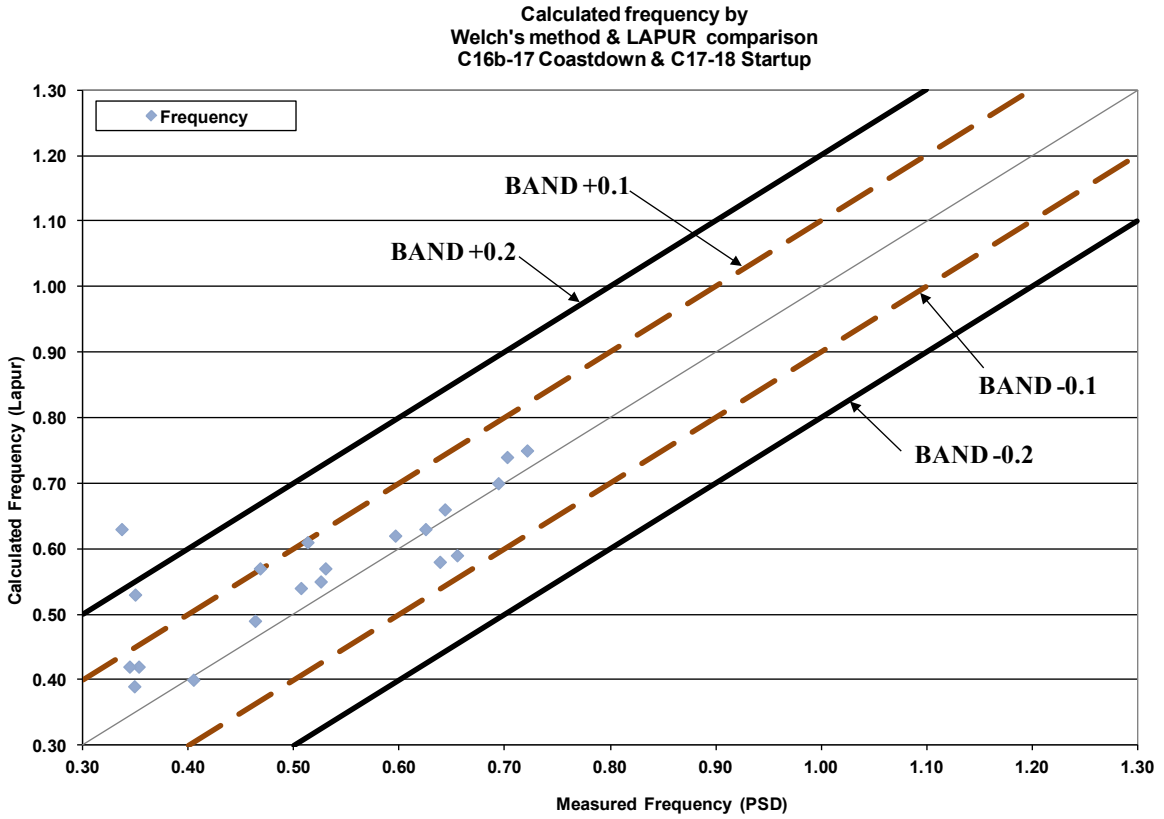
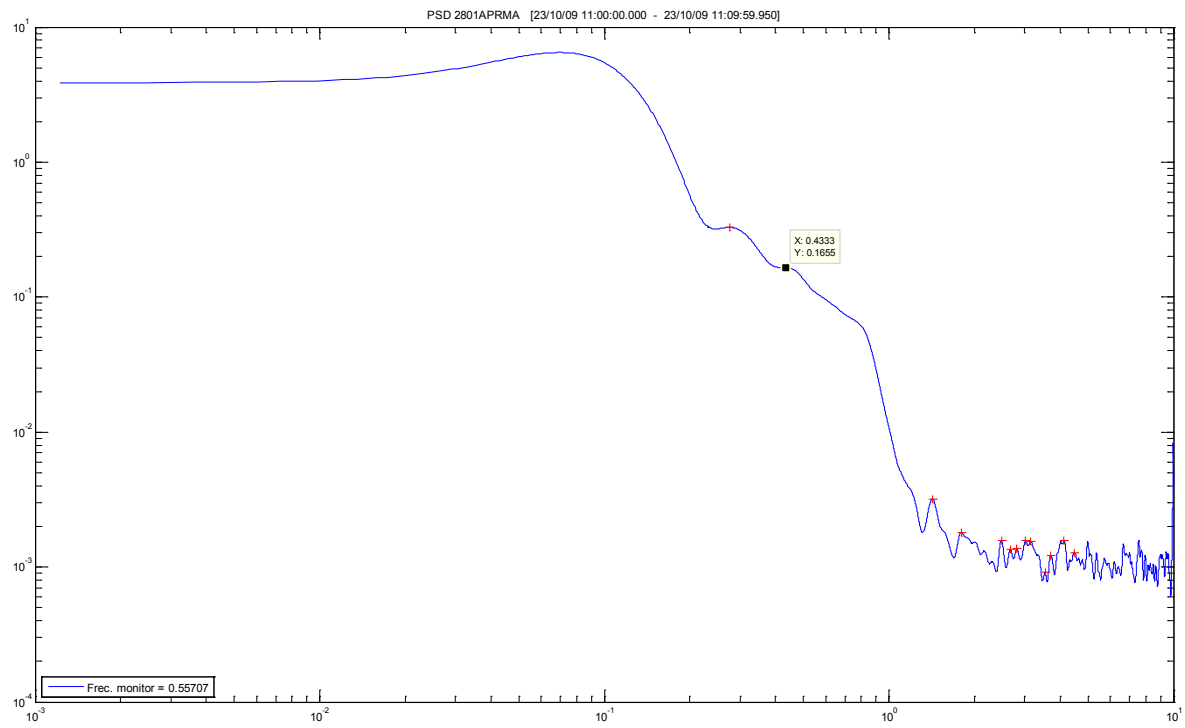
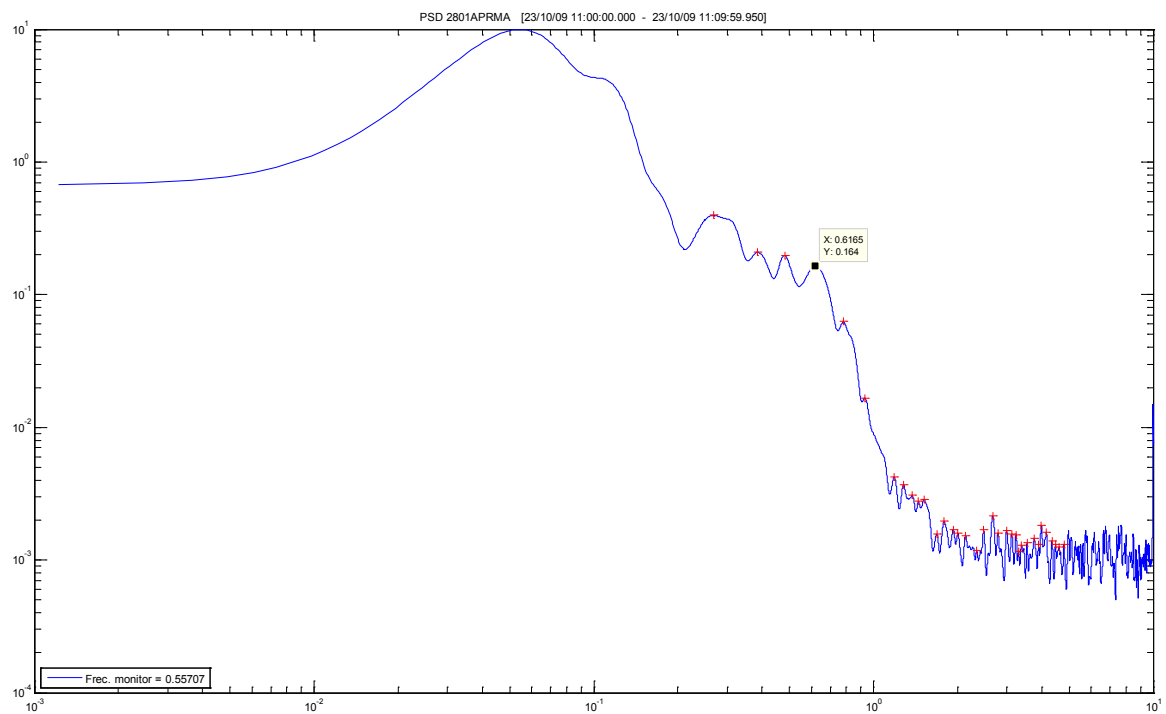


Figure 6.8 Comparison of Welch's method periodogram and LAPUR-calculated frequency



**Figure 6.9 Welch's method periodogram at 0.1 Hz resolution**



**Figure 6.10 Welch's method periodogram at 0.05 Hz resolution  
(peak close to LAPUR frequency)**

## **6.5 Decay Ratio and Frequency Validation: Cofrentes Cycle 6 Instability**

### **6.5.1 Event Description**

Shortly after 12 o'clock noon on January 29, 1991, a nuclear thermal-hydraulic instability event occurred during the start-up sequence approximately 30 h after a scram for full power. Conditions at the plant at the time of the event were as follows.

- Middle of cycle at an exposure of 4478 MWD/ST of a planned 9500 MWD/ST cycle.
  - Recirculation pumps motors at low speed
  - Flow control valves at minimum position
- One feedwater train was out of service (6A) and the other (6B) was being placed in service.
- Steam bypass valves closed

The operators were withdrawing control rods when oscillations of approximately 10% peak-to-peak of scale were observed. Event descriptions and stability analysis performed with LAPUR can be also found in IT-CONUC-028, 2006).

### **6.5.2 Setup of the Core Configuration**

The core configuration was updated using SIMULATE 6.07.15. The first step consisted of identifying the closest SIMULATE restart file to the event, in this case at the beginning of the Cycle 6. This initial restart corresponded to SIMULATE input data from the core following runs. After locating the initial restart file, four SIMULATE runs were conducted to reproduce the core configuration at the beginning of the event.

The first run of SIMULATE updated the core burnup conditions and initialized the xenon transient. For this reason, the reactor was brought to previous scram (01/28/91) conditions. The second run reproduced the scram and considered the reactor shutdown interval until the next startup. Taking into account this time interval was necessary in order to perform the xenon transient calculation. The third run was necessary to enter the time in hours between the shutdown and the start-up beginning xenon transient calculation. The start-up beginning time was unknown, so the interval in hours between the shutdown and the criticality was used as an acceptable approximation. Finally, the fourth run was necessary to calculate the core configuration at the 01/29/91 state point.

### **6.5.3 LAPUR Input Data**

Core channels have been grouped in six regions. In Cycle 6, the core was composed of 8×8 fuel. Two independent LAPURX grouping criteria, one for wide core decay ratio calculation, maintaining a power fraction per the sixth region less than 20%, and a second criteria isolating the hottest channel in one additional region and the other ones with a power fraction less than 20%. Tables 6.1 and 6.2 show the final power distribution obtained.

**Table 6.1 Number of channels assigned to LAPUR for channel decay ratio calculations**

State point	Channel 1	Channel 2	Channel 3	Channel 4	Channel 5	Channel 6
012991	91	100	108	127	122	76
Power fraction	0.19863	0.19964	0.19833	0.19984	0.15016	0.05342

**Table 6.2 Number of channels assigned to LAPUR for channel decay ratio calculations**

State point	Channel 1	Channel 2	Channel 3	Channel 4	Channel 5	Channel 6	Channel 7
012991	1	91	100	109	127	120	76

Reactor conditions at the beginning of the event are illustrated in Table 6.3.

**Table 6.3 Reactor conditions at the beginning of the event**

System pressure	969.1 psia
Core inlet enthalpy	477.97 BTU/Lb
Core power	1180.7
Core flow rate	25.940E6 lb/h
Bypass flow rate	1.0631E6 lb/h

#### 6.5.4 LAPUR6 Results

SIMULATE and LAPUR core pressure drops are consistent. A summary of these results is shown in Table 6.4.

**Table 6.4 Simulate LAPUR pressure drops comparison**

State point	SIMULATE core pressure drop (psi)	LAPUR core pressure drop (psi)	Error (%)
012991	5.811	5.841	0.525

Additionally, the consistence between flow distribution from SIMULATE and LAPUR has been verified. Results are shown in Table 6.5.

**Table 6.5 Comparison of SIMULATE and LAPUR flow rate channels**

State Point 012991	SIMULATE (lb/h)	LAPUR (lb/h)	Error (%)
Channel 1	464754	455640	-1.961
Channel 2	522561	514090	-1.621
Channel 3	574250	567400	-1.193
Channel 4	685725	684480	-0.182
Channel 5	648533	663360	2.286
Channel 6	238338	248790	4.385

### 6.5.5 Decay Ratio Values Analysis

- Execution for wide-core decay ratio—global decay ratio is directly obtained from LAPURW output file
- Execution for channel decay ratio—Channel decay ratio is also obtained from LAPURW output file.
- Out-of-phase decay ratio is calculated. An estimated value of the eigenvalue for the first harmonic flux solution (-1.06\$) has been used.

The core-wide, out-of-phase, and the highest value of the individual thermal-hydraulic channel decay ratios (the hottest channel) are provided in Table 6.6.

**Table 6.6 State point 290191 decay ratio values**

Power (MW)	Flow (MLb/h)	Core decay ratio	Frequency (Hz)	Channel decay ratio (1HC)	Out-of-phase decay ratio (-1.06\$)
1108.4 (40.8)	25.94 (30.7%)	0.75	0.41	0.69	0.78

The high value of hottest channel decay ratio indicates the high susceptibility of the core to oscillate locally and out of phase.

### 6.5.6 APRMs Signal Analysis

APRMs signals are available from the event, as shown in Figure 6.11. Applying Welch's method with a Hanning window to APRM A, the periodogram in Figure 6.12 is obtained. A double peak is clearly identified: the natural frequency and one harmonic, the double of the natural frequency. During BWR unstable oscillations, the fundamental mode of oscillation does not appear alone, but it appears to be always accompanied by at least the first axial oscillation mode. From observations of actual reactor instability tests and 3-D code simulations, it appears that the fundamental mode always excites at least the first axial mode (and probably all higher axial mode harmonics). This fact is an apparent paradox because, in principle, the different harmonic modes are orthogonal to each other, and therefore, one cannot excite the other. In summary, this effect can be explained by the fact that the reactivity feedback is nonlinear, and thus, linear mode orthogonality theorems do not apply (March-Leuba, 1992).

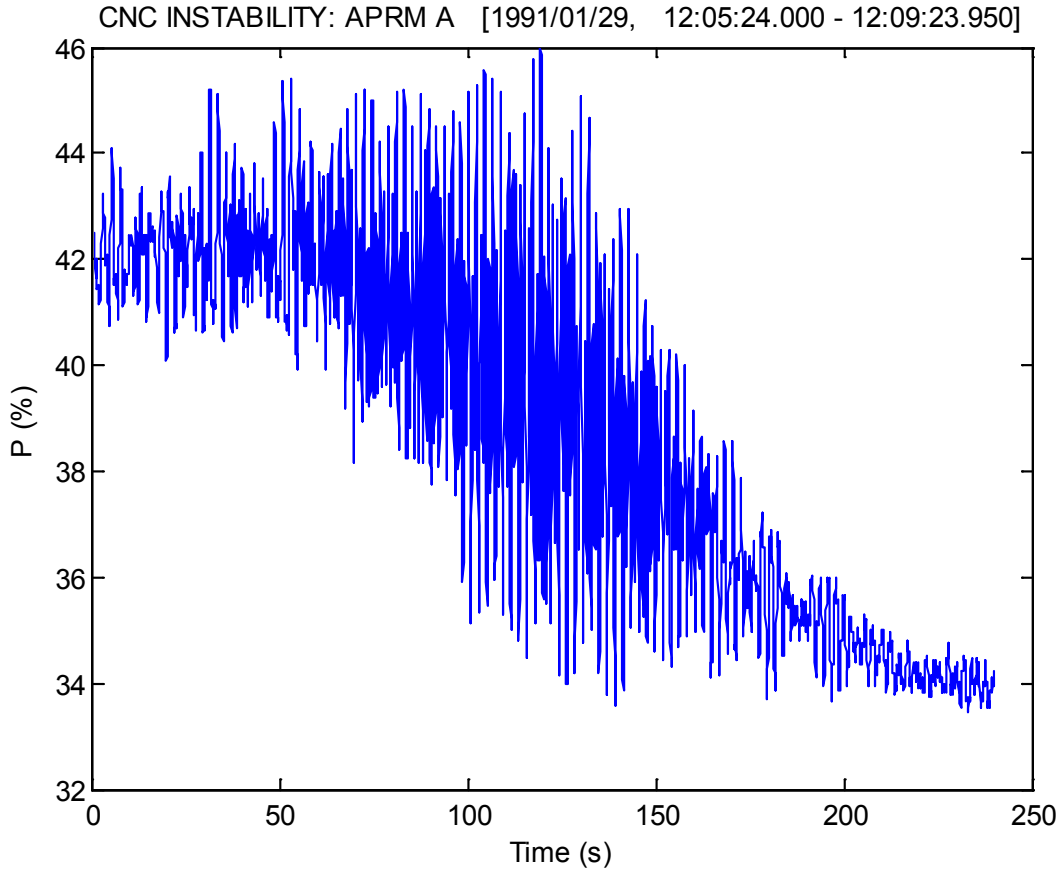


**Figure 6.11 APRM A 1991/01/29 Cofrentes instability event**

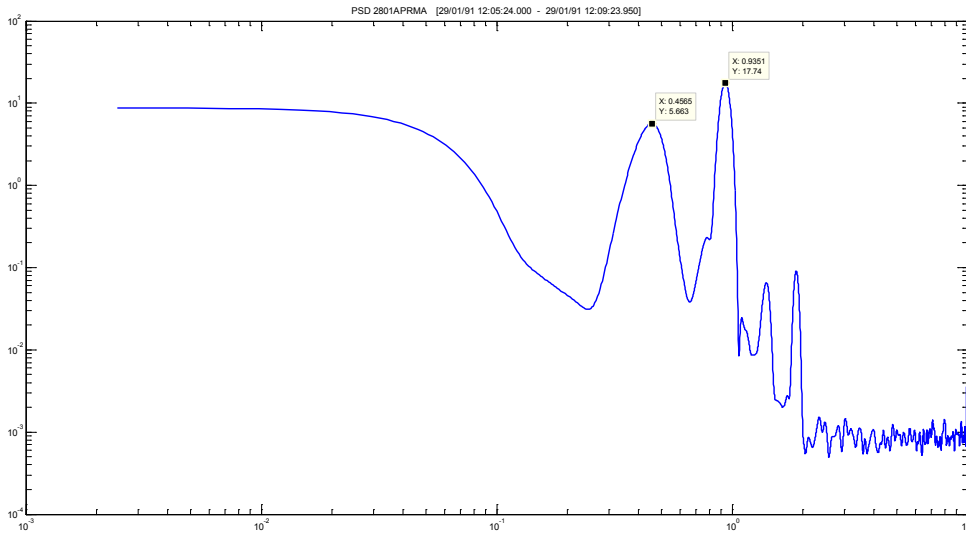


**Figure 6.12 PSD based on Welch's method periodogram (290191 Cofrentes instability)**

If a standard filter with a pass-band frequencies (0.3–1.3 Hz) is applied, as has been applied for analyses shown previously in this report, the mode with highest DR in the band is obtained which corresponds with the first axial mode (Table 6.7) and cannot be compared with wide-core decay ratios obtained from LAPUR.

In order to obtain autocorrelation-based decay ratios from fundamental mode and from the first axial oscillation mode, two types of notch Butterworth filter (Figure 6.13) have been applied to APRM signals in order to split up fundamental and first axial modes and obtain decay ratio separately. Figure 6.14 shows the effect of filters application in PSD. Results of applying a standard filter, filter type 1 and filter type 2, and filter specifications are shown in Table 6.7.

**Table 6.7 Filters applied to APRM signal**

	<b>Filter 1</b>	<b>Filter 2</b>
Pass-band frequencies	[0.3–0.6] Hz	[0.7–1.3] Hz
Stop-band frequencies	[0.2–4] Hz	[0.6–4] Hz
Pass-band ripple	1 dB	1 dB
Stopband attenuation	20 dB	20 dB

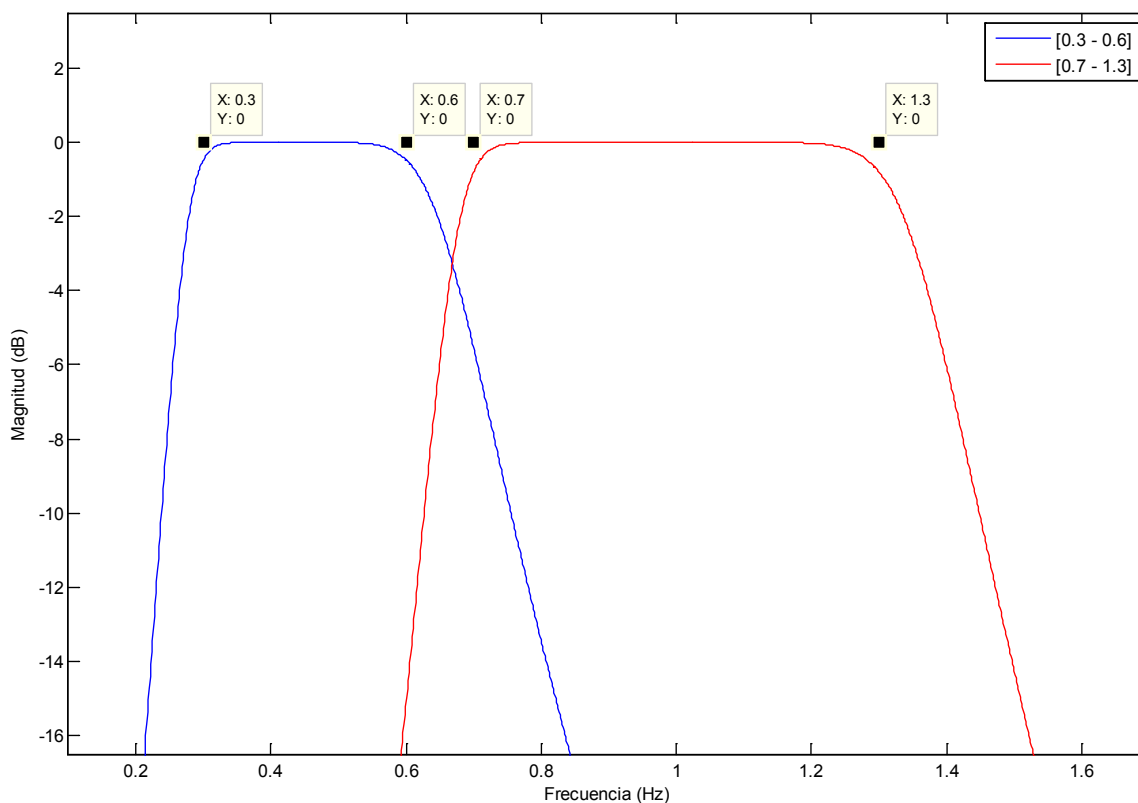


**Figure 6.13 Bode diagram of applied Butterworth filters to split up fundamental and first mode**

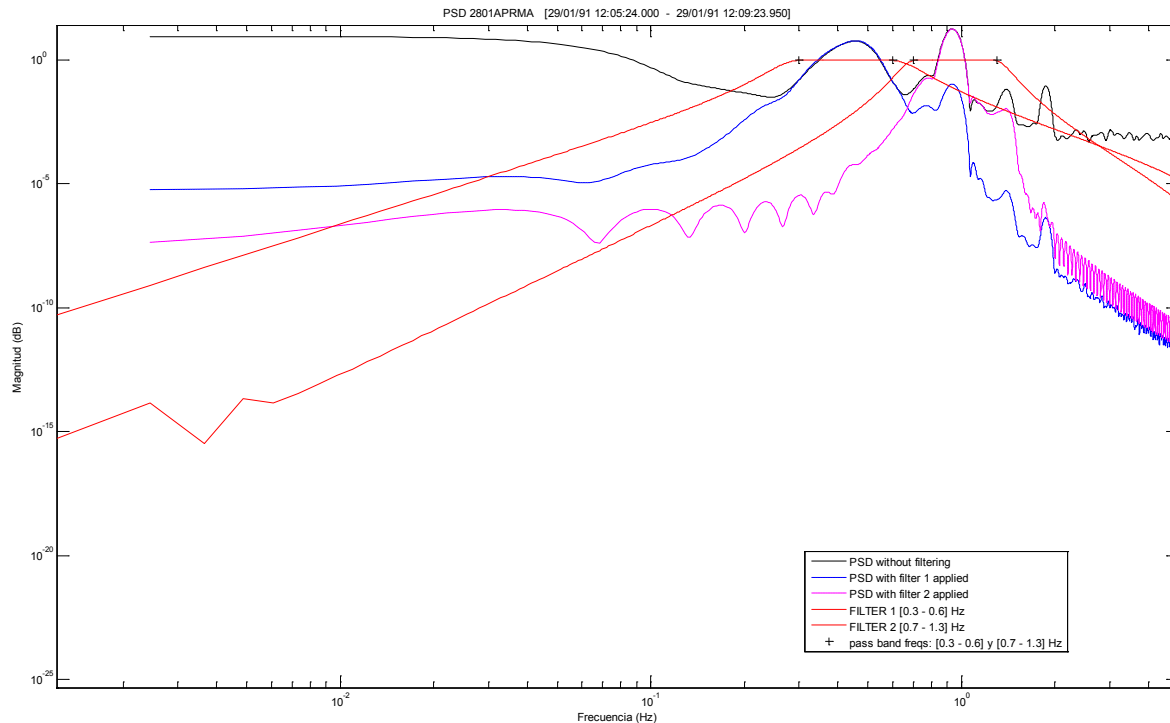


**Figure 6.14 Effect of type 1 and type 2 filtering in APRM A signal**

Note that the signal analysis with standard filter gives in the 7/8 APRM decay ratio for the harmonic, because of its highest decay ratio value. Agreement between results, filtering around fundamental frequency, and LAPUR wide-core results (decay ratio = 0.75 and frequency = 0.41 Hz) seems to be reasonable (Table 6.8).

## 6.6 LPRM and APRM Decay Ratio and Frequency Validation

Validations above are based on APRM data. Standard data acquisition system of the plant gives high enough sampling rate only for eight selected LPRMs (one from each APRM) selected from the  $33 \times 4$  levels = 132 LPRMs in the core. However, noise analysis of these LPRMs does not produce consistent noise analysis results. For decay ratio monitoring purposes, the availability of LPRM data with good properties in terms of noise quality is important. Capabilities for local analysis, coherence, and phase are welcome as well.

After searching the market for data acquisition systems with optima sampling rates and high-amplitude resolution in an analog-to-digital converter (16 bits), a RTP2316-M system was selected. The RTP2316-M Data Acquisition System was developed by RTP, a company with broad experience in the field of nuclear engineering. The model is a version of the RTP2300, which has been qualified as 1E Safety Class.

The system consists of the following:

- RTP2300-M chassis with 8 hot-swappable I/O cards with power input options of 115 V AC at 2.1 A, 230 V AC at 1.1 A or 24 V DC at 8 A. The chassis contains a dedicated PLD processor to perform I/O scanning.
- One node processor card, with a Mobile Intel Celeron Processor and 2 PCI-based 100 MHz full-duplex Ethernet controllers for input/output (I/O) communications.

**Table 6.8 Cofrentes 290191 instability (signal analysis results)**

FILTER 0.3-1.3 standard									
Sensor	Tiempo inicio	Tiempo fin tramo	DR 0.3-1.3	fRes 0.3-1.3	standard deviation	fPSD 1°	fPSD 2°	fPSD 3°	fPSD elegida
2801APRMA	05:24.0	09:23.9	1.00	0.94		0.94	0.46	0.78	0.94
2802APRMB	05:24.0	09:23.9	1.00	0.94		0.94	0.46	0.77	0.94
2803APRMC	05:24.0	09:23.9	1.01	0.95		0.94	0.47	0.78	0.94
2804APRMD	05:24.0	09:23.9	1.02	0.95		0.94	0.46	0.78	0.94
2805APRME	05:24.0	09:23.9	0.95	0.43		0.47	0.94	0.78	0.47
2806APRMF	05:24.0	09:23.9	0.51	0.42		0.94	0.46	0.79	0.46
2807APRMG	05:24.0	09:23.9	1.00	0.95		0.94	0.46	1.88	0.94
2808APRMH	05:24.0	09:23.9	1.03	0.94		0.94	0.46	0.78	0.94
FILTER 1 0.3-0.6						Aplicando el filtro también antes de la PSD:			
Sensor	Tiempo inicio	Tiempo fin tramo	DR 0.3-1.3	fRes 0.3-1.3	DR standard deviation	fPSD 1°	fPSD 2°	fPSD 3°	fPSD elegida
2801APRMA	05:24.0	09:23.9	0.74	0.47		0.46	0.77		0.46
2802APRMB	05:24.0	09:23.9	0.79	0.47		0.47	0.76		0.47
2803APRMC	05:24.0	09:23.9	0.78	0.47		0.46	0.77		0.46
2804APRMD	05:24.0	09:23.9	0.78	0.47		0.46	0.76		0.46
2805APRME	05:24.0	09:23.9	0.89	0.47		0.47	0.76		0.47
2806APRMF	05:24.0	09:23.9	0.80	0.47		0.46	0.77		0.46
2807APRMG	05:24.0	09:23.9	0.83	0.47		0.47	0.77		0.47
2808APRMH	05:24.0	09:23.9	0.68	0.47		0.46	0.77		0.46
		average	0.78	0.47	0.06			average	0.46
FILTER 2 0.7-1.3						Aplicando el filtro también antes de la PSD:			
Sensor	Tiempo inicio	Tiempo fin tramo	DR 0.3-1.3	fRes 0.3-1.3	DR standard deviation	fPSD 1°	fPSD 2°	fPSD 3°	fPSD elegida
2801APRMA	05:24.0	09:23.9	0.98	0.94		0.94	0.79	1.09	0.94
2802APRMB	05:24.0	09:23.9	0.98	0.94		0.94	0.78	1.09	0.94
2803APRMC	05:24.0	09:23.9	0.97	0.94		0.94	0.78	1.09	0.94
2804APRMD	05:24.0	09:23.9	0.98	0.94		0.94	0.78	1.09	0.94
2805APRME	05:24.0	09:23.9	0.98	0.94		0.94	0.78	1.09	0.94
2806APRMF	05:24.0	09:23.9	0.98	0.94		0.94	0.79	1.09	0.94
2807APRMG	05:24.0	09:23.9	0.98	0.94		0.94	0.79	1.09	0.94
2808APRMH	05:24.0	09:23.9	0.98	0.94		0.94	0.78	1.09	0.94
		average	0.98	0.94	0.002			average	0.94

- Two analog input cards: 8436/51 isolated analog input cards with eight input channels for ±10 V input data. Each of the eight channels is isolated with an anti-aliasing low-pass filter, multiplexed, and amplified before entering to a 16 bits bipolar A/D converter.
- Ethernet output connections to a computer for data collection.

APRM-C and related LPRMs analog volts data were connected to RTP2316-M input cards (Table 6.9).

**Table 6.9 RTP2316-M input channels**

Signals for each channel from RTP 8436/51 analog input cards		
Card 1	Card 2	Channel
APRM C	14-47A	CH0
22-23B	14-15A	CH1
22-23B → OPTOISOLATOR	46-15A	CH2
38-39B	46-31C	CH3
LOOP A JP FLOW	14-31C	CH4
LOOP B JP FLOW	30-47C	CH5
DOME PRESSURE	30-15C	CH6
38-07B	38-23D	CH7

APRM-C was bypassed in order to guarantee that any spurious signal could progress to any channel of the reactor protection system (RPS) due to was only a temporary connection. LPRM 22-23B was connected through an optoisolator to verify its effect in the noise quality.

### 6.6.1 New Data Acquisition System Test during Cycle 18 Sequence Exchanges (June 2010, September 2010)

During two consecutives control rod sequence exchanges, June and September 2010, data was taken according Table 6.9 scheme.

The June 2010 control rod sequence exchange, as shown in Figure 6.15, includes the verification of power flow map rod lines, specifically the 80% rod line.

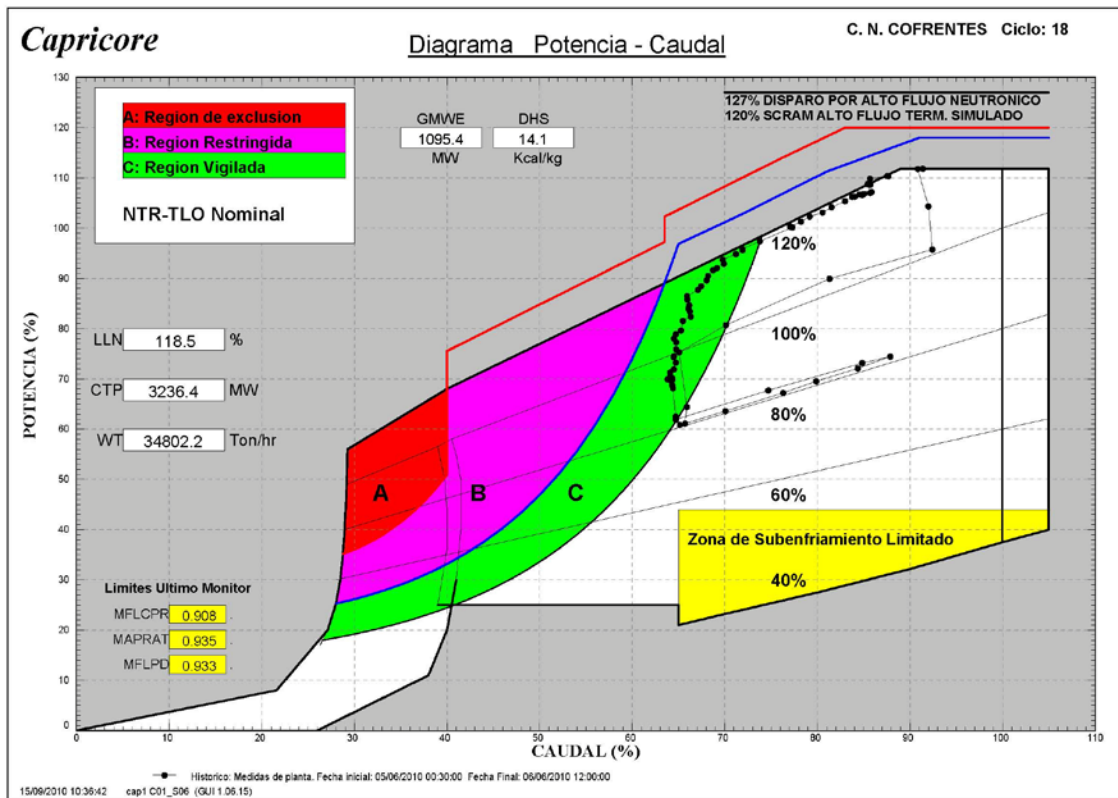


Figure 6.15 June 2010 control sequence exchange roadmap

Figure 6.16 (September 2010) shows a typical control rod sequence exchange. As can be seen in figures, control rod exchange is carried out between in the region C, E1A monitoring region. Conservatively, the right boundary of this region is considered the locus of power flow map conditions with a wide-core decay ratio of 0.4.

The procedure is clear: recirculation FCV closing to 70% of core flow; control rod insertion to 60–50% of power; sequence exchange at low power to minimize pellet clad interaction (PCI) contact in cladding; withdraw control rod to reach the PCI envelope; and finally increase core flow opening recirculation FCV, maintaining an increase of power around 20 MWe/h (60 MW thermal/h).

## 6.6.2 Signal Analysis

Signal quality results are summarized in Figure 6.17.

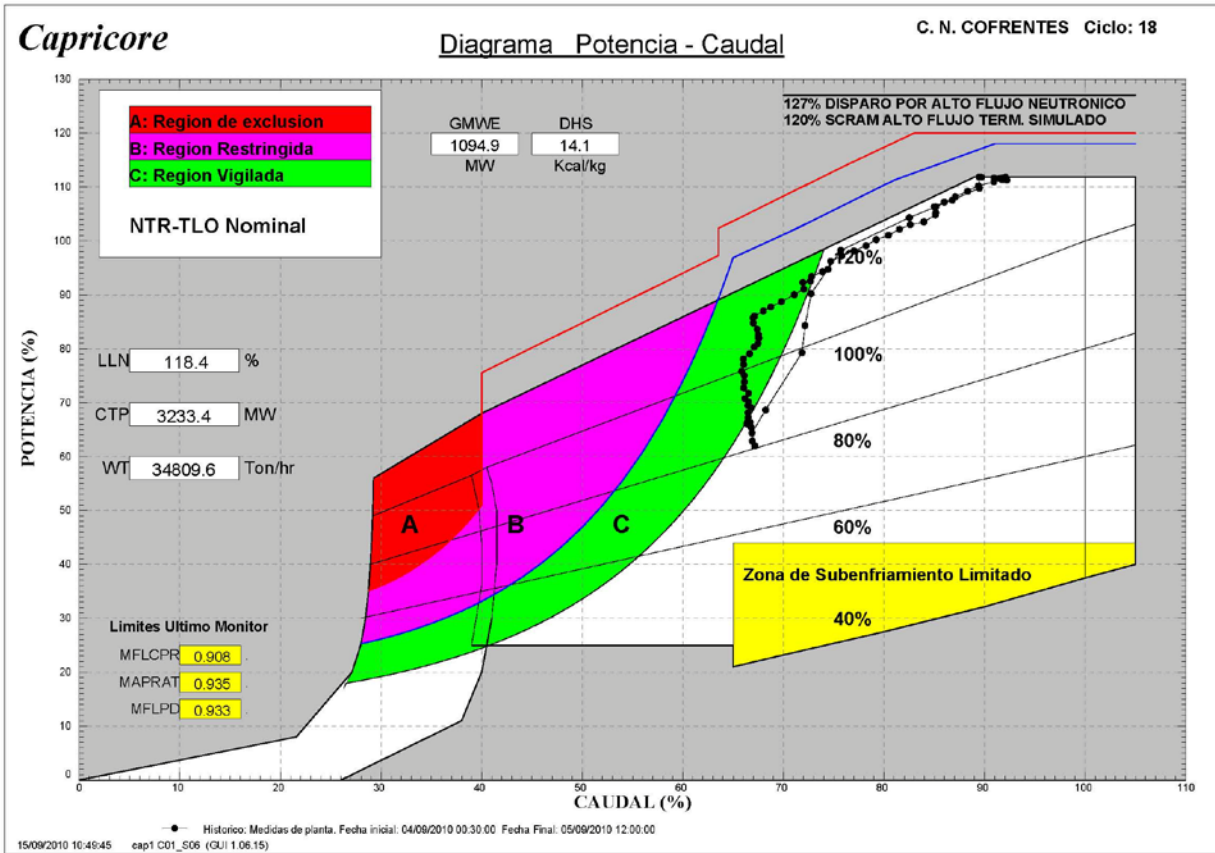
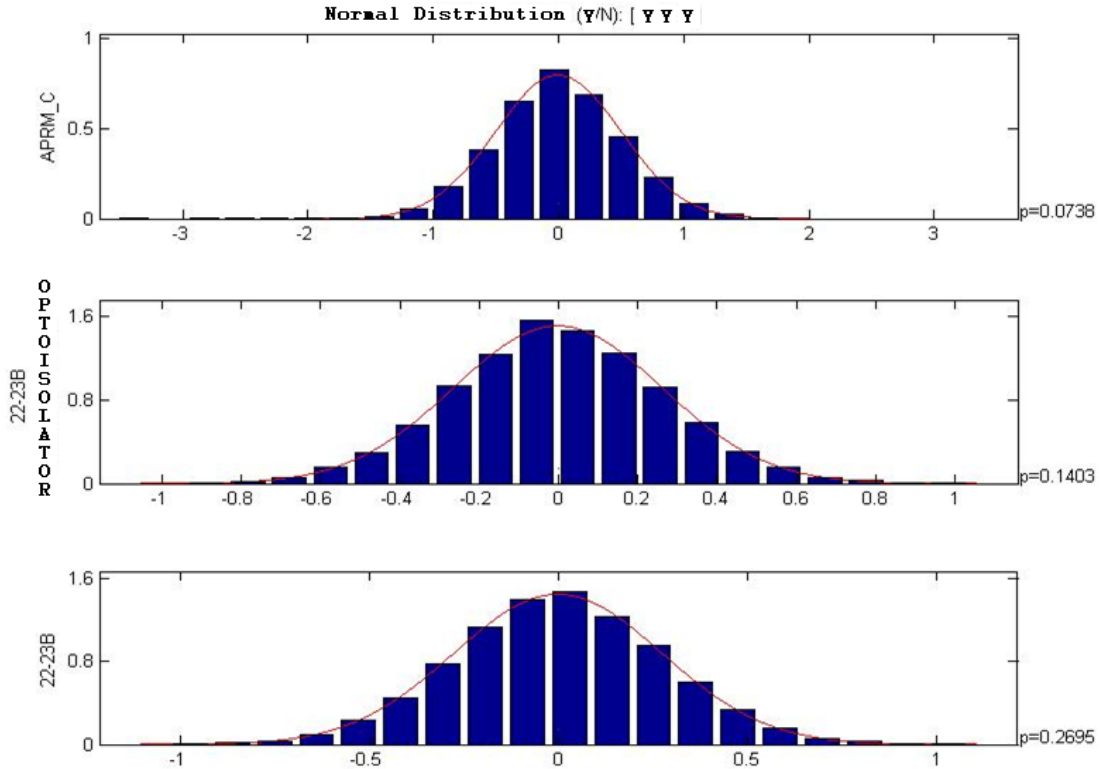


Figure 6.16 September 2010 control sequence exchange roadmap



**Figure 6.17 Histogram of APRM-C and LPRM 22-23B with and without optoisolator**

Applying the Kolmogorov-Smirnoff normality test to the signal indicates in some cases that noise distribution is normal. The test is not satisfied in all of the cases, but the appearance of the histogram shows a clear normality of signals. Gaussian noise is expected for conditions where the signal is not to be highly autocorrelated (low decay ratio). In case of high decay ratio values, the distribution would look like a sinusoid in Gaussian noise. The distribution of LPRM signal through the optoisolator seems to be unaffected from a statistics standpoint.

### 6.6.3 Decay Ratio Results

In Figure 6.18 a sample of June and September 2010 decay ratio values is shown. First of all, decay ratio values are lower than 0.2 for all of the state points.

Frequency and decay ratio trends seem to be reasonable. There is a higher inaccuracy in frequency estimation from autocorrelation function, especially for high flow and low decay ratios.

Figures 6.19 and 6.20 show the decay ratio and frequency agreement comparing autocorrelation and LAPUR-based data, respectively.

Decay ratios obtained are smaller than 0.2. Frequencies based on autocorrelation are higher than those predicted by LAPUR, especially for high core flow (higher than 70%). Decay ratio from these state points is very low, and this could cause numerical difficulties in determining the frequency from the autocorrelation function.

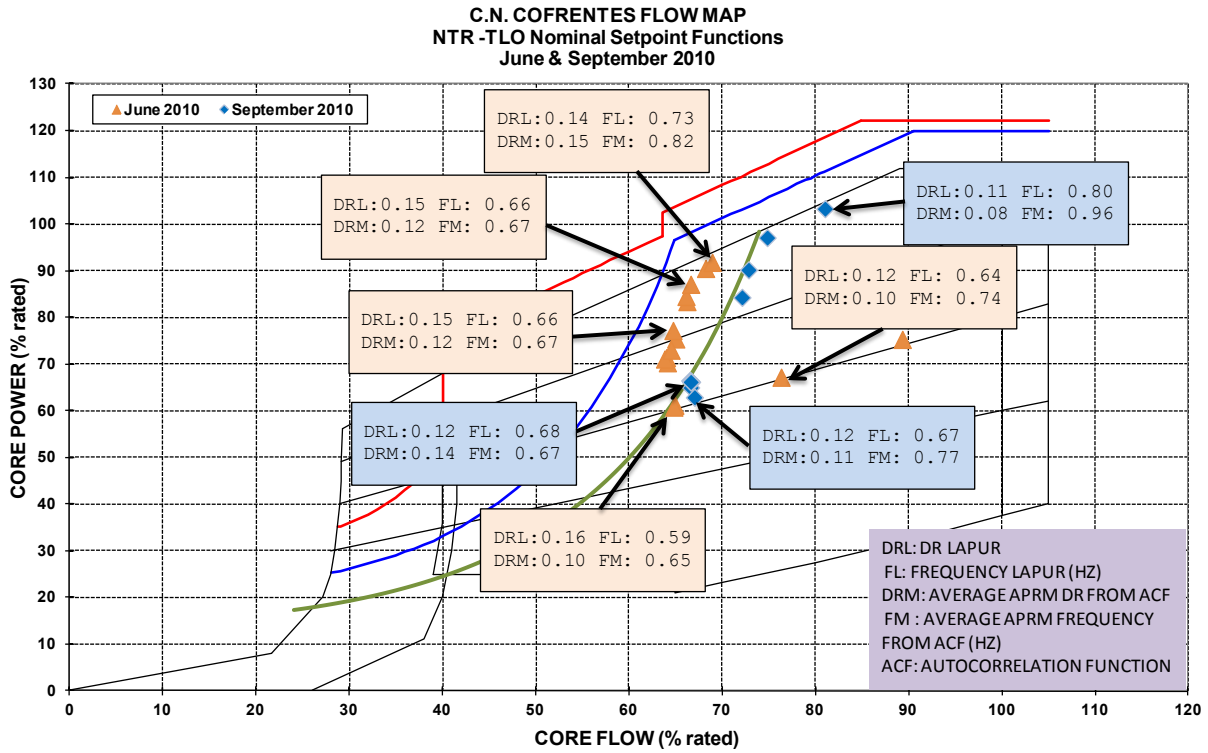


Figure 6.18 Decay ratio sample for June and September 2010 maneuvers

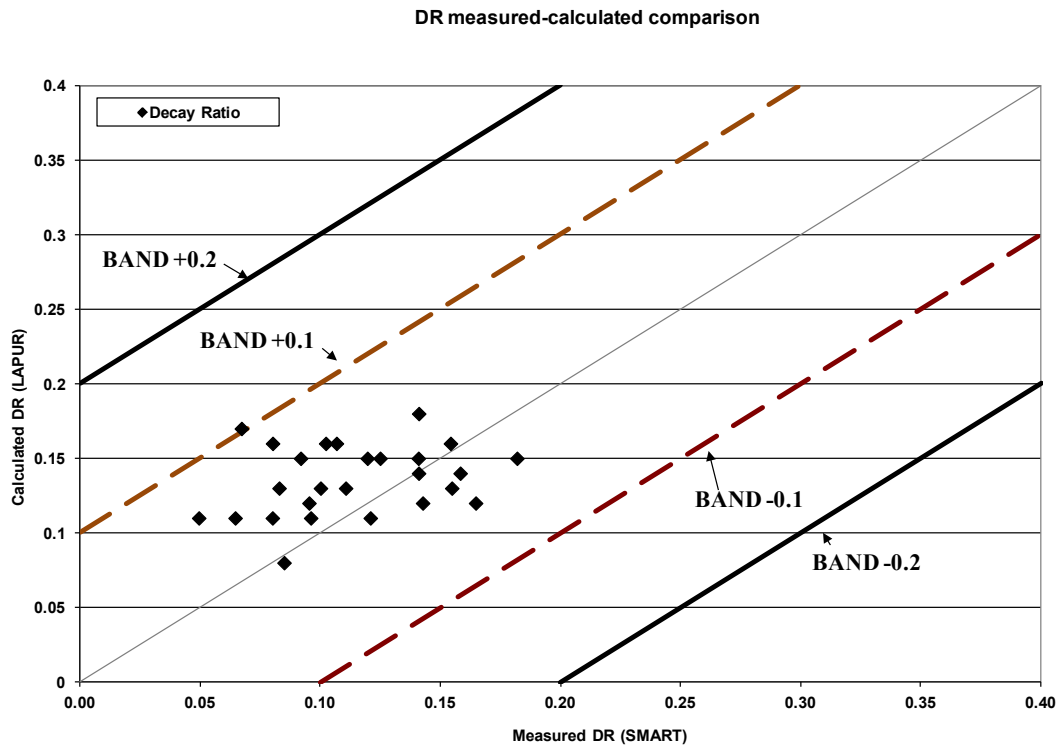


Figure 6.19 June and September 2010 maneuver—decay ratio comparison

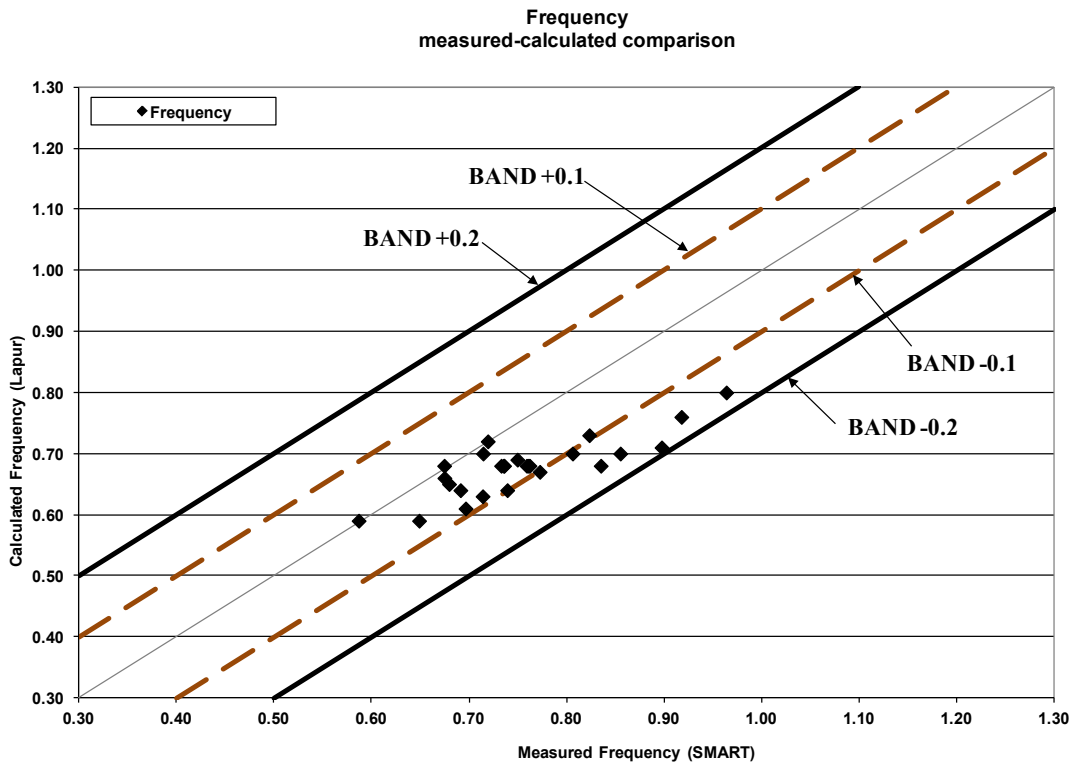


Figure 6.20 June and September 2010 maneuver—frequency comparison

## 6.7 LPRM Data

Due to better noise resolution capabilities of the RTP system, decay ratios from LPRMs can be obtained.

Figure 6.21 shows reasonable agreement among LPRM, APRM C and LAPUR decay ratios taking into account the increased noncorrelated noise, which LPRM signal usually contains.

Figure 6.22 shows the frequency comparison. The agreement is very good until the frequency is less than 0.8 Hz for signal and 0.7 Hz from LAPUR, for a core flow less than 70%. Decay ratio from these state points is very low, and this could cause numerical difficulties in determining the frequency from the autocorrelation function.

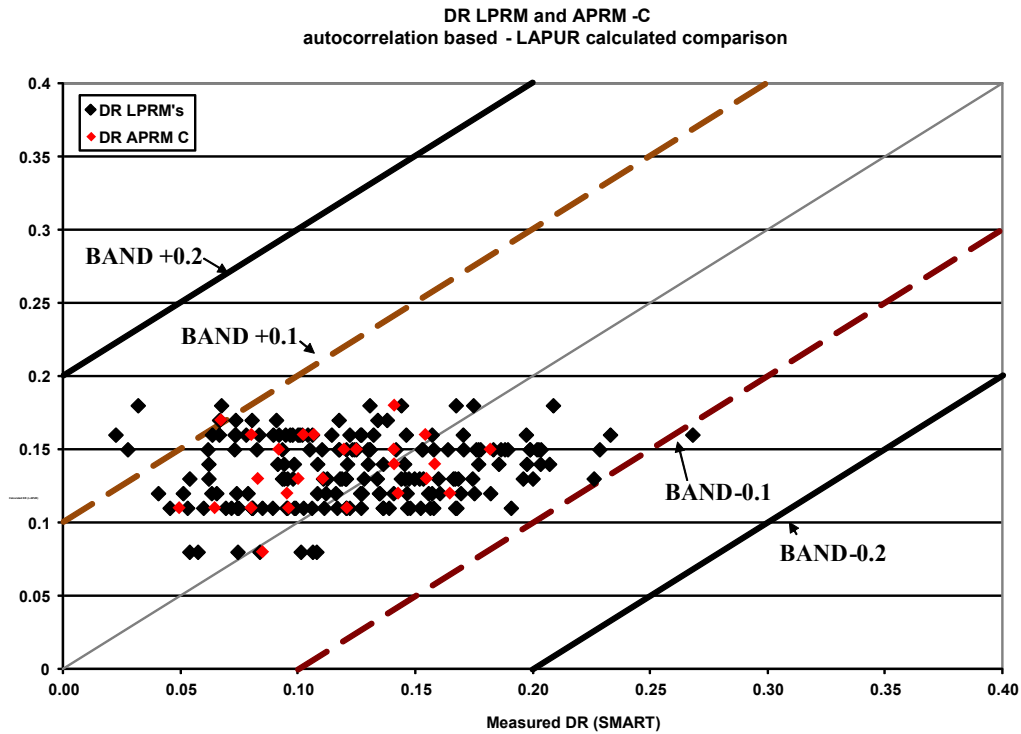


Figure 6.21 LPRM and APRM-C decay ratio from autocorrelation versus LAPUR decay ratio comparison—September and June 2010 sequence exchange

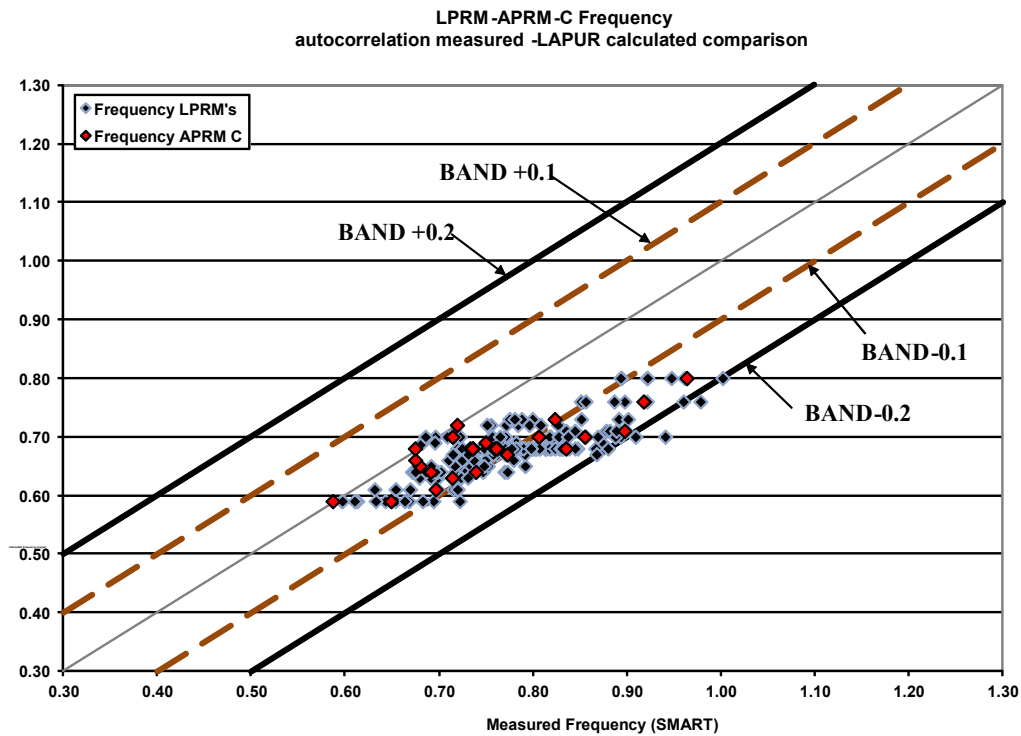


Figure 6.22 LPRM and APRM-C frequency autocorrelation-based versus LAPUR decay ratio comparison—September and June 2010 sequence exchange

## CONCLUSIONS

Generic validation of the components of pressure drop obtained with the new models implemented in LAPUR6 r.0 was performed (using default friction models of SIMULATE-3). Comparisons of LAPUR6 with SIMULATE-3 showed a very good agreement. Components that are dependent on void fractions (elevation and acceleration) showed slight discrepancies due to the void fractions predicted by SIMULATE-3 and LAPUR6 not being equal. However, the relative contribution of these components to the total pressure drop is very low, and the effect can be considered to be negligible.

FRIGG-2 LOOP experimental void fractions data and LAPUR6 were also compared. Their agreement was similar to those of other codes with three or four equations and dynamic or algebraic slip.

Figures 7.1 and 7.2 show all available Cofrentes plant data from start-up, sequence exchange, and coastdowns.

Reasonable agreement was observed, and the majority of predictions are in the  $\pm 0.1$  band. Frequency is reasonably predicted up to 70% of the flow rate (0.7 Hz for LAPUR and 0.8 for autocorrelation-based frequency).

Table 7.1 shows results obtained for Cofrentes instability on January 29, 1991. Agreement for wide-core decay ratio is very good. LAPUR6 and autocorrelation-based decay ratios and frequency show very consistent results.

**Table 7.1 Cofrentes instability results**

<b>State point</b>	<b>Power (MW)</b>	<b>Flow (MLb/h)</b>	<b>Core decay ratio</b>	<b>Frequency (Hz)</b>	<b>Channel decay ratio (1HC)</b>	<b>Out-of-phase decay ratio (-1.06\$)</b>
012991	1108.4 (40.8)	25.94 (30.7%)	0.75	0.41	0.69	0.78
Autocorrelation-based estimation			0.78	0.47		0.98

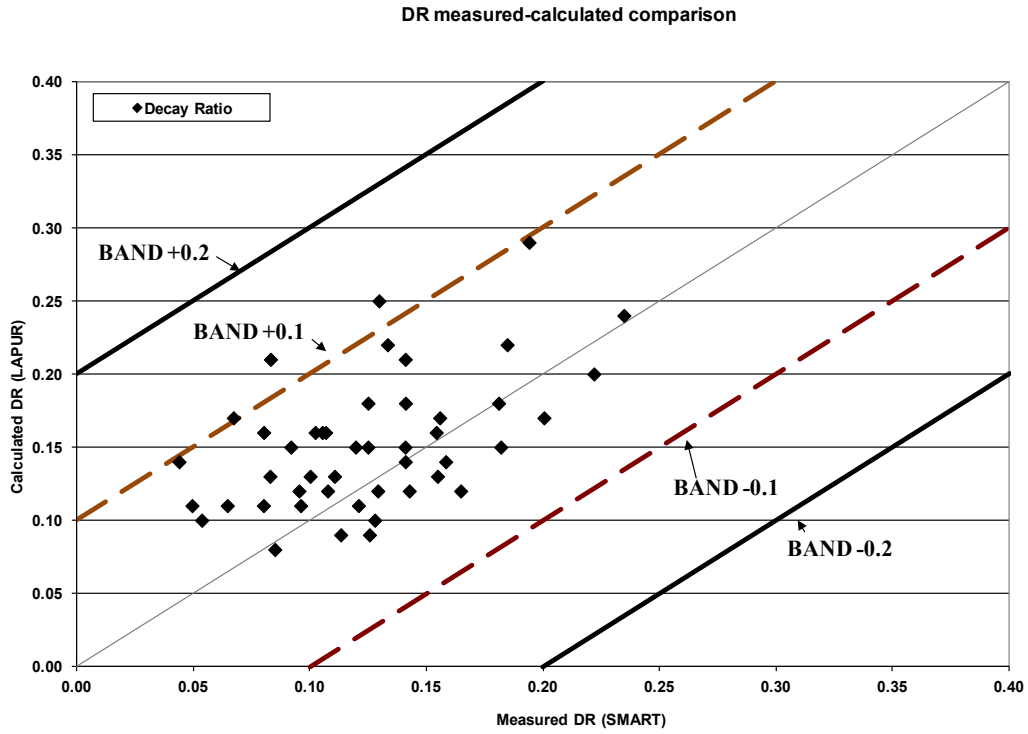


**Figure 7.1 Decay ratio autocorrelation based on LAPUR calculation**

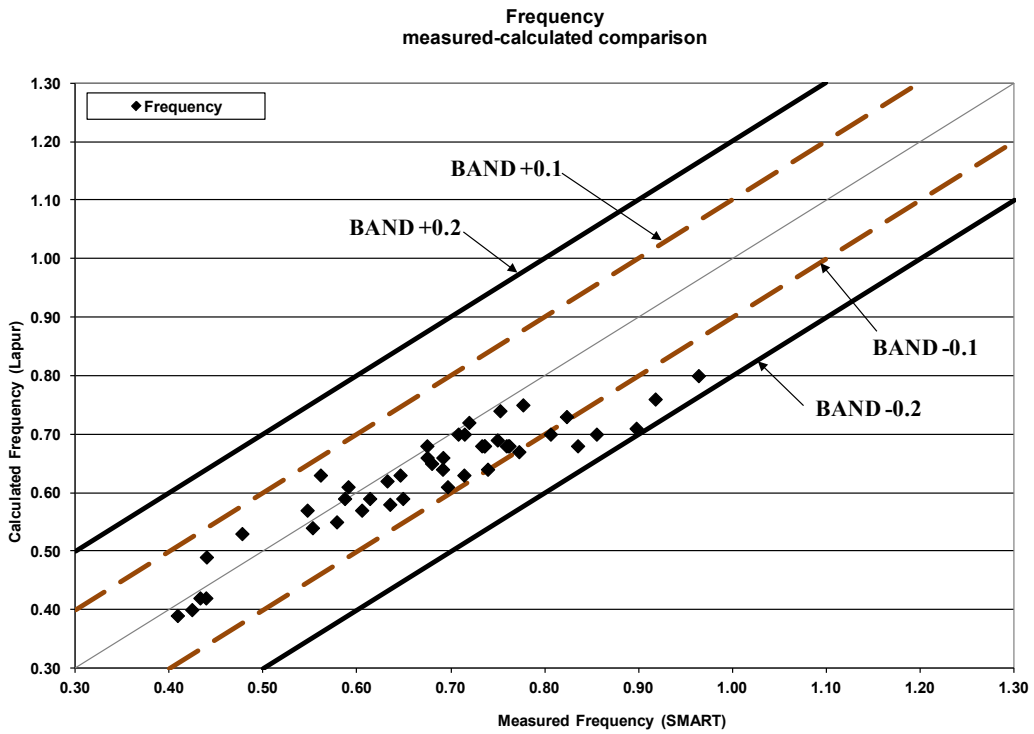


**Figure 7.2 Frequency autocorrelation based on LAPUR calculation**

## REFERENCES

- Albendea, M., and A. Crespo (2000). "CAPRICORE: A New on-line Monitoring System," EPHISOR 2000 ANS International Topical Meeting on Advances in Reactor Physics and Mathematics and Computation into the Next Millennium.
- CC-COSNU-415 (2006). *Validación de los nuevos modelos t/h de LAPUR6*.
- Chisholm, D. (1973). "Pressure Gradients Due to Friction During the Flow of Evaporating Two-phase Mixtures in Smooth Tubes and Channels," *Journal Heat Mass Transfer*, Vol. 16, Pergamon Press, Great Britain, pp. 347–358.
- Escrivá, A., J. L. Muñoz Cobo, J. Melara, M. Albendea, and J. March-Leuba (2008). *LAPUR 6.0 Users Manual*, NUREG/CR-6958, October.
- Escrivá, A., and J. March-Leuba (2000). *LAPUR 5.2 Verification and User's Manual*, NUREG/CR-6696, ORNL/TM-2000/340, November.
- FIBWR: A Steady-state Core Flow Distribution Code for Boiling Water Reactors Computer Code User's Manual* (1981). EPRI NP-1924-CCM, July.
- Harris, F. (1978). "On the Use of Windows for Harmonic Analysis with the Discrete Fourier Transform," *Proceedings of the IEEE*, Vol. 66, No. 1.
- IBERDROLA (2011). "Verificación del Modelo Termo-hidráulico de SIMULATE-3 para CN Cofrentes, IT\_CONUC-075 rev 6.
- IT-COSNU-260 (2006). Descripción del programa LIP, July.
- March-Leuba, J. (1984). "Dynamic Behavior of Boiling Water Reactor," PHD Dissertation, December.
- March-Leuba, J. (1992). *Density Wave Instabilities in Boiling Water Reactors*, NUREG CR/6003, October.
- Methodology and Procedure for Calculation of Core and Channel Decay Ratios with Lapur* (2006). IT-CONUC-028, rev. 4, July.
- Montesinos, M. E., J. L. Muñoz-Cobo, C. González, A. Escrivá, C. Lora, J. Melara, and M. Albendea (2010). "Utilización del monitor SMART V2.1, para el cálculo de estabilidad de un reactor de agua en ebullición," 36 Reunión Anual de la Sociedad Nuclear Española, Santiago de Compostela, October.
- Otaduy, P. J., and J. March-Leuba (1990). *LAPUR User's Guide*, NUREG/CR-5421.
- Proakis, J. G., and D. G. Manolakis (1998). *Tratamiento digital de señales. Principios, algoritmos y aplicaciones*, Prentice Hall, Madrid.
- RETRAN-3D—A Program for Transient and Thermal-Hydraulic Analysis for Complex Fluid Systems.* Vol. 4 Assessment manual (2006), NP-7450(A) Rev. 1.
- Studsvik (2007). *SIMULATE-3 User's Manual*, SSP-95/15, Rev. 4.
- Tofiño, Y. (2004). "Predictor de estabilidad para la vigilancia continua de un reactor tipo BWR," Proyecto Fin de Carrera. ETSI de Minas. Premio Mejor Proyecto Fin de Carrera SNE.
- Universidad Politécnica de Valencia (2006). *Improvements Made in LAPUR5 to Obtain LAPUR6*.

UPV Chemical Engineering Department (1998). *Aplicación de LAPUR para el cálculo del margen de estabilidad en reactores BWR*, DIQN-98/003, report prepared for Iberdrola, S. A., July.

Verdu, G., D. Ginestar, J. L. Muñoz-Cobo, J. Navarro, M. J. Palomo, P. Lansaker, J. M. Conde, and E. Sartori (2001). *Forsmark 1 & 2 Boiling Water Reactor Stability Benchmark: Time Series Analysis Methods for Oscillation during BWR Operation*, NEA/NSC/DOC (2001) 2, OECD, June.



**BIBLIOGRAPHIC DATA SHEET**

(See instructions on the reverse)

2. TITLE AND SUBTITLE

Validation of LAPUR 6.0 Code

3. DATE REPORT PUBLISHED

MONTH

YEAR

03

2012

4. FIN OR GRANT NUMBER

JCN J4430

5. AUTHOR(S)

Jose Melara, Carmen Lora (Iberdrola Ingenieria y Construccion)  
Alberto Escrivá, Jose Luis Muñoz-Cobo (Universidad Politécnica de Valencia)  
Manuel Albendea (Iberdrola Generación)  
Jose March-Leuba (ORNL)

6. TYPE OF REPORT

Technical

7. PERIOD COVERED (Inclusive Dates)

8. PERFORMING ORGANIZATION - NAME AND ADDRESS (If NRC, provide Division, Office or Region, U.S. Nuclear Regulatory Commission, and mailing address; if contractor, provide name and mailing address.)

Oak Ridge National Laboratory  
PO Box 2008  
Oak Ridge, TN 37831

9. SPONSORING ORGANIZATION - NAME AND ADDRESS (If NRC, type "Same as above"; if contractor, provide NRC Division, Office or Region, U.S. Nuclear Regulatory Commission, and mailing address.)

Division of Safety Systems  
Office of Nuclear Reactor Regulation  
U.S. Nuclear Regulatory Commission  
Washington, DC 20555-0001

10. SUPPLEMENTARY NOTES

Dr. T. L. Huang, Project Manager

11. ABSTRACT (200 words or less)

The capabilities of the computer code LAPUR have been upgraded. A new version, LAPUR6 r.0, has been implemented and validated for computing friction and local losses and capabilities for modelling bundles with variable cross areas. This report documents a twofold validation of the new thermal-hydraulic model implemented in LAPUR6. First, a comparison of each component of the pressure drop for a single-channel model using LAPUR6 and SIMULATE-3 was performed, the result of which showed very good agreement. Slight discrepancies in void fractions between the two codes were found, but the effect on total pressure drop was negligible. In addition, the LAPUR6 void fraction model was tested against FRIGG-2 void fraction data. Void fractions predicted by LAPUR6 showed deviations similar to those of other thermal-hydraulic codes when benchmarked against FRIGG 2 experimental data.

An extensive validation comparing measured against calculated core-wide (CW) decay ratios was also conducted. A set of Average Power Range Monitor (APRM) signals were recorded at steady state during the final coastdowns for Cycles 16b and 17 and start-up for Cycles 17 and 18 in Cofrentes Nuclear Power Plant (NPP). A detailed simulation of these activities was conducted with SIMULATE-3 using cycle-specific CASMO-4 cross sections and the recorded operating data. Selected quasi-steady-state points were analyzed using noise techniques, and decay ratio values were compared to LAPUR6 results. Finally, Cycle 6 Cofrentes out-of-phase (OOP) instability was reproduced using LAPUR6, and the resulting decay ratios showed excellent agreement with the measured data.

12. KEY WORDS/DESCRIPTORS (List words or phrases that will assist researchers in locating the report.)

LAPUR  
BWR  
BWR Stability

13. AVAILABILITY STATEMENT

unlimited

14. SECURITY CLASSIFICATION

(This Page)

unclassified

(This Report)

unclassified

15. NUMBER OF PAGES

16. PRICE



Federal Recycling Program





**UNITED STATES  
NUCLEAR REGULATORY COMMISSION**  
WASHINGTON, DC 20555-0001  
-----  
OFFICIAL BUSINESS

**NUREG/CR-7124**

**Validation of LAPUR 6.0 Code**

**March 2012**